

PHD PROGRAMME IN MOLECULAR AND
TRANSLATIONAL MEDICINE
DIMET

**Novel insights into the protective role of
miR-133a in the heart and its
therapeutic application for the
treatment of cardiac pathologies**

Dr. Vittoria Di Mauro

Matr. No. 787800

Cycle XXIX

Academic Year 2015-2016

Tutor: Prof. Roberto Giovannoni

Co-Tutor: Prof. Gianluigi Condorelli

Supervisor: Daniele Catalucci

Coordinator: Prof. Andrea Biondi

Table of contents

Chapter 1: *General Introduction*

Chapter 2: *Scope of the thesis*

Chapter 3: *The Wnt canonical pathway controls DNMT3B transcription via nuclear-relocalization of miR-133a in cardiac cells*

Chapter 4: *MiR-133 modulates the β_1 -Adrenergic Receptor transduction cascade*

Chapter 5: *Bio-Inspired Negatively-Charged Calcium Phosphate Nanocarriers for Cardiac Delivery of MicroRNAs*

Chapter 6: *MiR-153/Kv7.4: a novel molecular axis in the regulation of hypertension*

Chapter 7: *The importance of being ncRNAs: from bit players as “junk DNA” to rising stars on the stage of the pharmaceutical industry*

Chapter 1

General Introduction

1. The discovery of microRNAs

The pioneering event that led to the discovery of animal microRNAs (miRNAs) was in the early 1980s, when the loss-of-function mutation of an heterochronic gene, named *lin-4*, capable to control the timing of development of nematodes, was reported to lead to an increased number of molts and continued synthesis of larval specific proteins in in *C. elegans* ^[1]. Only several years later, two independent studies further characterized the mechanism of action of *lin-4*. Indeed, it was demonstrated that *lin-4* does not code for a protein but rather just a pair of short RNA transcripts capable to regulate the timing of larval development by translational repression of *lin-14* that, in turn, encodes for nuclear proteins. The authors hypothesized that this regulation was due to sequence complementarity between *lin-4* and the 3'-Untranslated Region (UTR) of *lin-14* mRNAs ^[2, 3]. Thereafter, a second heterochronic switch gene, *let-7*, expressed in the late stages of larval development, was found to have a complementary sequence to the 3'-UTR of *lin-14*, as well as other mRNAs ^[4].

Initially, these transcripts were defined as small temporal (st)RNAs and considered of limited relevance. Nonetheless, since the discovery of *let-7*, a multitude of other (st)RNAs were identified in different organisms, the majority of which sharing a highly conservation in sequence, thus reflecting their extreme importance and finally gave rise to the modern definition of microRNAs (miRNAs) ^[5].

2. Structure and biogenesis of miRNAs

Mature miRNAs are defined as single stranded RNA molecules of 21-26 nucleotides (nt) in length, generated from a longer hairpin-shaped transcript ^[6].

Even though it was originally believed that most miRNA genes were located in intergenic regions ^[7, 8], in the last decade different analyses of miRNA gene locations pointed out that the majority ($\approx 70\%$) of mammalian miRNA genes were located in defined transcription units (TUs) ^[9]. Moreover, many miRNA genes were found in the introns of either protein-coding or non-coding genes, and in some cases present in either an exon or an intron ('mixed'), depending on the alternative splicing pattern. Thus, miRNA genes can be categorized based on their genomic locations: intronic miRNA in protein-coding TU; intronic miRNA in non-coding TU, and exonic miRNA in non-coding TU (Figure 1). Additionally, approximately 50% of known miRNAs are found in cluster, and they are transcribed as polycistronic products.

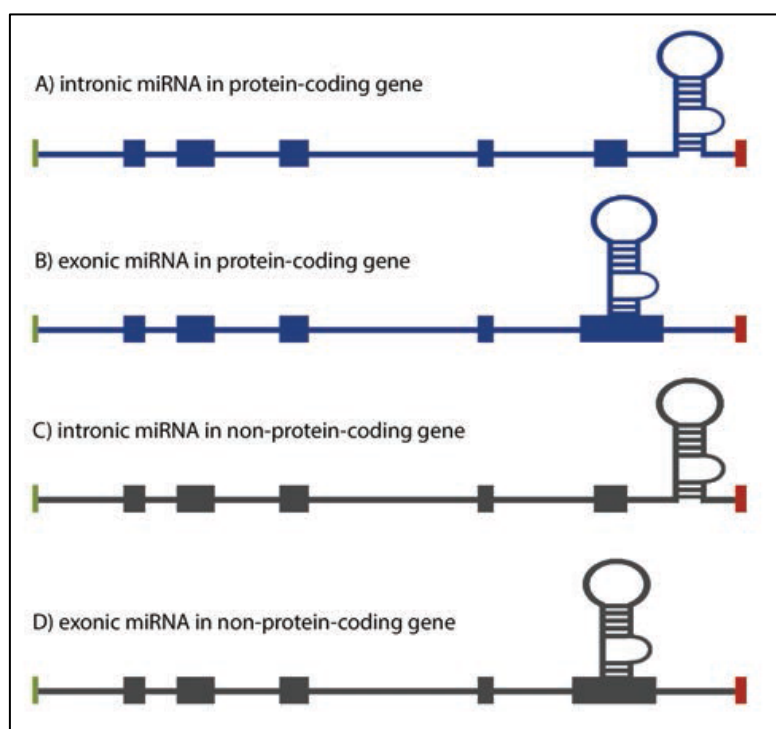


Figure 1. The genomic classification of miRNA genes. The miRNA gene localization in the genome can be classified in: **A)** intronic miRNA within the non-coding TU; **B)** exonic miRNA within the non-coding TU; **C)** intronic miRNA within the coding TU; **D)** exonic miRNA within the coding TU. Adapted from *Al-Moundhri M. et al., 2015* ^[10].

Whatever the origin, the transcription of miRNA gene by the RNA polymerase II, generates a RNA product, defined primary miRNA (pri-miRNA), which is several hundred nucleotides long and has a 33-nt stem-loop conformation comprising a 5'-end cap structure and a polyadenylated 3'-tail sequence ^[6]. Within the nucleus this pri-miRNA is cropped into a shorter product (60-70 nts), named pre-miRNA, by a multiprotein complex containing the RNase III Drosha and the DiGeorge syndrome critical region 8 (DGCR8) ^[11-13]. The pre-

miRNA exits from the nucleus through the Exportin-5 (XPO5)/RanGTP^[14]. Specifically, the hydrolysis from RanGTP to RanGDP causes the release of pre-miRNA into the cytosol in which it is further cleaved by the RNase III DICER to give rise to a 22-24 nucleotide miRNA duplex^[15]. This duplex is unwound by a helicase activity, and one strand, so called “passenger” strand (or miRNA*) is usually degraded, while the other strand, named “guide” strand, accumulates as mature miRNA. Then, miRNAs are loaded into the Argonaute proteins (Ago1-4), which bind the 3’-end of miRNAs with the Piwi-Argonaute-Zwille (PAZ) domain. The association between Argonaute, Dicer and miRNA forms a ribonulceoprotein complex called miRNA-induced silencing complex (miRISC) through which mature miRNAs elicit their biological function^[16] (Figure 2).

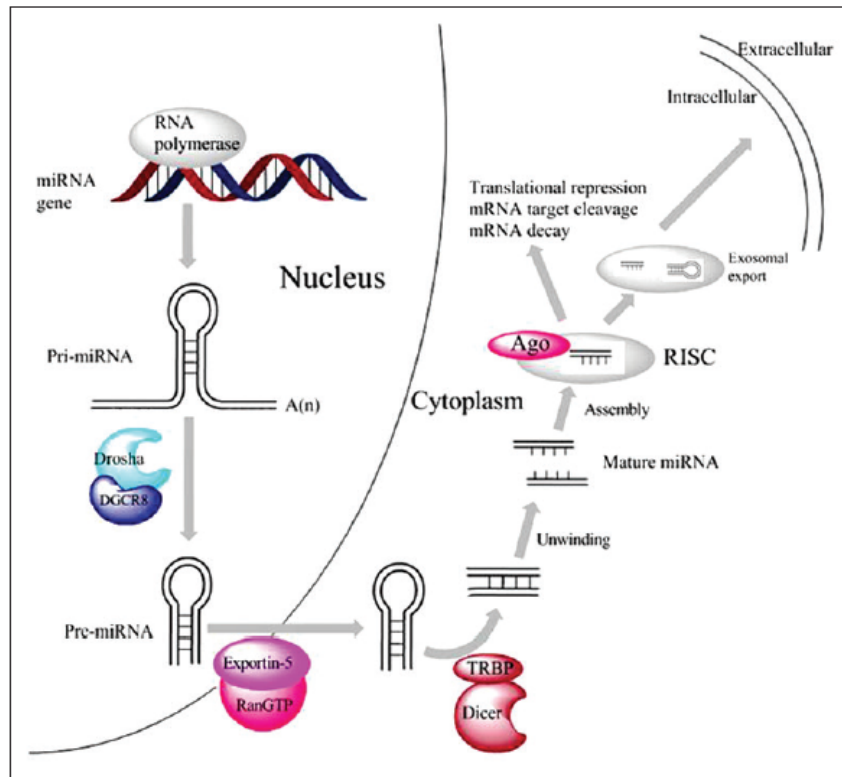


Figure 2. The biogenesis of miRNAs. The transcription of miRNA gene by RNA polymerase II produces a transcript called pri-miRNA. This pri-miRNA is cleaved by the Drosha-DGCR8 complex and forms the pre-miRNA. This is transported to cytoplasm from nucleus by the XPO5/RanGTP cofactor. The pre-miRNA is processed into a miRNA duplex, which is unwound to form mature miRNA. The guide strand binds to Ago to form RNA-induced silencing complex (miRISC). Adapted from *Liu N et al., 2015* ^[17].

3. MiRNA mechanism of action: the “old canonical” Vs “new non-canonical”

Canonically, mature miRNAs are believed to elicit their action in the cytosol of cells. In particular, the main function of miRNAs is the negative modulation of gene expression at post-transcriptional level,

through the well accepted mechanism of endogenous RNA interference (RNAi)^[18]. Indeed, miRNAs guide the miRISC complex to target mRNAs at the cytoplasmic processing-bodies (P-bodies)^[19, 20]. Here, miRNAs bind to the 3'-UTR of target mRNAs, typically forming an imperfect duplex. Although multiple mismatches are tolerated between miRNAs and their targets, a high sequence complementarity in the so called “seed region” of miRNA (nts 2-7) is necessary for the proper target recognition ^[21, 22]. The exact mechanism through which miRNAs regulate gene expression is still subject of discussion, nevertheless it is well accepted that based on the overall degree of complementarity with their targeted mRNA, miRNAs can either block mRNA translation or induce degradation. In fact, high levels of complementarity lead to the cut at specific nucleotide position through the slicer activity of Ago2 ^[23]. On the contrary, the presence of mismatches and bulges results into a block of translation rather than a decrease in mRNA abundance (Figure 3).

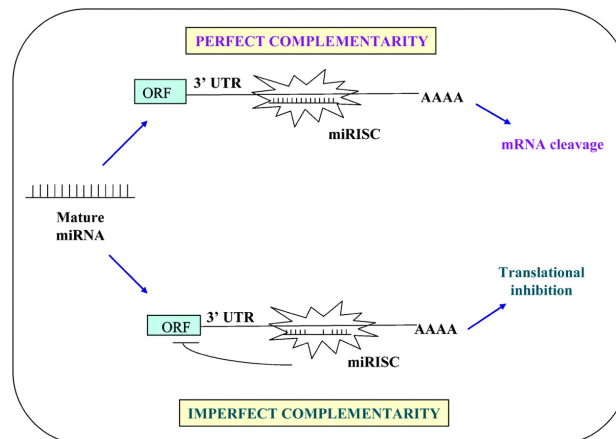


Figure 3. The canonical mechanism of miRNA action. MiRNAs regulate gene expression by binding to complementary sites in the target mRNA. Imperfect binding between miRNAs and the site in 3'-UTR of mRNA gene blocks target gene

expression at the level of protein translation. MiRNAs that bind to their mRNA targets with perfect (or nearly perfect) complementarity with mRNA target induce target mRNA cleavage. Adapted from *Paranjape T. et al., 2009* ^[24].

Beyond this canonical mechanism of action, in the last years different works have highlighted how this paradigm of miRNA function is not absolute. Indeed, many works showed that mature miRNAs could relocate into the nucleus and, in some cases, be even more abundant in the nucleus than in the cytoplasm ^[25-28].

In support of the observation that mature miRNAs are present in cell nuclei, studies have also reported the localization of Ago proteins in the human cell nucleus ^[29]. This evidence suggests a potential role of Ago proteins inside this compartment as enhancer of nuclear miRNA function. More evidence of nuclear presence for both mature miRNAs and component of RNAi machinery, consequently led researchers to test the hypothesis of the existence of a cellular machinery involved in their cytoplasmic-nuclear transport (Figure 4) ^[21, 30].

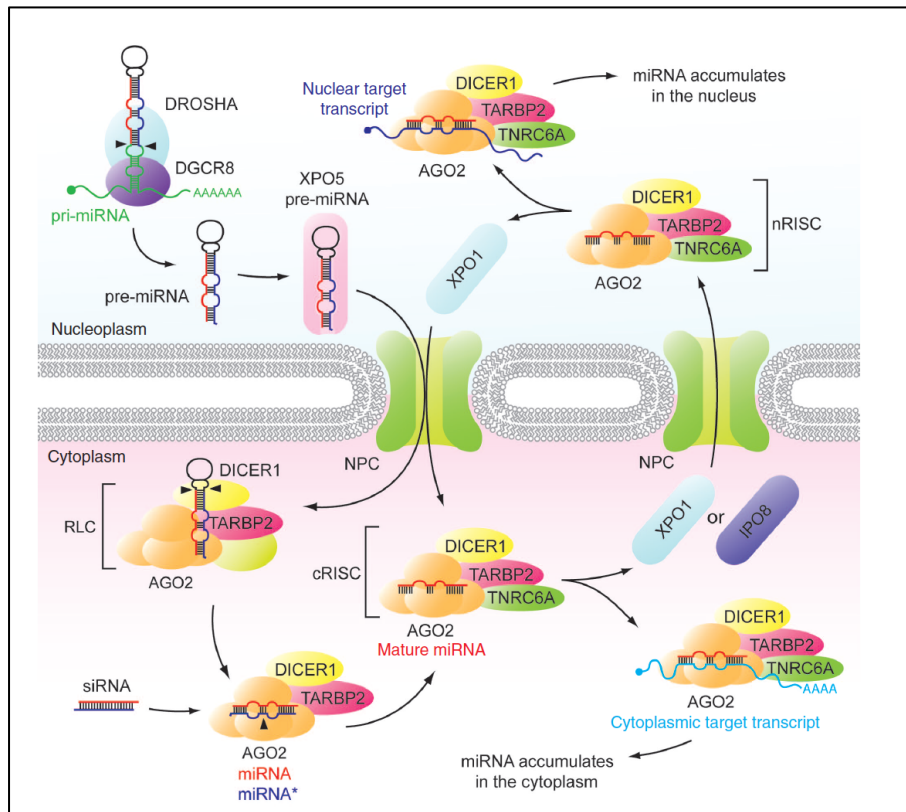


Figure 4. The nuclear-cytoplasmic machinery of miRNAs. In the canonical view, miRNAs interact with Nuclear Pore Complex (NPC) during their biogenesis. Pre-miRNAs are exported outside the nucleus through XPO5. Mature miRNAs, in association with components of RNAi machinery, can also re-locate into the nucleus through Exportin-1 (XPO1) or Importin-8 (IPO8). Adapted from *Roberts TC et al., 2014* ^[21].

Importins and exportins mediate the translocation of molecules through the NPC. In 2009 *Castanotto et al.* showed for the first time that XPO1 facilitates the transport of mature miRNAs from the cytosol to the nucleus in human cells ^[31]. Few years later, another evidence of a dedicated machinery for the cytosol-nucleus shuttling of miRNAs and miRISC components came from the work of *Zisoulis et*

al. In this paper, the authors showed that depletion of XPO1 by RNA interference resulted in a lower nuclear localization of Argonaute-like Gene 1 (ALG-1), the Argonaute protein in *C. elegans* [32]. Moreover, other works also demonstrated implications of IPO8 in nuclear import of miRNAs [33]. Indeed, upon IPO8 knock-down localization of AGO2 was shifted from the nucleus to the cytoplasm in human cells [34].

Although the functions of cytoplasmic miRNAs are well established, the role of nuclear miRNAs is only starting to be uncovered. One of the first hypothesis was the idea of nucleus as recycling compartment of miRNAs, in order to sequester them from the cytoplasm and fine-regulate their impact on mRNAs targets [30]. Nevertheless, the simultaneous presence into cell nuclei of RNAi factors, strongly suggested a more sophisticated action of nuclear miRNAs. Indeed, analysis of miRNA-mRNA-Argonaute interactions by high-throughput [35, 36] sequencing of RNAs isolated by cross-linking immunoprecipitation (HITS-CLIP) in mouse brain showed for the first time that a substantial number of Ago-mRNA tags mapped to intronic region and long non-coding RNAs (lncRNA) sequences [37, 38]. Additionally, several studies also revealed that some miRNAs can regulate the biogenesis of other miRNAs directly into the nucleus [39]. Moreover, different works also demonstrated an active function of miRNAs in the modulation of the epigenetic landscape of target genes. Indeed, in the work of *Kim et al.*, the authors found a putative site for miR-320 in the promoter of RNA Polymerase III Subunit D (POLR3D) of human cells. Interestingly, the binding of miR-320 in this site was able to induce the enrichment of AGO1 and chromatin modifier that, in turn, leads to the heterochromatinization of the locus

and the subsequent transcriptional gene silencing (TGS) [40]. Subsequently, many other works described analogue mechanisms of action for other miRNAs, included transcriptional activation (TGA) of target genes [35, 36, 41, 42] (Figure 5).

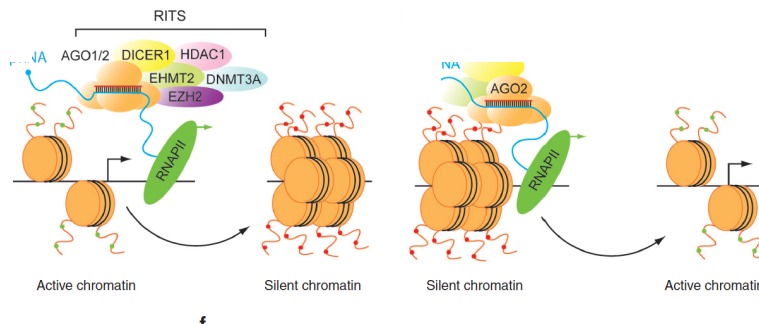


Figure 5. The epigenetic function of nuclear miRNAs. Transcriptional gene silencing (TGS) or transcriptional gene activation (TGA) is mediated by miRNAs through recruitment of specific epigenetic enzymes in the regulatory region of target genes. Adapted from Roberts T. *et al.*, 2014 [21].

4. The miRNA impact in the physiology and pathophysiology of organism: a specific focus on miR-1 and miR-133 in the heart

As discovery of human miRNAs increased, the main goal of research was gradually focused towards functional characterization of miRNAs in the contest of human diseases [43]. The connection between miRNAs and disease resulted immediately obvious, because the majority of miRNAs were found to play key roles in many biological processes such as cell division and death [44, 45], cellular metabolism [44, 45], intracellular signaling [46], immunity and cell movement [47, 48]. Indeed, since the miRNA first discovery, a plethora of studies demonstrated that deregulation in their expression proportionately

affects these critical processes, and as a result, leads to various pathological and often malignant outcomes ^[43].

In the contest of cardiovascular system, the heart is the first organ to form in embryos and it is also the most sensitive to many stimuli and stresses. Consequently, also the faint perturbation during cardiogenesis can lead to catastrophic consequences ^[49]. Indeed, congenital heart diseases affect nearly the 1% of all new-borns and for this, it is considered the leading cause of death worldwide ^[50]. Thus, it is not surprising that many efforts have been made into the understanding of development, physiology and pathology of the cardiovascular system. In this contest, only in the last years different studies started to unravel the role of various miRNAs in cardiovascular pathophysiology. So far, two related muscle specific miRNAs, the miR-1 and miR-133, have been extensively characterized for their important role in the control of proliferation and differentiation of muscle cells.

MiR-1 is a highly conserved miRNA and it was found in nematodes, flies and vertebrates ^[6]. Moreover, miR-1 is the most abundant miRNA in mammalian heart, accounting for almost 40% of all miRNAs in the adult murine heart ^[51, 52]. The miR-1 family comprises the miR-1 and miR-206 subfamily. The latter is not expressed in cardiac cells. For what concern the miR-1 subfamily, it is made up of two related transcripts, miR-1-1 and miR-1-2, encoded by two distinct genes located in chromosome 2 and 18, respectively. During mammalian heart development, miR-1-1 starts to be expressed in the inner curvature of heart loop and atria, for then becoming widespread in all heart as development goes on. MiR-1-2 is much more present in

ventricles ^[53]. In mammals, the cardiac expression of miR-1 is controlled by the serum response factor (SRF), that recruits the co-factor myocardin to muscle-specific genes to finely control differentiation ^[54].

The miR-133 family includes miR-133a-1, miR-133a-2 and miR-133b, and is expressed from bicistronic units together with miR-1. Indeed, an ancient duplication from a common precursor is thought to have resulted in two loci for miR-1/miR-133 cluster in vertebrates, with identical mature sequences (Figure 6) ^[55].

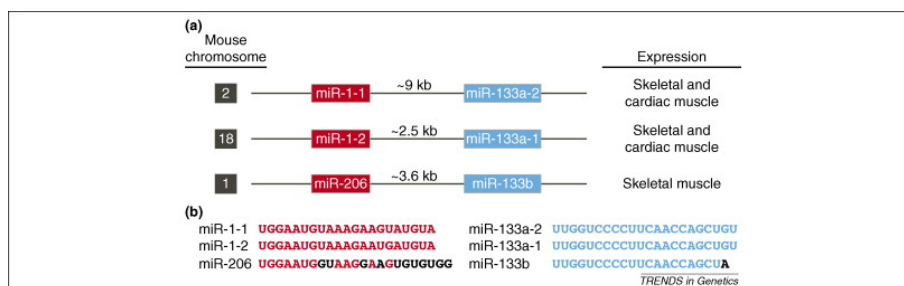


Figure 6. Genomic organization of miR-1/133 cluster. MiR-133a-1 and miR-133a-2 share identical sequences, whereas miR-133b differs by 2 nucleotides at the 3'-terminus. Also, miR-1-1 and miR-1-2 differ between each other for 3 nucleotides at 3'-terminus. Each of the three miR-133 miRNAs is transcribed as a bicistronic transcript with miR-1-2, miR-1-1, or miR-206, as indicated. Genomic distances between the miR coding regions in the mouse genome and expression patterns of each miR cluster are shown. Modified from *Olson E. et al., 2008* ^[56].

MiR-133 is expressed both in skeletal and cardiac muscle. In the latter, its expression is temporally dependent, with increased level from embryonic day (E) 12.5 to at least E18.5 in mouse ^[57]. Similarly to miR-1, the muscle specific-expression of miR-133 is controlled by SRF that, in turn, is also down-regulated in a negative feedback loop

by miR-133 itself. During development, miR-1 and miR-133 work cooperatively to promote mesoderm differentiation of Embryonic Stem Cells (ESCs) and blocking endodermal and ectodermal cell fates [58]. On the other hand, in later stages of development, they have opposing roles in defining cardiac lineage fate. In fact, miR-1 promotes cardiac myocytes differentiation, directly inhibiting the translation of Hand2, a transcription factor demonstrated to regulate the ventricular cardiomyocyte expansion [53]. On the contrary, miR-133 keeps them in a more undifferentiated state (Figure 7) [58, 59].

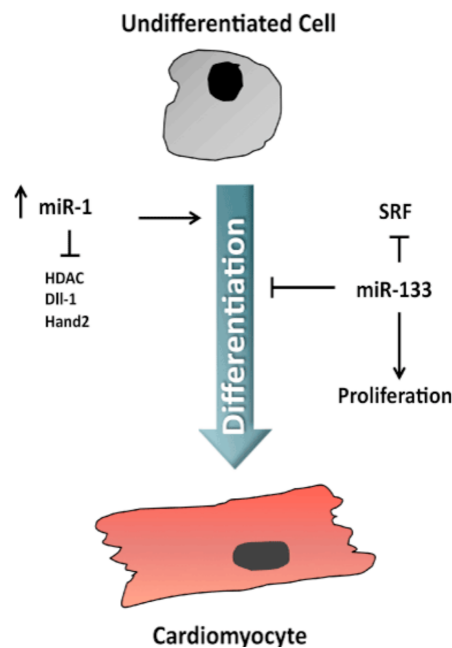


Figure 7. MiR-1 and miR-133 during heart development. During cardiomyocyte differentiation, expression levels of miR-1 and miR-133 increase. In later stages of cardiac lineage differentiation, miR-1 and miR-133 elicit opposite functions. MiR-1 induces the differentiation by inhibiting the expression of Hand2 that, in turn, regulates the expression of cardiac specific genes. Conversely, miR-133 inhibits the differentiation by blocking the expression of SRF, thus promoting cell proliferation. Modified from *Serradifalco C. et al., 2012* [59].

The evidences that pointed out miR-1 and miR-133 as key regulators of cardiac development, also led researchers to question whether alterations in their expression could cause cardiac defects.

In line with this, overexpression of miR-1, under control of the β -myosin heavy chain (β -MHC) promoter, was demonstrated to impair embryonic mouse heart development and it was associated with thin-walled ventricles, heart failure and lethality at E13.5 ^[53]. Moreover, also homozygous deletion of miR-1-2 in mice causes lethality, with incomplete penetrance, between E15.5 and birth because of ventricular-septal defects (VSDs) ^[52].

In contrast to the extreme sensitivity of murine heart to perturbation of miR-1, mice that lack of either miR-133a-1 or miR-133a-2 do not display any evident developmental phenotype ^[60]. Anyway, deletion of both miR-133a genes causes lethal VSDs in half of double-mutant embryos or neonates. MiR-133a double mutants that survive to adulthood succumb for cardiac dysfunction by 5-6 months of age or sudden cardiac death ^[60]. In fact, miR-133a-double-mutant hearts are characterized by increased cardiomyocyte proliferation and apoptosis, sarcomere alteration and cardiac fibrosis ^[60].

The importance of these two miRNAs during heart development is also reflected in postnatal cardiac pathophysiology. In fact, one of the major response of the heart to both biomechanical stresses and pathological stimuli is to undergo cardiac remodelling defined as cardiac hypertrophy ^[49, 61]. From a phenotypic point of view, cardiac hypertrophy is characterized by an increase in cardiomyocyte size or myofibrillar volume in order to sustain cardiac output in response to stress stimuli. This remodelling is accompanied by a re-activation of

fetal genes, suggesting that molecular events that control cardiac gene expression in heart development are also implicated in regulating postnatal remodelling ^[62].

In this contest, different studies unravelled the critical role of miR-1 and miR-133, which were found to inversely correlate with the onset of cardiac hypertrophy ^[57]. In an *in vitro* model of cardiac hypertrophy, using primary cardiomyocytes, the overexpression of miR-1 or miR-133 was able to block cellular hypertrophic growth ^[49, 57, 63, 64]. Conversely, prolonged *in vivo* inhibition of miR-133 in heart led to a marked hypertrophic response ^[57].

5. MiRNAs as novel therapeutic targets and their potential application in the pharmaceutical industries

The profound role of miRNAs into the cardiovascular system and, as above described, often in the onset of cardiac dysfunctions, led the scientific community to question whether they could be good targets for therapeutic applications. Indeed, although most efforts in this field have been done in cancer therapy, the application of miRNA-based approaches in the cardiovascular area is a rapidly expanding area towards pre-clinical and clinical phases ^[65]. To date, two are the main strategies to manipulate miRNAs. Indeed, based on whether the targeted miRNA expression has to be downregulated or to re-introduced, the current strategies can be classified into: 1) the “antisense inhibition of mature miRNA”, or 2) the “replacement of miRNA functions through mimicry-based approaches” ^[66].

Currently, miRNA therapeutic inhibition can be achieved by three approaches: 1) expression vectors (miRNA sponges); 2) small-

molecule inhibitors, and 3) antisense oligonucleotides (ASOs) ^[66]. The first technology is based on the use of a reporter vector that contains multiple miRNA-binding sites. Once delivered into cells, the binding sites would serve as decoy for the targeted miRNA, thereby reversing the suppression of endogenous target genes ^[67]. The second approach relied on low molecular-weight compounds, capable to interfere with different steps of miRNA pathways. In fact, these small molecules can hinder the transcription of pri-miRNAs, inhibit miRNA processing by interfering with Dicer activity, or even impair their loading into AGO2 to form an active RNA-induced silencing complex (RISC) ^[68]. The third technology is so far the most studied and used. It is based on chemically modified miRNA-targeting antisense oligonucleotides (anti-miRNAs) designed to target and bind specific miRNAs with high affinity. Nowadays, various chemical modifications (*i.e.* 2'-OME; cholesterol and Locked Nucleic Acid) are available in order to ameliorate the cellular uptake and the specificity of these anti-miRNAs ^[57, 69-71].

No less than the antisense approaches, also the therapeutic up-regulation of miRNAs has become a goal for pharmaceutical industries. However, despite the significant efforts made far, the current approaches to optimize miRNA overexpressing tools have been rather inadequate ^[72]. The strategy for replacing a miRNA is based on synthetic RNA-duplex known as “mimic”. However, since they must act as a miRNA and recognized by the RISC complex, the chemical modifications have been limited ^[73]. Thus, further studies in developing chemical stabilization and/or delivery modifications are required to improve the biological.

In addition to the ongoing research towards the improvement of chemical modification used for the down- or up-modulation of the altered miRNAs, a further difficulty is the successful and safe delivery of the therapeutic compound to target tissues. In this contest, the world of nanomaterials seems to represent the capstone for overcoming this obstacle. In fact, nanostructured biomaterials with their physiochemical properties such as small size, biocompatibility and biodegradable chemical composition, reactivity and functional structure, might successfully square up the drug delivery limitations of traditional approaches ^[74]. Moreover, the possibility to incorporate therapeutic molecules within nanocarriers and the non-immunogenicity of some biomaterials can facilitate the therapeutic preservation against potential immunogenicity reactions and enzymatic degradation, respectively ^[75]. Furthermore, functionalization of nanocarriers with cell-specific targeting moieties (*i.e.* aptamers or peptides) can improve the specific targeting of final tissues preventing the onset of side effects, due to uncontrolled biodistribution of the drug in other organs.

References

1. Chalfie, M., H.R. Horvitz, and J.E. Sulston, *Mutations that lead to reiterations in the cell lineages of C. elegans*. Cell, 1981. **24**(1): p. 59-69.
2. Lee, R.C., R.L. Feinbaum, and V. Ambros, *The C. elegans heterochronic gene lin-4 encodes small RNAs with antisense complementarity to lin-14*. Cell, 1993. **75**(5): p. 843-854.
3. Wightman, B., I. Ha, and G. Ruvkun, *Posttranscriptional regulation of the heterochronic gene lin-14 by lin-4 mediates temporal pattern formation in C. elegans*. Cell, 1993. **75**(5): p. 855-862.
4. Reinhart, B.J., et al., *The 21-nucleotide let-7 RNA regulates developmental timing in Caenorhabditis elegans*. nature, 2000. **403**(6772): p. 901-906.
5. Huang, Y., et al., *Biological functions of microRNAs: a review*. Journal of physiology and biochemistry, 2011. **67**(1): p. 129-139.
6. Latronico, M.V., D. Catalucci, and G. Condorelli, *Emerging role of microRNAs in cardiovascular biology*. Circulation Research, 2007. **101**(12): p. 1225-1236.
7. Lagos-Quintana, M., et al., *Identification of novel genes coding for small expressed RNAs*. Science, 2001. **294**(5543): p. 853-858.
8. Lau, N.C., et al., *An abundant class of tiny RNAs with probable regulatory roles in Caenorhabditis elegans*. Science, 2001. **294**(5543): p. 858-862.

9. Rodriguez, A., et al., *Identification of mammalian microRNA host genes and transcription units*. Genome research, 2004. **14**(10a): p. 1902-1910.
10. Al-Khanbashi, M. and M. Al-Moundhri, *Micro-ribonucleic acid and carcinogenesis: breast cancer as an example*. Oncology reviews, 2015. **9**(1).
11. Lee, Y., et al., *The nuclear RNase III Drosha initiates microRNA processing*. Nature, 2003. **425**(6956): p. 415-419.
12. Han, J., et al., *The Drosha-DGCR8 complex in primary microRNA processing*. Genes & development, 2004. **18**(24): p. 3016-3027.
13. Landthaler, M., A. Yalcin, and T. Tuschl, *The human DiGeorge syndrome critical region gene 8 and its D. melanogaster homolog are required for miRNA biogenesis*. Current biology, 2004. **14**(23): p. 2162-2167.
14. Kim, V.N., *MicroRNA precursors in motion: exportin-5 mediates their nuclear export*. Trends in cell biology, 2004. **14**(4): p. 156-159.
15. Bartel, D.P., *MicroRNAs: target recognition and regulatory functions*. cell, 2009. **136**(2): p. 215-233.
16. Peters, L. and G. Meister, *Argonaute proteins: mediators of RNA silencing*. Molecular cell, 2007. **26**(5): p. 611-623.
17. Liu, N. and Y. Tu, *Systematic review of microRNAs and its therapeutic potential in glioma*. Cancer Translational Medicine, 2015. **1**(2): p. 50.

18. Filipowicz, W., et al., *Post-transcriptional gene silencing by siRNAs and miRNAs*. Current opinion in structural biology, 2005. **15**(3): p. 331-341.
19. Liu, J., et al., *MicroRNA-dependent localization of targeted mRNAs to mammalian P-bodies*. Nature cell biology, 2005. **7**(7): p. 719-723.
20. Liu, J., et al., *A role for the P-body component GW182 in microRNA function*. Nature cell biology, 2005. **7**(12): p. 1261-1266.
21. Roberts, T.C., *The microRNA biology of the mammalian nucleus*. Molecular Therapy—Nucleic Acids, 2014. **3**(8): p. e188.
22. Lewis, B.P., et al., *Prediction of mammalian microRNA targets*. Cell, 2003. **115**(7): p. 787-798.
23. Liu, J., et al., *Argonaute2 is the catalytic engine of mammalian RNAi*. Science, 2004. **305**(5689): p. 1437-1441.
24. Paranjape, T., F. Slack, and J. Weidhaas, *MicroRNAs: tools for cancer diagnostics*. Gut, 2009. **58**(11): p. 1546-1554.
25. Meister, G., et al., *Human Argonaute2 mediates RNA cleavage targeted by miRNAs and siRNAs*. Molecular cell, 2004. **15**(2): p. 185-197.
26. Politz, J.C.R., F. Zhang, and T. Pederson, *MicroRNA-206 colocalizes with ribosome-rich regions in both the nucleolus and cytoplasm of rat myogenic cells*. Proceedings of the National Academy of Sciences, 2006. **103**(50): p. 18957-18962.

27. Hwang, H.-W., E.A. Wentzel, and J.T. Mendell, *A hexanucleotide element directs microRNA nuclear import*. Science, 2007. **315**(5808): p. 97-100.
28. Liao, J.-Y., et al., *Deep sequencing of human nuclear and cytoplasmic small RNAs reveals an unexpectedly complex subcellular distribution of miRNAs and tRNA 3' trailers*. PLoS one, 2010. **5**(5): p. e10563.
29. Robb, G.B., et al., *Specific and potent RNAi in the nucleus of human cells*. Nature structural & molecular biology, 2005. **12**(2): p. 133-137.
30. Liang, H., et al., *Nuclear microRNAs and their unconventional role in regulating non-coding RNAs*. Protein & cell, 2013. **4**(5): p. 325-330.
31. Castanotto, D., et al., *CRMI mediates nuclear-cytoplasmic shuttling of mature microRNAs*. Proceedings of the National Academy of Sciences, 2009. **106**(51): p. 21655-21659.
32. Zisoulis, D.G., et al., *Autoregulation of microRNA biogenesis by let-7 and Argonaute*. Nature, 2012. **486**(7404): p. 541-544.
33. Weinmann, L., et al., *Importin 8 is a gene silencing factor that targets argonaute proteins to distinct mRNAs*. Cell, 2009. **136**(3): p. 496-507.
34. Wei, Y., et al., *Importin 8 regulates the transport of mature microRNAs into the cell nucleus*. Journal of Biological Chemistry, 2014. **289**(15): p. 10270-10275.
35. Place, R.F., et al., *MicroRNA-373 induces expression of genes with complementary promoter sequences*. Proceedings of the National Academy of Sciences, 2008. **105**(5): p. 1608-1613.

36. Majid, S., et al., *MicroRNA-205-directed transcriptional activation of tumor suppressor genes in prostate cancer*. Cancer, 2010. **116**(24): p. 5637-5649.
37. Leucci, E., et al., *microRNA-9 targets the long non-coding RNA MALAT1 for degradation in the nucleus*. Scientific reports, 2013. **3**: p. 2535.
38. Chi, S.W., et al., *Argonaute HITS-CLIP decodes microRNA-mRNA interaction maps*. Nature, 2009. **460**(7254): p. 479-486.
39. Tang, R., et al., *Mouse miRNA-709 directly regulates miRNA-15a/16-1 biogenesis at the posttranscriptional level in the nucleus: evidence for a microRNA hierarchy system*. Cell research, 2012. **22**(3): p. 504-515.
40. Kim, D.H., et al., *MicroRNA-directed transcriptional gene silencing in mammalian cells*. Proceedings of the National Academy of Sciences, 2008. **105**(42): p. 16230-16235.
41. Chu, Y., et al., *Involvement of argonaute proteins in gene silencing and activation by RNAs complementary to a non-coding transcript at the progesterone receptor promoter*. Nucleic acids research, 2010. **38**(21): p. 7736-7748.
42. Li, L.-C., et al., *Small dsRNAs induce transcriptional activation in human cells*. Proceedings of the National Academy of Sciences, 2006. **103**(46): p. 17337-17342.
43. Li, Y. and K.V. Kowdley, *MicroRNAs in common human diseases*. Genomics, proteomics & bioinformatics, 2012. **10**(5): p. 246-253.
44. Ng, R., et al., *A microRNA-21 surge facilitates rapid cyclin D1 translation and cell cycle progression in mouse liver*

- regeneration*. The Journal of clinical investigation, 2012. **122**(3): p. 1097-1108.
45. Rayner, K.J., et al., *Inhibition of miR-33a/b in non-human primates raises plasma HDL and lowers VLDL triglycerides*. Nature, 2011. **478**(7369): p. 404-407.
46. Zhang, P., et al., *MiR-155 is a liposarcoma oncogene that targets casein kinase-1 α and enhances β -catenin signaling*. Cancer research, 2012. **72**(7): p. 1751-1762.
47. Taganov, K.D., et al., *NF- κ B-dependent induction of microRNA miR-146, an inhibitor targeted to signaling proteins of innate immune responses*. Proceedings of the National Academy of Sciences, 2006. **103**(33): p. 12481-12486.
48. Png, K.J., et al., *A microRNA regulon that mediates endothelial recruitment and metastasis by cancer cells*. Nature, 2012. **481**(7380): p. 190-194.
49. Callis, T.E. and D.-Z. Wang, *Taking microRNAs to heart*. Trends in molecular medicine, 2008. **14**(6): p. 254-260.
50. Rosamond, W., et al., *Heart disease and stroke statistics—2008 update*. Circulation, 2008. **117**(4): p. e25-e146.
51. Porrello, E.R., *microRNAs in cardiac development and regeneration*. Clinical science, 2013. **125**(4): p. 151-166.
52. Zhao, Y., et al., *Dysregulation of cardiogenesis, cardiac conduction, and cell cycle in mice lacking miRNA-1-2*. Cell, 2007. **129**(2): p. 303-317.
53. Zhao, Y., E. Samal, and D. Srivastava, *Serum response factor regulates a muscle-specific microRNA that targets Hand2 during cardiogenesis*. Nature, 2005. **436**(7048): p. 214-220.

54. Wang, D.-Z., et al., *Activation of cardiac gene expression by myocardin, a transcriptional cofactor for serum response factor*. Cell, 2001. **105**(7): p. 851-862.
55. Chen, J.-F., et al., *The role of microRNA-1 and microRNA-133 in skeletal muscle proliferation and differentiation*. Nature genetics, 2006. **38**(2): p. 228-233.
56. van Rooij, E., N. Liu, and E.N. Olson, *MicroRNAs flex their muscles*. Trends in Genetics, 2008. **24**(4): p. 159-166.
57. Care, A., et al., *MicroRNA-133 controls cardiac hypertrophy*. Nature medicine, 2007. **13**(5): p. 613-618.
58. Ivey, K.N., et al., *MicroRNA regulation of cell lineages in mouse and human embryonic stem cells*. Cell stem cell, 2008. **2**(3): p. 219-229.
59. Serradifalco, C., G. Zummo, and V. Felice, *MicroRNA and Cardiac Stem Cell Therapy*. J Clin Exp Cardiol S, 2012. **11**: p. 2.
60. Liu, N., et al., *microRNA-133a regulates cardiomyocyte proliferation and suppresses smooth muscle gene expression in the heart*. Genes & development, 2008. **22**(23): p. 3242-3254.
61. Hunter, J.J. and K.R. Chien, *Signaling pathways for cardiac hypertrophy and failure*. New England Journal of Medicine, 1999. **341**(17): p. 1276-1283.
62. Heineke, J. and J.D. Molkentin, *Regulation of cardiac hypertrophy by intracellular signalling pathways*. Nature reviews Molecular cell biology, 2006. **7**(8): p. 589-600.

63. Sayed, D., et al., *MicroRNAs play an essential role in the development of cardiac hypertrophy*. *Circulation research*, 2007. **100**(3): p. 416-424.
64. Castaldi, A., et al., *MicroRNA-133 modulates the β 1-adrenergic receptor transduction cascade*. *Circulation research*, 2014. **115**(2): p. 273-283.
65. Esteller, M., *Non-coding RNAs in human disease*. *Nat Rev Genet*, 2011. **12**(12): p. 861-74.
66. Christopher, A.F., et al., *MicroRNA therapeutics: Discovering novel targets and developing specific therapy*. *Perspectives in clinical research*, 2016. **7**(2): p. 68.
67. Ebert, M.S., J.R. Neilson, and P.A. Sharp, *MicroRNA sponges: competitive inhibitors of small RNAs in mammalian cells*. *Nature methods*, 2007. **4**(9): p. 721-726.
68. Gumireddy, K., et al., *Small-Molecule Inhibitors of MicroRNA miR-21 Function*. *Angewandte Chemie International Edition*, 2008. **47**(39): p. 7482-7484.
69. Bonauer, A., et al., *MicroRNA-92a controls angiogenesis and functional recovery of ischemic tissues in mice*. *Science*, 2009. **324**(5935): p. 1710-1713.
70. Van Rooij, E., et al., *Dysregulation of microRNAs after myocardial infarction reveals a role of miR-29 in cardiac fibrosis*. *Proceedings of the National Academy of Sciences*, 2008. **105**(35): p. 13027-13032.
71. Elmén, J., et al., *LNA-mediated microRNA silencing in non-human primates*. *Nature*, 2008. **452**(7189): p. 896-899.

72. Thum, T., *MicroRNA therapeutics in cardiovascular medicine*. EMBO molecular medicine, 2012. **4**(1): p. 3-14.
73. van Rooij, E., A.L. Purcell, and A.A. Levin, *Developing microRNA therapeutics*. Circulation research, 2012. **110**(3): p. 496-507.
74. Singh, S., et al., *Nanoparticle based drug delivery system: advantages and applications*. Indian Journal of Science and Technology, 2011. **4**(3): p. 177-180.
75. Di Mauro, V., et al., *Bioinspired negatively charged calcium phosphate nanocarriers for cardiac delivery of MicroRNAs*. Nanomedicine, 2016. **11**(8): p. 891-906.

Chapter 2

Scope of the thesis

So far, a plethora of studies demonstrated the importance of miRNAs, in embryo development and in the onset of basically all kinds of pathologies. In the cardiac system, the role of miR-133a was extensively characterized from embryogenesis to the development of cardiac defects. Nevertheless, much remains to be learned about the functions of miR-133a. The main scope of my PhD thesis was to investigate these additional functions of miR-133a firstly in cardiac development, focusing on its potential ability to control signal pathways at the transcriptional level, and secondly in the already well characterized cardiac pathologies.

Moreover, the ultimate goal of my research was to translate the additional roles of miR-133a into its therapeutic use by developing a new strategy that, based on the use of nanomaterials, allows for the specific and controlled delivery of miR-133a into the cardiac system.

Chapter 3

The Wnt canonical pathway controls DNMT3B transcription via nuclear-relocalization of miR-133a in cardiac cells.

**Vittoria Di Mauro^{1,2,3}, Silvia Crasto³, Federico Colombo³, Elisa Di Pasquale^{2,3}
and Daniele Catalucci^{2,3}**

1) University of Milan Bicocca, Piazza dell'Ateneo Nuovo, 1 - 20126, Milan

2) CNR-IRGB UOS Milan, Via Fantoli 1 5/16 -20131 Milan,

3)Flow cytometry core, Humanitas Clinical and Research Center, via Alessandro Manzoni
113-20089 Rozzano, Milan

Abstract

Cardiac diseases represent the leading cause of death worldwide, mainly due to the poor capacity of the heart to self-repair after injury. Thus, molecular pathways, associated with repair and regeneration of damaged cardiac cells, are of great interest from a therapeutic point of view. One of the pivotal transduction cascades regulating the development of the heart is the Wnt β -catenin signaling pathway. This pathway is mainly silent in the healthy heart but it is re-expressed under pathological conditions, whereby the majority of works aimed at defining the molecular effects of its re-activation during cardiogenesis, rather than its inhibition, which on the contrary still remains a poor explored territory.

MicroRNAs (miRNAs), which are additional regulators of developmental processes, included those occurring during

cardiogenesis, have been recently shown to be down-stream effectors of the Wnt canonical pathway. Although, miRNAs mainly inhibit gene expression at post-transcriptional level in the cytosol, latest evidences showed that they could relocalize into the nuclear compartment after maturation and recognize complementary genomic sites in gene promoters, thus directly regulating gene expression.

Here, we showed for the first time that inactivation of the Wnt canonical pathway is responsible for the inhibition of DNA Methyltransferase 3B (DNMT3B) via nuclear re-localization of mature miR-133a. DNMT3B is an important gene involved in cardiac development and strongly repressed upon inactivation of canonical Wnt signaling. In this setting, miR-133a shuttles to the nucleus in complex with AGO2 via an importin 8 (IPO8)-mediated process. In the nucleus, the miR-133a-AGO2 complex represses the expression of DNMT3B by binding an evolutionary conserved miR-133a putative site in the promoter. Conversely, the impairment of miR-133a-promoter binding by application of a miR-133a selective target protector significantly restores DNMT3B gene expression.

Furthermore, the transcriptional repression of DNMT3B relies on a feedback loop mediated by AGO2-miR-133a complex, that works as interface between DNMT3B enzyme and its own promoter. This results in a hypermethylation of promoter sequence and in the consequent silencing of the gene.

Finally, we found that AGO2-miR-133a/ Wnt canonical pathway axis is an important checkpoint for *in vitro* recapitulation cardiogenesis. Indeed, hESCs-derived cardiomyocytes with alteration in the interplay between nuclear action of AGO2-miR133a and Wnt canonical

signaling, displayed defects in maturation, reflected by a reduced expression genes involved in contractility and calcium handling. Taken together indicate that AGO2-miR-133a/ Wnt canonical pathway axis play a key role in cardiogenesis and it is mandatory for the proper differentiation and maturation of derived-cardiomyocytes.

Introduction

The Wnt β -catenin signalling pathway is an evolutionary conserved transduction cascade, which plays pivotal roles in animal development [76-79]. The central mediator of canonical Wnt pathway is β -catenin [80]. In absence of Wnt ligands (off-state) the β -catenin is marked for proteolytic degradation by the (APC) destruction complex [81, 82]. Thus, activation of Wnt responsive genes, involved in cell-fate, proliferation and survival, is prevented [83]. On the other hand, when Wnt ligands bind to Frizzled (Fz) receptors initiates the transduction cascade (on-state), which trigger the stabilization of cytosolic β -catenin, that translocates into the nucleus, interacts with T-cell Factor/lymphoid enhancer factor (TCF/LEF) transcription factors to induces the expression of Wnt-related genes [79, 84, 85].

In heart, this pathway is involved in the tight control of the proliferative and differentiative states occurring during cardiac development. In turn, the spatio-temporal regulation of Wnt canonical pathway itself is mandatory for proper differentiation of cardiac cells [86]. In fact, experiments conducted on an *in vitro* model of cardiogenesis, based on embryonic stem cells (ESCs), showed that initial enhancement followed by inhibition of Wnt canonical signalling results into an increase of terminally differentiated and

spontaneous contracting myocytes^[86, 87]. So far the major effort in characterizing the Wnt β -catenin signalling cascade have been done in the field of its positive regulation, given that it is re-activated in adult heart in response to injury^[88, 89]. On the contrary very few it is known about the negative modulation of Wnt pathway and its role in regulating heart formation and differentiation^[90]. Recently, microRNAs (miRNAs) a class of 20–25 nucleotides small noncoding RNAs, have been identified as major contributors in regulating Wnt β -catenin transduction cascade, by targeting multiple components of the signaling pathway. Indeed, miRNAs by incorporation into the RNA-induced silencing complex (RISC)^[11, 21, 91, 92] negatively regulates target messenger RNAs (mRNAs) either by translational repression or by mRNA degradation^[18]. However, despite the canonical post-transcriptional gene regulation in the cytosol is the prevailing view, recent studies have detected mature miRNAs in nuclear compartment^[25, 27, 93, 94], in which in association with proteins of miRNAs biogenesis (Argonautes) directly modulate transcription of target genes^[40, 95-97]. These evidences suggest a new level of interaction between signaling pathway and miRNAs in regulating the expression of responsive genes.

Here, we showed for the first time that inhibition of the Wnt- β -catenin canonical pathway induces a re-localization of mature miR-133a-3p in nuclei of HL-1 cardiac cells and directly targets the promoter of *de novo* DNA methyltransferase (DNMT3B) to repress its transcription. Moreover, using an in vitro model of cardiogenesis, we showed that transcriptional control of DNMT3B by nuclear miR-133a-3p after inactivation of Wnt canonical pathway is mandatory for

proper differentiation of human Embryonic Stem Cells (hESCs) into cardiomyocytes.

Methods

Cell line and culture

HL-1 cells were grown in Claycomb medium (Sigma-Aldrich) supplemented with 10% Fetal Bovine Serum (FBS) (Sigma-Aldrich), 1% penicillin-streptomycin (Pen-Strep 10000 U/ml, Lonza), 1% ultraglutamine (200 mM, Lonza), and 1 mM norepinephrine (Sigma-Aldrich) in gelatin/fibronectin precoated flasks. After reaching full confluence, cells were split according to Dr Claycomb's instructions. For the modulation of Wnt canonical pathway, HL-1 cells were stimulated with either 5 μ M IWR-1 (Sigma-Aldrich) or 5 μ M CHIR99021 (Selleck Chemicals) for 24-48 hours, before being collected.

Cardiac differentiation of Human Embryonic Stem Cells (hESCs)

Human Embryonic Stem Cell (hESCs) colonies were dissociated with 0.5 mM EDTA (Gibco Life Technologies) into single-cell suspension and resuspended in Essential 8 Medium (Life Technologies) on vitronectin-coated dishes at 37 °C with 5% CO₂. For cardiac differentiation, hESCs were cultured into hESC-CMs using a chemical defined monolayer differentiation protocol. hESCs were next cultured to 100% cell confluence into Matrigel Growth Factor Reduced (GFR) - coated plates and then treated for 24 hours with 12 μ M CHIR99021 (Selleck Chemicals) in RPMI+B27 supplement without insulin to activate the Wnt signaling pathway. On day 1, cells were placed on

RPMI+B27 without insulin. On days 3-4, cells were treated with 5 μ M IWR-1 (Sigma-Aldrich). On days 5 and 7, cells were replaced with RPMI+B27 without insulin. From day 10, cells were replaced with RPMI+B27 with insulin and cultured for 10 days from beating day. FACS-Sorting experiments were performed at days 3-10 during differentiation.

Extraction of Nuclear and Cytosolic fractions

The nuclear fraction of HL-1 cells was extracted using the PARISTM kit (Ambion). Cells were washed three times with phosphate-buffered saline (PBS) on ice, followed by centrifugation at 300 X g for 5 min. Cell pellets were resuspended in cell fraction buffer from the PARISTM kit, incubated on ice for 10 min, and then centrifuged at 500 X g for 5 min at 4°C. Nuclear pellets were homogenized with the cell disruption buffer from the PARISTM kit.

siRNA and Target site blocker transfection

A pool of two different siRNA-AGO2, siRNA-AGO1, a specific siRNA-IPO8, and siRNA-Scramble (Sigma-Aldrich) were transfected in HL-1 cells using the Lipofectamine 2000 (Life Technologies) according to the manufacturer's instructions. After 6 hours from transfection, culture medium was changed and HL-1 cells were treated with 5 μ M IWR-1 (Sigma Aldrich) as above-mentioned. 48 hours after treatment, gene expression was evaluated in total RNA.

Specific "Target site blocker" (TSB) designed for the putative binding site of miR-133a-3p in DNMT3B murine and human promoter was obtained by Exiqon. A dose curve of TSB or scramble control was

transfected in HL-1 cells using the Lipofectamine 2000 (Life Technologies), according to the manufacturer's instructions. After 6 hours from transfection, the medium was changed and the stimulation with IWR-1 was done as previously reported. For the hESC transfection, TSB or scramble were conjugated with fluorescein (FITC), and transfected at day 2 of cardiac differentiation using the ViaFect Reagent (PromegaTM), according to the manufacturer's protocol.

RNA isolation and quantification

Total RNA or RNA from subcellular fractions was extracted using the PureZol Reagent (Bio-Rad). Reverse transcription of RNA for miR-133a-3p, miR-19b-5p, miR-1-1 and U6 was performed using the miRCURY LNATM Universal RT microRNA PCR Polyadenylation and cDNA synthesis kit (Exiqon). Real time quantitative polymerase chain reaction (qRT-PCR) was performed with microRNA LNATM PCR primers (Exiqon) using the GoTaq Probe qPCR Master Mix (Promega). Relative expression was calculated using the $\Delta\Delta(Ct)$ method. The miRNA expression in the cells or nuclei was normalized to U6 snRNA, while gene mRNA expression in cells was normalized to GAPDH.

DNA constructs

For the BRET assay, Ago2 and Ago1 cDNAs were cloned into the pNLF1-N vector, while Dnmt3b and IPO8 cDNA were cloned into the HaloTag-pFN21A vector. All vectors for NanoLuciferase and BRET assays were obtained from Promega. To generate the *DNMT3B*

luciferase promoter plasmid, the region corresponding to -1 to -2500 from chromosome 2 was cloned into the pGL3-Enhancer vector (Promega). The mutated vector for the mir-133a-3p putative binding site was synthesized by GenScript (USA). All cloning steps were performed using the In-fusion HD Cloning Plus kit (Clontech).

Western analyses

Protein expression was evaluated in total or sub-fraction lysates by Western analyses according to standard procedures. Samples obtained from treated or not treated cells were homogenized in RIPA buffer (150mM NaCl, 10mM Tris-HCl pH 7.2, 0.1% SDS, 1% Triton-X100, 5mM EDTA, 100 μ M Na₃VO₄, 10mM NaF, and 1X Protease inhibitor (Thermo Fisher Scientific)), loaded onto a 8- or 12% Tris-Glycine Gel, separated by electrophoresis, and transferred to a nitrocellulose membrane (Bio -Rad). Antibodies against the following proteins were used: Ago2 (clone 11A9) and Ago1 (clone 4B1) were both provided by Helmholtz Zentrum Munchen; H3, H3 (trimethyl K27), H3 (trimethyl K24) from Abcam; DNMT3B (52A1018) from Active Motif; GAPDH (14C10) from Cell Signaling Technology. Image J software (National Institutes of Health) was used for densitometry analysis. Antibody concentrations used are the 2 μ g for AGO2 and AGO1; 1 μ g for DNMT3B; 0.1 μ g for GAPDH and H3; H3K27me3; H3K4me3

Nano-BRET Assay

The NanoBRET assay was performed as described by the manufacturer (Promega). Briefly, for protein-protein interaction

assays, HL-1 transfected cells were treated with 100nM NanoBRET 618 Ligand (Promega) and signals were detected 6 hours after treatment. Signals were detected using a Synergy H4 instrument (BioTek), and results were analyzed using Prism 6.0 software (GraphPad Software, CA).

Promoter Assay

Consensus sequences for the miR-133a-3p were computationally identified within the *DNMT3B* promoter (-2500). HL-1 cells were co-transfected with pGL3 Enhancer DNMT3B promoter WT or MUT and Renilla Vector (Promega) and stimulated with a dose curve of IWR-1 (0 to 50 μ M), and the firefly luciferase signal was detected 48 hours later with a Synergy H4 instrument (BioTek) as described by the manufacturer (Promega) and normalized to Renilla Luciferase. Results were analyzed using Prism 6.0 software (GraphPad Software, CA).

Chromatin Immunoprecipitation (CHIP) assay

For the Chromatin Immunoprecipitation experiments, HL-1 cells were seeded at density of 1×10^6 on gelatin/fibronectin plates and treated with IWR-1 for 48 hours as previously reported. The day of harvest, cells were cross-linked with 1% of formaldehyde for 10 min. Cross-linking reaction was stopped with 0.125 M Glycine for 5 min. Then, cells were washed with cold PBS and collected into IP Buffer (2 volumes of SDS Buffer - 100mM NaCl, 50mM Tris-HCl pH 8.1, 5mM EDTA pH 8.0, 0.5% SDS -, and 1 volume of Triton Dilution Buffer - 100mM NaCl, 100mM Tris-HCl pH 8.1, 5mM EDTA, 5%

Triton X-100 -). Samples were sonicated using the Bioruptor[®] Plus sonication device. Sonicated samples were then checked on 0.8% agarose gel. Samples were then clarified by centrifugation. Input was saved as 20% of clarified lysates, before adding 20 μ l of Dynabeads[®] Protein G (Thermo Fisher Scientific) and specific antibodies (AGO2; DNMT3B; H3K4me3; H3K27me3) at 4°C overnight. The day after, samples were washed several times with different buffers (Mixed Micelle Buffer: 20mM Tris-HCl pH 8.0, 150mM NaCl, 5mM EDTA pH 8.0, 1% Triton X-100, 0.2% SDS; Buffer 500: 50mM HEPES, 0.1% Deoxycholic Acid, 1% Triton X-100, 500mM NaCl, 1mM EDTA pH 8.0; LiCl detergent buffer: 10mM Tris-HCl pH 8.0; 0.5% Deoxycholic Acid, 0.5% NP40, 250mM LiCl). De-cross-linking was performed after adding 200mM NaCl at 65°C overnight. The following day, samples were incubated with 20ug/ml of Proteinase K at 45°C for 2 hours. DNA was then extracted using the UltraPure[™] Phenol:Chloroform:Isoamyl Alcohol (25:24:1, v/v) (Thermo Fisher Scientific) according to the manufacturer's instructions. qRT-PCR was then used to check final results.

Evaluation of methylation enrichment

The methylation enrichment (%) of GpC islands was determined using the MethylCollector[™]Ultra Kit (ActiveMotif), according to the manufacturer's instruction. The resulting methylated DNA was analyzed through qRT-PCR using specific primers to amplify the locus of miR-133a-3p putative binding site.

AGOs nuclear PULL-DOWN

HL-1 cells were seeded at density of 1×10^6 on gelatin/fibronectin plates and treated with IWR-1 for 48 hours as previously reported. Cells were collected and processed for nuclear extracts using the Nuclear Complex Co-IP Kit, according to the manufacturer's protocol. The nuclear protein lysate was then incubated with antibodies against AGO2; AGO1 or IgG, and 20 μ l of Dynabeads® Protein G (Thermo Fisher Scientific) at 4°C overnight on rotation. For protein analysis, samples were subjected to Western blot assays, while for miRNAs analysis, the RNA derived from AGO2; AGO1 or IgG pull-down assay was isolated and then analyzed through qRT-PCR.

Fluorescent In situ hybridization (FISH) and Duo-Link Assay

HL-1 cells were seeded at 5.0×10^4 cells/well on VWR Micro cover slips coated with gelatin/fibronectin in complete Claycomb medium, and then incubated overnight at 37°C with 5% CO₂. The following day, HL-1 cells were treated with 5 μ M IWR-1 for 24-48h. Then, cultured cells were fixed using 4% paraformaldehyde at room temperature, followed by treatment in PBS containing 0.2% Triton X-100 for 5 min. For miR-133a-3p or scramble staining, miRCURY LNA™ Detection probe was used. TSA amplification system (Life technologies) was used to detect miRNAs or scramble signal. After three washes with PBS, nuclei were counterstained with 4', 6-diamidino-2-phenylindole, dihydrochloride (Life Technology) for 5 min at room temperature. Fluorescent images were taken with a laser scanning confocal microscope (Olympus, FV1000/SIMS). For AGO2-DNMT3B interaction the Duo-Link assay (Sigma Aldrich) was

used following manufacturer's instructions.

FACS Sorting

FITC positive and negative hESC-derived cardiomyocytes were sorted using a FACSAria III instrument (Becton Dickinson, Franklin Lakes, CA, USA). Photomultiplier voltages and laser time delay were checked on a daily basis to assure the maximum reproducibility of the results.

Cell sorting was performed at room temperature using a 100 μm nozzle, 20 psi pressure, 3500 plate voltage and low speed to reduce cell stress to the minimum. Doublet discrimination was performed plotting events in a FSC-A vs. FSC-H dot plot.

Statistical Analysis

Data are presented as mean \pm SD. The normality of data was assessed with the Kolmogorov-Smirnov test. Statistical comparison was performed in at least 3 independent experiments with the Mann-Whitney test, and comparisons between groups were analyzed by ANOVA repeated-measures in combination with the Tukey multicomparison. Prism 6.0 software (GraphPad Software) was used to verify the normality of the data and for statistical calculation. A value of $P < 0.05$ was considered significant.

Results

Inhibition of canonical Wnt β -catenin signalling pathway induces nuclear re-localization of miR-133a-3p.

To investigate the hypothesis that Wnt β -catenin signalling pathway is responsible for a subcellular redistribution of miRNAs, we used a recently published inhibitor of the canonical Wnt β -catenin signalling response (IWR-1)^[98, 99]. After 24- and 48h treatment with IWR-1, the cardiac cell line HL-1 was collected and both cytosolic and nuclear fraction were isolated (Fig 1 A) and checked for purity with nuclear (U6 snRNA and histones) and cytoplasmic markers (GAPDH), by western blot and real-time reverse transcription PCR (qRT-PCR) analysis (Fig 1 B and C). The relative amount of miRNAs in both total cell extracts and sub-cellular fractions was measured by qRT-PCR. We found that inhibition of Wnt β -catenin signalling pathway, though treatment with IWR-1, induced an increase in the total level of both miR-133a-3p and miR-1 (Fig 1 D), but interestingly only miR-133a-3p showed enrichment in the nuclear compartment of HL-1 cells (Fig 1 E). Fluorescent in situ hybridization (FISH) experiments using an antisense LNA probe for mature miR-133a-3p, confirmed its nuclear enrichment after IWR-1 treatment (Fig. 1 F). To confirm the specificity of the signal we performed additional FISH experiment using a scramble-LNA probe and no signals were observed in HL-1 treated as above described (data not shown).

In contrast treatment of HL-1 cells with CHIR99021^[100], that mimics Wnt β -catenin on-state, did not induce an increase in relative abundance of mature miR-133a-3p and miR-1 in HL-1 cells, and furthermore no alteration in the sub-cellular compartment was also

observed (SI 1). Altogether these data demonstrate that inhibition of Wnt β -catenin cascade promotes a nuclear re-localization of miR-133a-3p in HL-1 cells.

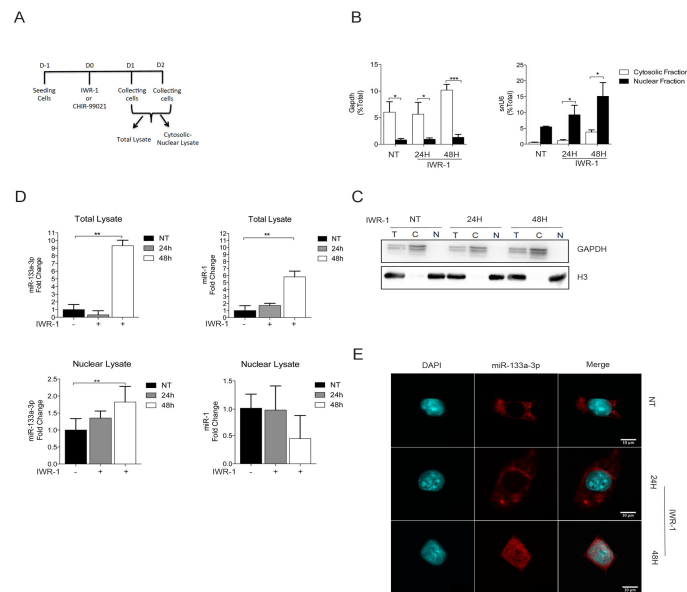


Figure 1. Sub-cellular distribution of mature miRNAs after chemical inhibition of Wnt β -catenin signalling pathway in HL-1 cells. A) Schematic representation of cellular treatment and sub cellular fractionation. B) and C) Control of fractionation purity through qRT-PCR (snRNAU6 and GAPDH) and Western Blot analysis (GAPDH and H3). D) qRT-PCR for mRNA level of miR-133a-3p and miR-1 in total cell lysate and in purified nuclear fraction. E) *FISH* experiment on HL-1 cells for detecting miR-133a-3p (RED) and co-stained with DAPI (BLUE) for nuclei visualization. (n=5, *p < 0.05; **p < 0.01)

Inhibition of Wnt β -catenin signalling pathway increases the presence of AGO2 loaded with miR-133a-3p into nuclei of HL-1 cells.

To further corroborate the nuclear presence of mature miR-133a-3p as consequence of inhibition Wnt β -catenin signalling pathway, we also

checked for presence of components of miRNAs biogenesis and function in nuclear compartment. Argonautes (AGOs) comprise a large family of evolutionary conserved proteins with a central role in both miRNAs biogenesis and function. Although it is widely accepted their function in the cytosol of cells, AGO2 and AGO1 were recently found to be present and active in nuclei of murine and human cells [101-103]. In line with this, we first checked for their presence in nuclei of HL-1 cells. As shown in Figure 2 A, we were able to observe the presence of both AGO2 and AGO1 in nuclear lysates of HL-1 treated or not with the inhibitor of Wnt canonical pathway. However as demonstrated by densitometry analysis (Fig 2 A), only AGO2 protein resulted increased in amount after inhibition of canonical Wnt cascade. Moreover to further understand the molecular mechanism underlying the nuclear re-localization of miR-133a-3p, we reasoned whether nuclear pool of AGO2 resulted loaded with miR-133a-3p. RNA immunoprecipitation assay indeed, revealed a significant higher enrichment for miR-133a-3p, after treatment with Wnt inhibitor, only for nuclear AGO2 (Fig 2 B and C). Thus, also confirming the differently distribution of AGO2 and AGO1 into nuclear compartment as response of IWR-1 stimulation.

Taken together these data demonstrate that in response to IWR-1 treatment AGO2 loaded with mature mir-133a-3p translocate into the nuclei of HL-1 cells.

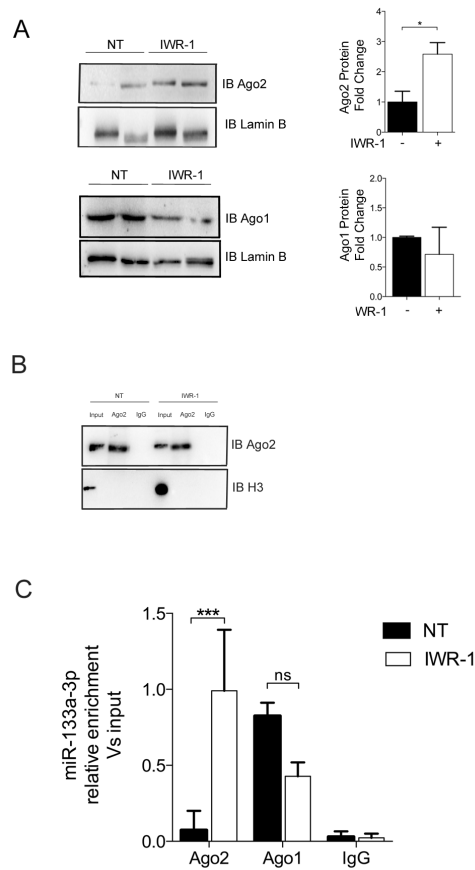


Figure 2. MiR-133a-3p is bound to AGO2 into nuclei of HL-1 cells after inhibition of Wnt β -catenin signalling pathway. A) Western blot assay and protein level representation for AGO2 and AGO1 on nuclear lysates of HL-1 cells treated or not with IWR-1. B) Western Blot assay for immunoprecipitated endogenous AGO2 on isolated nuclei of HL-1 treated or not with IWR-1. C) qRT-PCR on miRNAs after endogenous AGO2 or AGO1 immunoprecipitation from isolated nuclei of stimulated or not HL-1 cells with Wnt β -catenin signalling pathway inhibitors. (n=3, *p < 0.01;).**

AGO2 directly mediates the nuclear enrichment of mature miR-133a-3p

Consistently with previous data we next decided to further investigate the involvement of AGO2 and AGO1 in nuclear enrichment mature miR-133a-3p into the nucleus of HL-1 cells. To achieve this hypothesis a specific pool of siRNAs against AGO2 or AGO1 were used in presence or not of chemical inhibitors of Wnt β -catenin signalling pathway (Fig 3 A and C), Notably, based on the above observations, we found that the nuclear enrichment of miR-133a-3p resulted strongly reduced only in presence of siRNAs against AGO2 (Fig 3 B and D), These results were additionally confirmed by FISH experiments in which the transient silencing of AGO2, but not of AGO1, affects the nuclear distribution of miR-133a-3p in HL-1 cells. (Fig 3 E and F). Overall these results showed that AGO2 is involved in the nuclear re-localization of miR-133a-3p in response to inhibition of canonical Wnt pathway.

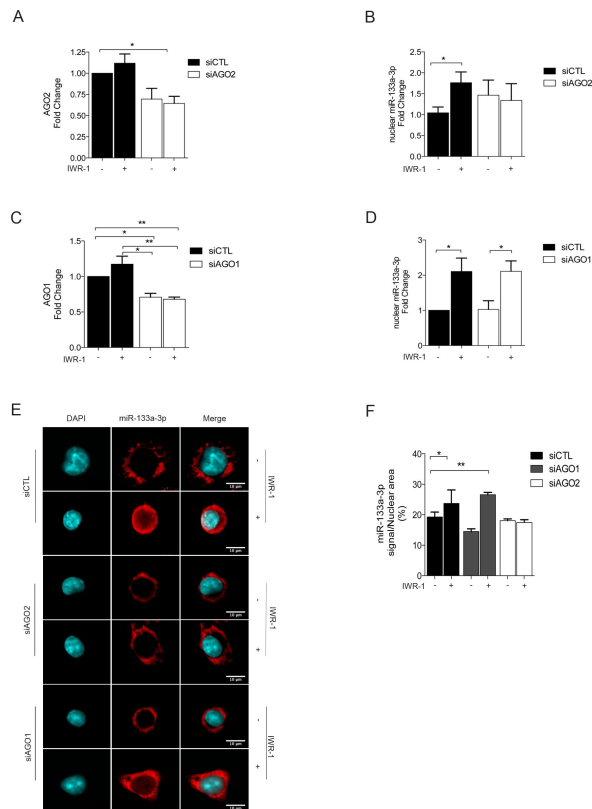


Figure 3. AGO2 is responsible for the nuclear re-localization of miR-133a-3p in HL-1 cells in response of IWR-1 treatment. A) and C) qRT-PCR for AGO2 and AGO1 mRNA levels after transient transfection of specific siRNAs. B) and D) qRT-PCR for mature miR-133a-3p on isolated nuclei of HL-1 cells, in presence or not of Wnt β -catenin signalling pathway inhibitor. E) *FISH* experiment for miR-133a-3p (RED) and co-stained with DAPI (BLUE), performed in HL-1 cells, treated or not with IWR-1 and in presence or not of siRNAs for AGO2 or F) Graphic representation of miR-133a-3p detection signal above nuclear area in presence or not of Wnt β -catenin signalling pathway inhibitor and siRNAs against AGO2 or AGO1. (n=6, *p < 0.05; **p < 0.01).

The karyopherin β family member Importin8 (IPO8) impacts the shuttling of miR133a-3p/AGO2 complex from cytosol to nucleus of HL-1 cell

Beyond member of miRNAs biogenesis, other proteins have been demonstrated to be involved in the cytosol-nuclear shuttling of mature miRNAs. Among these, a recent paper showed a specific member of karyopherin β family, named importin8 (IPO8), which is involved in the transport of mature miRNAs between cytoplasm and nucleus in mammalian cells^[34]. To demonstrate whether IPO8 was also involved in the translocation of mature miR-133a-3p as consequence of negative regulation of Wnt β -catenin signalling pathway, we transiently transfected HL-1 with specific siRNAs against IPO8 (Fig 4 A). After the knocking down of IPO8 the relative enrichment of mature miR-133a-3p inside nuclei of HL-1 with inactivated Wnt β -catenin signalling pathway was completely abolished (Fig. 4 B). These results were additionally confirmed by FISH experiment (Fig 4 C) in which miR-133a-3p nuclear signal resulted negatively affected by the silencing of IPO8. To better appreciate the involvement of IPO8 in nuclear shuttling of miR-133a-3p, we performed a bioluminescence resonance energy transfer (BRET) assay between AGO2 and IPO8 fusion proteins, that revealed that interaction between these two proteins happens only in presence of the inhibitor of Wnt β -catenin signalling pathway (Fig 4 D). These data showed that the IPO8 is another important component of the machinery responsible for nuclear re-localization of miR-133a in HL-1 cells.

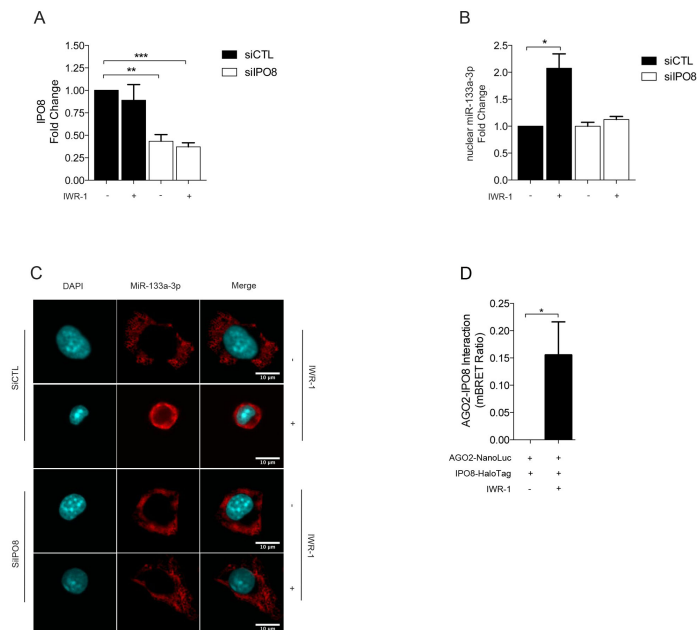


Fig 4. Nuclear enrichment of miR-133a-3p after Wnt β -catenin signalling pathway is dependent on the interaction between AGO2 and IPO8. **A)** qRT-PCR for IPO8 mRNA after transient transfection of specific siRNAs. **B)** qRT-PCR for mature miR-133a-3p in isolated nuclei of HL-1 cells treated as indicated. **C)** FISH experiment on HL-1 cells with inactivated or not Wnt β -catenin signalling pathway, and treated with siRNAs as indicated. miR-133a-3p (RED); DAPI (BLUE), **D)** IPO8-AGO2 affinity evaluated as measure of bioluminescence resonance energy transfer (BRET) assay in HL-1 cells transfected with AGO2 NanoLuc and IPO8-Halo and treated as indicated (n=3 *p < 0.05; **p < 0.01; *** p < 0.001).

DNMT3B expression depends on nuclear activity of miR-133a after inhibition of canonical Wnt pathway

In the last years the epigenetic regulation has demonstrated to be important in development and differentiation research^[104]. In particular, cardiogenesis is defined as a complex process associated with dramatic changes in epigenetic modification^[105] in response to

modulation of signalling pathways. Thereby to identify gene candidates for a direct miR-133a-3p transcriptional regulation after inhibition of canonical signalling pathway, we first checked the expression of different genes encoding for transcription factors and epigenetic enzymes (SI 3). Among these genes, the most modulated resulted the *de novo* DNA methyltransferase 3B (DNMT3B).

DNA methylation is an epigenetic modification that mainly involves methylation of CpG islands in the promoter genes. Specific catalytically active enzymes, including “maintenance” methyltransferase (DNMT1) and “*de novo*” methyltransferase (DNMT3A and DNMT3B) add methyl groups to CpG residues, thereby modifying the accessibility of DNA to the transcriptional machinery. Altered regulation of cytosine methylation has been linked to cardiovascular diseases (CVDs) development and progression ^{[106, 107], [108-110]}.

In HL-1 cells treatment with IWR-1 leads to a down-regulation of DNMT3B both at transcriptional and post-transcriptional level (Fig 5 A). To verify whether miR-133a-3p may be involved in negatively regulating DNMT3B expression, we used bioinformatics approach to scan -2 kb of DNMT3B promoter sequence for putative binding sites complementary to miR-133a-3p. As shown in figure 5 B at -50 bp from the “transcription start site” (TSS) in the DNMT3B promoter there is a putative binding site for miR-133a-3p, which resulted partially conserved also in human. To verify the inhibitor effect of miR-133a-3p on promoter of DNMT3B, we first cloned the promoter sequence of DNMT3B containing the putative binding site for miR-133a-3p into the pgl3-ancher vector (SI 4 A). As demonstrated in SI

4 B, the firefly luciferase activity of the DNMT3B WT promoter resulted reduced in a dose dependent manner by IWR-1 treatment. On the other hand no significant effect were found when the experiment were conducted using the mutated form of the DNMT3B promoter (SI 4 B). Based on data that not putative binding sites for miR-133a-3p were find in the 3'UTR of DNMT3B, to effectively asses whether or not the miR-133a-3p nuclear enrichment was directly linked to the transcriptional control of this gene, we checked for DNMT3B expression in presence of specific siRNAs against AGO2 and IPO8. As expected, in presence of siRNAs against AGO2 or IPO8 the down-regulation of DNMT3B is strongly reduced (Fig 5 C). On the contrary in presence of siRNAs against AGO1, the expression of DNMT3B is comparable to the scramble condition.

Ultimately, to prove that the transcriptional down-regulation of DNMT3B was correlated to the binding of miR-133a-3p on the putative site in the gene promoter, we transfected HL-1 cells with a specific “Target site blocker” (TSB) oligonucleotide. TSB oligonucleotide competes with the miRNA for the binding to the specific genomic region, thus preventing its annealing to the target sequence and its consequent action. Consistently, the application of the TSB was able to revert the negative down-regulation of DNMT3B transcription as consequence of inactivation of Wnt canonical signalling (Fig 5 D). Taken together these results demonstrated that miR-133a-3p, trough directly binding on DNMT3B promoter was able to induce a transcriptional down-regulation of this gene.

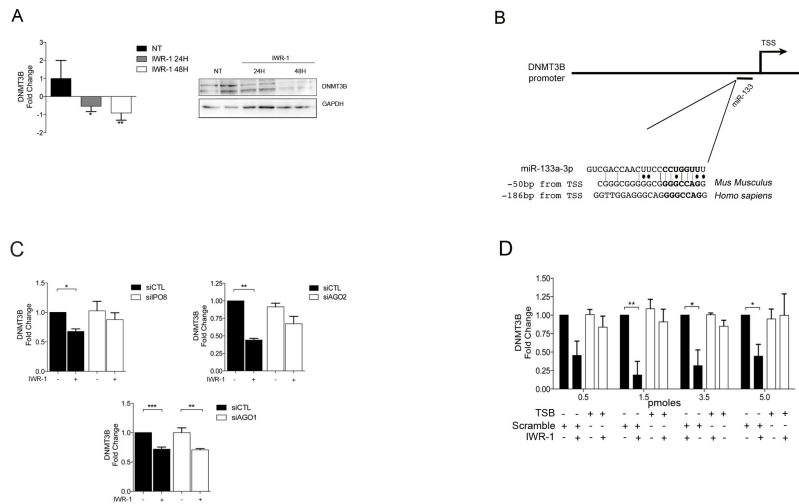


Figure 5. A miR-133a-3p binding site in DNMT3B promoter is responsible for gene transcriptional down-regulation. **A)** qRT-PCR and Western blot analysis in HL-1 cells for DNMT3B after treatment with IWR-1. Representative experiments are shown (n=3). **B)** Scheme of DNMT3B promoter and identification of the conserved miR-133a-3p putative binding site. **C)** qRT-PCR for DNMT3B in HL-1 cells transfected with siRNAs against IPO8, AGO2 or AGO1. Representative experiments are shown (n=5). **D)** qRT-PCR for DNMT3B on HL-1 cells transfected with Target site blocker (TSB) oligonucleotide or scramble and stimulated or not with IWR-1. Representative experiments are shown (n=4). (p < 0.05; **p < 0.01).

miR-133a-3p/AGO2 complex is recruited on DNMT3B promoter and induce an repressive epigenetic re-arrangement.

Different studies demonstrated the involvement of Argonaute proteins in small RNA-induced gene transcriptional regulation^[42, 102, 111]. Indeed, Kim H. et al, demonstrated that miR-704 directs AGO1, and tri-methyl histone H3 lysine 27 (H3K27me3) within the POLR3D promoter, thereby inducing a miRNA-directed transcriptional gene silencing (TGS) in mammalian cells^[40].

In line with this, and based on our data of involvement of AGO2 in nuclear re-localization of miR-133a-3p we specifically analysed the binding of AGO2 on the promoter region of DNMT3B in proximity of miR-133a-3p. As shown in Fig. 6 A chromatin immunoprecipitation (ChIP) followed by real-time quantitative PCR (qPCR) assay revealed an enrichment in binding of AGO2 in region overlapping the miR-133a-3p predicted site in DNMT3B promoter after inactivation of Wnt canonical pathway. Moreover, we also found a significant enrichment of the histone repressive marker (H3K27me3) in proximity of the miR-133a-3p binding site in DNMT3B promoter (Fig 6 B). Conversely the histone active modification H3 Lysine 4 trimethylation (H3K4me3) of transcription activation is much more enriched in basal condition (Fig 6 C). Taken together, these results suggest that miR-133-3p recruits AGO2 on DNMT3B promoter and induce a transcription regulation of the gene through epigenetic changes associated with transcriptional repression.

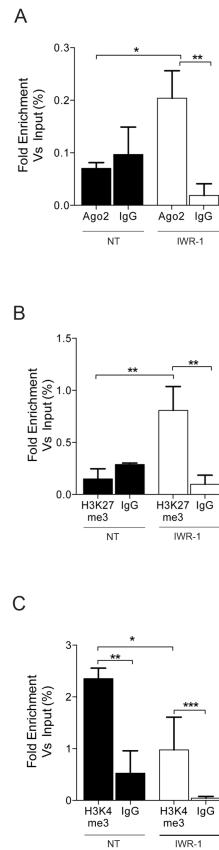


Fig. 6 AGO2/miR-133a-3p associates to DNMT3B promoter and induces epigenetic changes associated with transcription repression. A), B) and C) chip assay evaluating the enrichment of AGO2; H3K27me3 and H3K4me3 in proximity of miR-133a-3p putative binding site in DNMT3B promoter. Representative experiments are shown (3<n<4). (*p < 0.05; **p < 0.01; *p < 0.001).**

The AGO2/miR-133a-3p complex mediates repression of DNMT3B through miRNA-directed DNA methylation on its own promoter.

Recently in plants and lower organisms have been reported that small interference RNAs (siRNAs) are used to target specific genomic regions to mediate transcriptional gene silencing^[112]. This mechanism

relies on the RNA-directed DNA methylation targeting system (RdDM), in which small RNAs of 21-24 nucleotides are incorporated into Argonaute 4 complex (AGO4) and guide DRM1/2, the homologues of mammalian DNMT3A/B to their corresponding genomic DNA ^[113-115]. Thus, the discoveries that plants and animals share DNA methylation features ^[112] raised the challenge whether RdDM is also present in mammals. In fact, it was recently demonstrated that in human cells siRNAs can target GpC islands within promoter of a specific gene and promote transcriptional gene silencing through DNA-methyltransferase-dependent mechanism consistent with the phenomenon observed in plants^[116].

Since miR-133a-3p putative binding site in DNMT3B promoter is located into a GpC island we evaluated the enrichment of DNMT3B in correspondence of miR-133a-3p putative binding site after canonical Wnt inactivation. Chromatin immunoprecipitation assay followed by quantitative polymerase chain reaction revealed significant enrichment for DNMT3B after inactivation on Wnt canonical pathway in correspondence of miR-133a-3p putative binding site (Fig 7 A). Notably, BRET assay demonstrated that physical interaction between AGO2 and DNMT3B is miRNA-mediated, since HL-1 transfection with the target site blocker against the putative miR-133a-3p binding site completely abolished this interaction (Fig 7 B). Additionally, physical interaction between endogenous AGO2 and DNMT3B, assessed by Duo-Link proximity ligation assay, resulted increased by treatment of IWR-1 (Fig 7 C). Ultimately, the methylation rate in within DNMT3B promoter in proximity of miR-133a-3p binding site resulted increased after

inhibition of Wnt canonical pathway (Fig 7 D). Taken together, this data suggest a specific DNMT3B negative-feedback loop miRNA-mediated responsible for the gene silencing of DNMT3B.

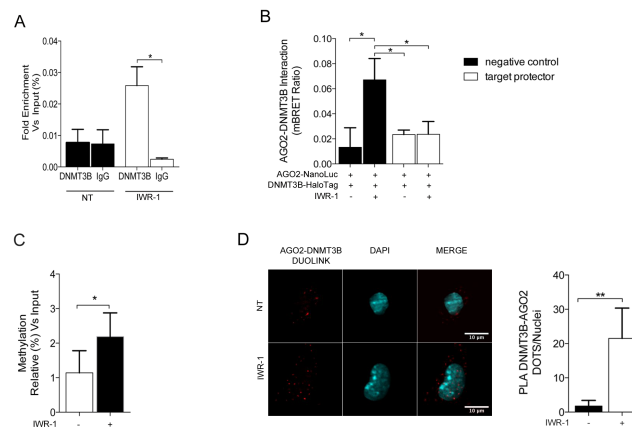


Fig. 7 AGO2/miR-133a-3p induces DNMT3B transcriptional gene silencing via a negative feed-back loop dependent from DNMT3B itself. **A)** ChIP assay for evaluating DNMT3B enrichment of in proximity of miR-133a-3p putative binding site in DNMT3B promoter. **B)** qRT-PCR for detection of DNA methylated assay in HL-1 cells treated as indicated. **C)** DNMT3B-AGO2 protein interaction as measured by bioluminescence resonance energy transfer (BRET) assay in HL-1 cells transfected with AGO2 NanoLuc and DNMT3B-Halo and treated as indicated (N=4) Representative experiments are shown (p < 0.05; **). **D)** Duo-Link assay performed to visualize interaction between endogenous AGO2 with DNMT3B (RED) in HI-1 treated or not with IWR-1 and counter-stained with DAPI (BLUE).

AGO2/miR-133a-3p mediated transcriptional regulation of DNMT3B is essential for proper differentiation of hESCs into mature cardiomyocytes

The Wnt β -catenin signalling is a key regulator of cardiac development both *in vivo* and *in vitro* [117]. Indeed, for *in vitro* differentiation of human Embryonic Stem Cells (hESCs), a first

artificial activation of Wnt/ β -catenin signalling (with a pharmacological agonist e.g. CHIR99021) followed by experimental inhibition of endogenous Wnt signalling (with a pharmacological antagonist e.g. IWR-1) leads pluripotent cells to differentiate into rhythmically contracting cardiomyocytes^[118, 119]. In line with this, we tested hypothesis in which the AGO2/miR-133a-3p mediated transcriptional regulation of DNMT3B could be confirmed in this *in vitro* model of cardiogenesis, and whether could have a role in the proper differentiation of hESCs into cardiomyocytes. To achieve this we first verified the nuclear enrichment of miR-133a-3p during cardiac differentiation of hESCs. As reported in figure 8 A, differentiating hESCs were treated with IWR-1 at day 3. As shown in figure 8 B qRT-PCR for mature miR-133a-3p on isolated nuclei of differentiating hESCs revealed an enrichment of miRNA at day 5. Consistently with previous results DNMT3B mRNA level resulted strongly down-regulated at after inactivation of Wnt β -catenin signalling pathway. These data confirmed our previous results in which inactivation of Wnt signalling pathway induces a re-localization of miR-133a-3p and a down-regulation of DNMT3B.

To further understand the role of this miR-133a-3p-mediated molecular mechanism, we transfected differentiating hESCs with target site blocker conjugated with FITC at day 2 of differentiation. FITC⁺ cells were then sorted at day 3 and day 10. As shown in Fig 8 C, qRT-PCR on sorted cells revealed that the target site blocker prevented the transcriptional repression of DNMT3B gene as compared to scramble condition, thus confirming that the regulation of this gene is directly dependent on miR-133a-3p binding on the

putative binding site within the promoter. Moreover, *de novo* DNA methylation is known to be important for proper cardiac development in terms of orchestrating cardiac gene expression, and abnormal DNA methylation is linked to the onset of congenital heart disease [120]. In line with this we decided to evaluate how the impairment of AGO2/miR-133a-3p mediated transcriptional down-regulation of DNMT3B affect maturation of hESCs derived cardiomyocytes. As shown in fig 8 D differentiating hESCs transfected with target site blocker express low levels of structural cardiac genes involved in contractility (e.g aMHC; TNNI2) or in calcium signalling (e.g. CACNA).

These results corroborate the hypothesis that miR-133a-3p directed transcriptional down-regulation of DNMT3B is essential for correct *in vitro* cardiac differentiation of hESCs cells.

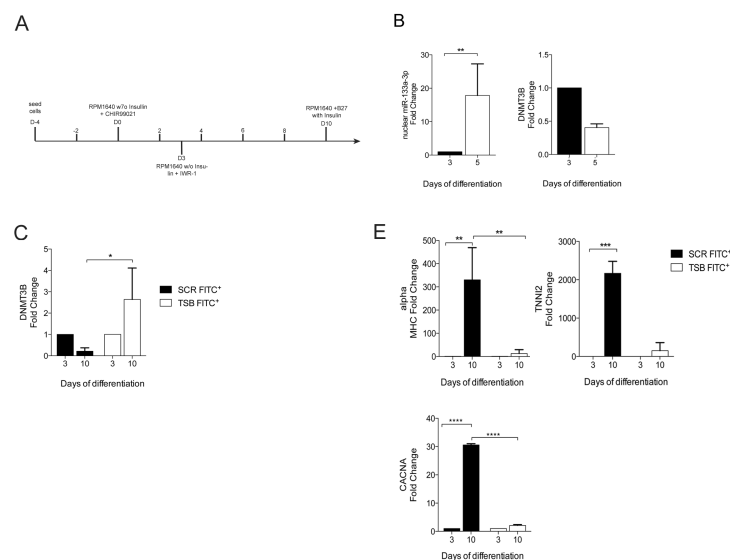


Figure 8. The nuclear relocation of AGO2/miR-133a-3p complex is essential for differentiation of hESCs into mature cardiomyocytes. A) Schematic representation of cardiac differentiation protocol of hESCs. **B)** qRT-PCR from

isolated nuclei and total cell lysate of differentiating hESCs, for miR-133a and DNMT3B, respectively. C) qRT-PCR on sorted cells for DNMT3B and treated as indicated. D) qRT-PCR on alphaMHC; TNNI2; CACNA genes in differentiating hESCs. (n=3, *p < 0.05; **p < 0.01; ***p < 0.001).

Discussion

Heart is the first organ to form and function during embryogenesis, thus life of all organisms strictly depends on its uninterrupted function [121]. Since heart has poor capacity to generate new cardiac muscle cells in response to injury, and since current drugs and mechanical devices can only transiently improve cardiac function, the scientific community aimed to extensively characterize molecular mechanism to offer new opportunities for therapeutically long term treatment of heart diseases. In this contest the Wnt β -catenin cascade tightly controls expression of genes involved in cardiac development, via the canonical post transcriptional action of miRNAs on downstream targets. However, it has now been shown that miRNAs can also bind to the promoter regions of genes to regulate gene expression [35, 36, 102, 122].

Our study showed for the first time that negative modulation of Wnt canonical signaling induced an up-regulation and a subsequent nuclear re-localization of mature miR-133a. Given this specific subcellular distribution of miR-133a, we further checked for nuclear presence of proteins related to miRNAs functions. Indeed, we were also able to found a different cellular distribution for AGOs proteins, in which AGO2 rather than AGO1 is much more enriched in nuclear compartment of HL-1 cells in response to Wnt inactivation. Consistently, AGO1 or AGO2 RNAs-bound immunoprecipitation,

followed by qRT-PCR, showed a switch in miR-133a binding to AGO2 in cells stimulated with inhibitor of Wnt canonical pathway. Thus, these data suggest a selective role for AGO2 in mediating nuclear function of miR-133a.

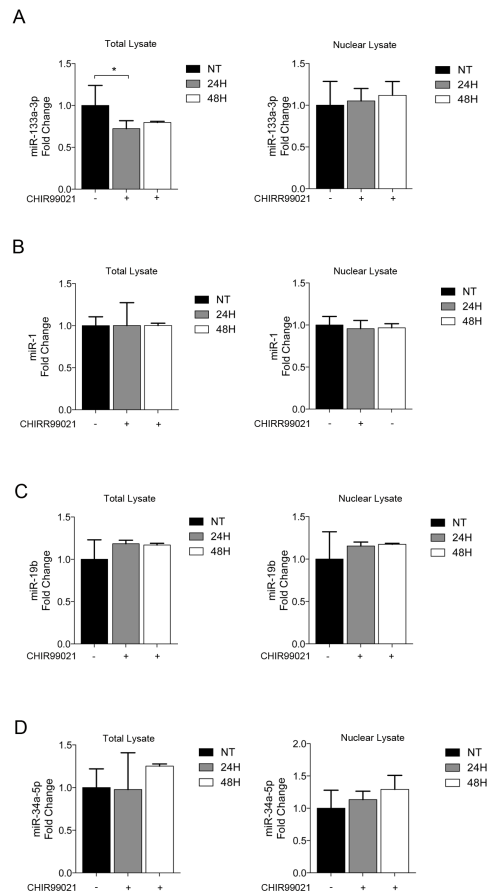
Moreover, the nuclear enrichment of AGO2-miR-133a-3p is mediated by the karyopherin IPO8. Similarly to their canonical mechanism of miRNAs action mRNA target gene, when present in nuclei, miRNAs can bind to specific genomic region based on base-pair complementarity^[35]. Into nuclei of cardiac cells, AGO2/miR-133a-3p complex binds to the promoter sequence of DNMT3B, which is an epigenetic enzyme strongly down-regulated in response to inactivation of Wnt β -catenin signaling pathway. This down-regulation of DNMT3B is dependent on the physical binding of miR-133a-3p on the promoter region, indeed when this interaction is prevented by the application of a competitive oligonucleotide (TSB), the negative modulation of DNMT3B is abolished. Several evidences also demonstrated that nuclear miRNAs regulates genes at transcriptional level, by modification of their epigenetic state^[35]. In line with this, we found that nuclear AGO2-miR-133a caused the down-regulation of DNMT3Bs by first inducing enrichment the histone repressive marker H3K27me3 and then through a negative feed-back loop, that led DNMT3B itself to methylate its own promoter.

We also showed for the first time that the link between inactivated Wnt β -catenin and nuclear function of miR-133a-3p is an essential checkpoint for cardiac differentiation in an *in vitro* model of cardiogenesis based on hESCs. In fact, the transcriptional control of DNMT3B is mandatory for differentiation of hESCs cell into mature

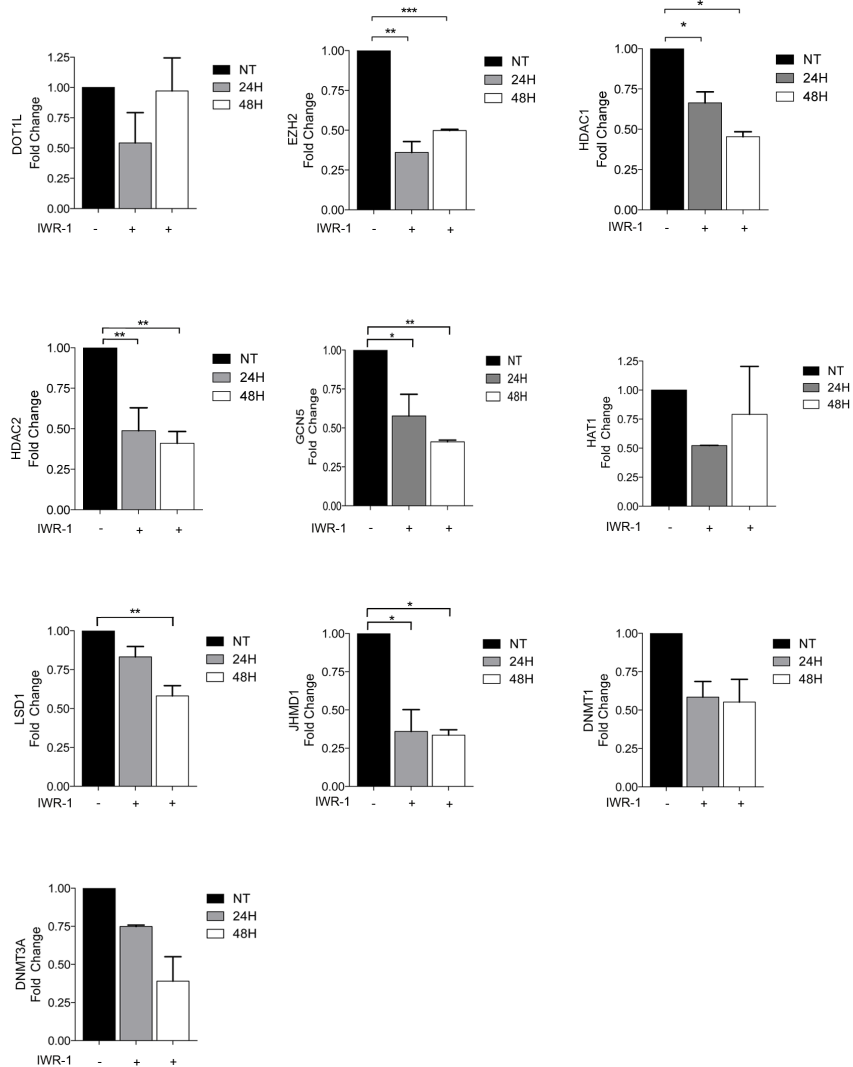
cardiomyocytes, since we showed that the impairment of miR-133a binding within DNMT3B promoter, results in a reduced maturation of hESC-derived cardiomyocytes, as demonstrated by reduced expression of genes involved in contractility and calcium handling.

Our results might open a new challenge towards a better characterization of those mechanisms involved in cardiac differentiation for their future translation in the discovery treatment for human cardiac diseases.

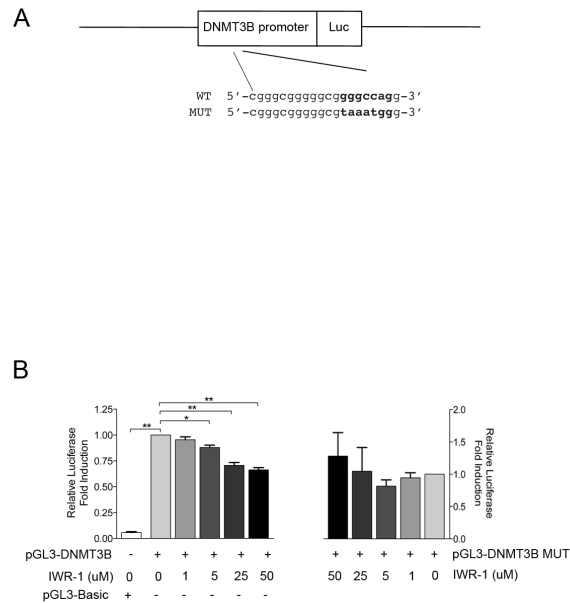
Supplementary figures



Supplementary figure 1. Sub-cellular distribution of mature miRNAs after chemical activation of Wnt β -catenin signalling pathway in HL-1 cells. A) and B) qRT-PCR for mRNA level of miR-133a-3p and miR-1 in total cell lysate and in purified nuclear fraction. C and D) qRT-PCR for mRNA level of miR-34a-5p and miR-19b in total cell lysate and in purified nuclear fraction (n=5, *p < 0.05).



Supplementary figure 2. Gene expression analysis of epigenetic enzymes after inactivation of canonical Wnt pathway. qRT-PCR on HL-1 total cell lysate treated as indicated. (n=3, *p < 0.05; **p < 0.01; ***p < 0.001).



Supplementary Figure 3. Analysis of DNMT3B promoter activity in HL-1 cells after treatment with IWR-1. **A)** Scheme and sequence of intact (WT) or mutated (MUT) putative binding site of miR-133a-3p within DNMT3B promoter-luciferase reporter vectors. **B)** dual-luciferase assay showing the activity of DNMT3B promoter WT and MUT and empty vector (pGL3-Basic) in HL-1 cells treated with a dose curve of IWR-1. (n=4, *p < 0.05; **p < 0.01).

References

1. Nüsslein-Volhard, C. and E. Wieschaus, *Mutations affecting segment number and polarity in Drosophila*. Nature, 1980. **287**(5785): p. 795-801.
2. Rijsewijk, F., et al., *The Drosophila homology of the mouse mammary oncogene int-1 is identical to the segment polarity gene wingless*. Cell, 1987. **50**(4): p. 649-657.
3. McMahon, A.P. and R.T. Moon, *Ectopic expression of the proto-oncogene int-1 in Xenopus embryos leads to duplication of the embryonic axis*. Cell, 1989. **58**(6): p. 1075-1084.
4. Logan, C.Y. and R. Nusse, *The Wnt signaling pathway in development and disease*. Annu. Rev. Cell Dev. Biol., 2004. **20**: p. 781-810.
5. Peifer, M., et al., *wingless signal and Zeste-white 3 kinase trigger opposing changes in the intracellular distribution of Armadillo*. DEVELOPMENT-CAMBRIDGE-, 1994. **120**: p. 369-369.
6. Behrens, J., et al., *Functional interaction of an axin homolog, conductin, with β -catenin, APC, and GSK3 β* . Science, 1998. **280**(5363): p. 596-599.
7. Hart, M.J., et al., *Downregulation of β -catenin by human Axin and its association with the APC tumor suppressor, β -catenin and GSK3 β* . Current Biology, 1998. **8**(10): p. 573-581.
9. Arce, L., N. Yokoyama, and M. Waterman, *Diversity of LEF/TCF action in development and disease*. Oncogene, 2006. **25**(57): p. 7492.

10. Vlad, A., et al., *The first five years of the Wnt targetome*. Cellular signalling, 2008. **20**(5): p. 795-802.
11. Naito, A.T., et al., *Developmental stage-specific biphasic roles of Wnt/ β -catenin signaling in cardiomyogenesis and hematopoiesis*. Proceedings of the National Academy of Sciences, 2006. **103**(52): p. 19812-19817.
12. Mummery, C.L., et al., *Differentiation of human embryonic stem cells and induced pluripotent stem cells to cardiomyocytes*. Circulation research, 2012. **111**(3): p. 344-358.
13. Cai, C.-L., et al., *Isl1 identifies a cardiac progenitor population that proliferates prior to differentiation and contributes a majority of cells to the heart*. Developmental cell, 2003. **5**(6): p. 877-889.
14. Tseng, A.-S., F.B. Engel, and M.T. Keating, *The GSK-3 inhibitor BIO promotes proliferation in mammalian cardiomyocytes*. Chemistry & biology, 2006. **13**(9): p. 957-963.
15. Foley, A.C. and M. Mercola, *Heart induction by Wnt antagonists depends on the homeodomain transcription factor Hex*. Genes & development, 2005. **19**(3): p. 387-396.
16. Roberts, T.C., *The microRNA biology of the mammalian nucleus*. Molecular Therapy—Nucleic Acids, 2014. **3**(8): p. e188.
17. Lee, Y., et al., *MicroRNA genes are transcribed by RNA polymerase II*. The EMBO journal, 2004. **23**(20): p. 4051-4060.

18. Lee, Y., et al., *The nuclear RNase III Drosha initiates microRNA processing*. Nature, 2003. **425**(6956): p. 415-419.
19. Yi, R., et al., *Exportin-5 mediates the nuclear export of pre-microRNAs and short hairpin RNAs*. Genes & development, 2003. **17**(24): p. 3011-3016.
20. Filipowicz, W., et al., *Post-transcriptional gene silencing by siRNAs and miRNAs*. Current opinion in structural biology, 2005. **15**(3): p. 331-341.
21. Meister, G., et al., *Human Argonaute2 mediates RNA cleavage targeted by miRNAs and siRNAs*. Molecular cell, 2004. **15**(2): p. 185-197.
22. Hwang, H.-W., E.A. Wentzel, and J.T. Mendell, *A hexanucleotide element directs microRNA nuclear import*. Science, 2007. **315**(5808): p. 97-100.
23. Park, C.W., et al., *Mature microRNAs identified in highly purified nuclei from HCT116 colon cancer cells*. RNA biology, 2010. **7**(5): p. 606-614.
24. Khudayberdiev, S.A., et al., *A comprehensive characterization of the nuclear microRNA repertoire of post-mitotic neurons*. 2013.
25. Kim, D.H., et al., *MicroRNA-directed transcriptional gene silencing in mammalian cells*. Proceedings of the National Academy of Sciences, 2008. **105**(42): p. 16230-16235.
26. Tan, Y., et al., *Transcriptional inhibition of Hoxd4 expression by miRNA-10a in human breast cancer cells*. BMC molecular biology, 2009. **10**(1): p. 12.

27. Zardo, G., et al., *Polycombs and microRNA-223 regulate human granulopoiesis by transcriptional control of target gene expression*. *Blood*, 2012. **119**(17): p. 4034-4046.
28. Qu, H., et al., *miRNA-558 promotes tumorigenesis and aggressiveness of neuroblastoma cells through activating the transcription of heparanase*. *Human molecular genetics*, 2015. **24**(9): p. 2539-2551.
29. Chen, B., et al., *Small molecule-mediated disruption of Wnt-dependent signaling in tissue regeneration and cancer*. *Nature chemical biology*, 2009. **5**(2): p. 100-107.
30. Huang, S.-M.A., et al., *Tankyrase inhibition stabilizes axin and antagonizes Wnt signalling*. *Nature*, 2009. **461**(7264): p. 614-620.
31. Ye, S., et al., *Pleiotropy of glycogen synthase kinase-3 inhibition by CHIR99021 promotes self-renewal of embryonic stem cells from refractory mouse strains*. *PloS one*, 2012. **7**(4): p. e35892.
32. Huang, V., et al., *Ago1 Interacts with RNA polymerase II and binds to the promoters of actively transcribed genes in human cancer cells*. *PLoS Genet*, 2013. **9**(9): p. e1003821.
33. Huang, V., et al., *Upregulation of Cyclin B1 by miRNA and its implications in cancer*. *Nucleic acids research*, 2012. **40**(4): p. 1695-1707.
34. Gagnon, K.T., et al., *RNAi factors are present and active in human cell nuclei*. *Cell reports*, 2014. **6**(1): p. 211-221.

35. Wei, Y., et al., *Importin 8 regulates the transport of mature microRNAs into the cell nucleus*. Journal of Biological Chemistry, 2014. **289**(15): p. 10270-10275.
36. Latham, T., N. Gilbert, and B. Ramsahoye, *DNA methylation in mouse embryonic stem cells and development*. Cell and tissue research, 2008. **331**(1): p. 31-55.
37. Liu, Z., et al., *WNT signaling promotes Nkx2. 5 expression and early cardiomyogenesis via downregulation of Hdac1*. Biochimica et Biophysica Acta (BBA)-Molecular Cell Research, 2009. **1793**(2): p. 300-311.
38. Baubec, T., et al., *Genomic profiling of DNA methyltransferases reveals a role for DNMT3B in genic methylation*. Nature, 2015. **520**(7546): p. 243-247.
39. Baccarelli, A., et al., *Repetitive element DNA methylation and circulating endothelial and inflammation markers in the VA normative aging study*. Epigenetics, 2010. **5**(3): p. 222-228.
40. Nührenberg, T.G., et al., *Cardiac myocyte de novo dna methyltransferases 3a/3b are dispensable for cardiac function and remodeling after chronic pressure overload in mice*. PloS one, 2015. **10**(6): p. e0131019.
41. Vujic, A., et al., *Experimental heart failure modelled by the cardiomyocyte-specific loss of an epigenome modifier, DNMT3B*. Journal of molecular and cellular cardiology, 2015. **82**: p. 174-183.
42. Okano, M., et al., *DNA methyltransferases Dnmt3a and Dnmt3b are essential for de novo methylation and mammalian development*. Cell, 1999. **99**(3): p. 247-257.

43. Li, L.-C., et al., *Small dsRNAs induce transcriptional activation in human cells*. Proceedings of the National Academy of Sciences, 2006. **103**(46): p. 17337-17342.
44. Morris, K.V., et al., *Small interfering RNA-induced transcriptional gene silencing in human cells*. Science, 2004. **305**(5688): p. 1289-1292.
45. Verdel, A., et al., *Common themes in siRNA-mediated epigenetic silencing pathways*. International Journal of Developmental Biology, 2009. **53**(2-3): p. 245-257.
46. Matzke, M., et al., *RNA-mediated chromatin-based silencing in plants*. Current opinion in cell biology, 2009. **21**(3): p. 367-376.
47. Qi, Y., et al., *Distinct catalytic and non-catalytic roles of ARGONAUTE4 in RNA-directed DNA methylation*. Nature, 2006. **443**(7114): p. 1008-1012.
48. Denis, H., M.N. Ndlovu, and F. Fuks, *Regulation of mammalian DNA methyltransferases: a route to new mechanisms*. EMBO reports, 2011. **12**(7): p. 647-656.
49. Kawasaki, H. and K. Taira, *Induction of DNA methylation and gene silencing by short interfering RNAs in human cells*. Nature, 2004. **431**(7005): p. 211-217.
50. Gessert, S. and M. Kühl, *The multiple phases and faces of wnt signaling during cardiac differentiation and development*. Circulation research, 2010. **107**(2): p. 186-199.
51. Rao, J., et al., *Stepwise clearance of repressive roadblocks drives cardiac induction in human ESCs*. Cell stem cell, 2016. **18**(3): p. 341-353.

52. Nakahama, H. and E. Di Pasquale, *Generation of cardiomyocytes from pluripotent stem cells*. Patient-Specific Induced Pluripotent Stem Cell Models: Generation and Characterization, 2016: p. 181-190.
53. Chamberlain, A.A., et al., *DNA methylation is developmentally regulated for genes essential for cardiogenesis*. Journal of the American Heart Association, 2014. **3**(3): p. e000976.
54. Majid, S., et al., *MicroRNA-205-directed transcriptional activation of tumor suppressor genes in prostate cancer*. Cancer, 2010. **116**(24): p. 5637-5649.
55. Place, R.F., et al., *MicroRNA-373 induces expression of genes with complementary promoter sequences*. Proceedings of the National Academy of Sciences, 2008. **105**(5): p. 1608-1613.

Chapter 4

MiR-133 modulates the β_1 Adrenergic Receptor transduction cascade

Alessandra Castaldi, PhD; Tania Zaglia, PhD; Vittoria Di Mauro, MSc; Pierluigi Carullo, BSc; Giacomo Viggiani, MSc; Giulia Borile, MSc; Barbara Di Stefano, PhD; Gabriele Giacomo Schiattarella, MD; Maria Giovanna Gualazzi, PhD; Leonardo Elia, PhD; Giuliano Giuseppe Stirparo, MSc; Maria Luisa Colorito, PhD; Gianluigi Pironti, PhD; Paolo Kunderfranco, PhD; Giovanni Esposito, MD, PhD; Marie-Louise Bang, PhD; Marco Mongillo, MD, PhD; Gianluigi Condorelli, MD, PhD; Daniele Catalucci, PhD

Razionale. The sympathetic nervous system plays a fundamental role in the regulation of myocardial function. During chronic pressure overload, over-activation of the sympathetic nervous system induces the release of catecholamines, which activate β -adrenergic receptors (β ARs) in cardiomyocytes (CMs) and lead to increased heart rate and cardiac contractility. However, chronic stimulation of β ARs leads to impaired cardiac function and β -blockers are widely used as therapeutic agents for the treatment of cardiac disease. MiR-133 is highly expressed in the myocardium and is involved in controlling cardiac function through regulation of mRNA translation/stability.

Objective. To determine whether miR-133 affects β AR signaling during progression to heart failure.

Methods and Results. Based on bioinformatic analysis, β_1 AR and other components of the β_1 AR signal transduction cascade, including adenylate cyclase VI and the catalytic subunit of the cAMP-dependent protein kinase A (PKA), were predicted as direct targets of miR-133 and subsequently validated by experimental studies. Consistently, cAMP accumulation and activation of downstream targets were repressed by miR-133 overexpression in both neonatal and adult CMs following selective β_1 AR stimulation. Furthermore, gain- and loss-of-function studies of miR-133 revealed its role in counteracting the deleterious apoptotic effects caused by chronic β_1 AR stimulation. This was confirmed *in vivo* using a novel cardiac-specific TetON-miR-133 inducible transgenic mouse model (Tg133). When subjected to transaortic constriction, Tg133 mice maintained cardiac performance and showed attenuated apoptosis and reduced fibrosis compared to control mice.

Conclusions. MiR-133 controls multiple components of the β_1 AR transduction cascade and is cardioprotective during heart failure.

Keywords: β_1 adrenergic receptor, microRNA, cardiomyocyte, cAMP,

receptor signaling pathway.

Non-standard Abbreviations and Acronyms

AC_{VI}	Adenylate cyclase VI
aAR	α-adrenergic receptors
cAMP	Cyclic adenosine monophosphate
CLB	Clenbuterol
Ctl	Control
CM	Cardiomyocyte
Dox	Doxycycline
FRSK	Forskolin
GRK	G protein-coupled receptor kinase
IBMX	Isobutylmethylxantine
ICI	ICI-118,551
IGF-1	Insulin-like growth factor 1
MHC	Myosin heavy chain
MiR	MicroRNA
nCM	Neonatal cardiomyocyte
NE	Norepinephrine
PLN	Phospholamban
PKA	Protein kinase A
PKA C-Beta	Catalytic subunit beta of cAMP-dependent protein kinase A
TAC	Transaortic constriction
Tg	Transgenic
UTR	Untranslated region

The sympathetic nervous system plays a pivotal role in the regulation of myocardial function. However, hyperactivation of this pathway can cause or accelerate cardiac pathology and is inversely correlated with survival.[123-126] These detrimental effects are caused by increased levels of circulating catecholamines, which act on cardiomyocytes (CMs) mainly through chronic stimulation of beta-adrenergic receptors (β ARs). In the heart, different β AR subtypes are expressed with the β_1 and β_2 subtypes being the most abundant.[127]

β_1 AR belongs to a class of seven-transmembrane G protein-coupled receptors[128] that, when stimulated, trigger the activation of G-proteins (Gs),[129] which, in turn, activate specific adenylyl cyclases (i.e. AC_V and AC_{V1} in the heart).[130] This elicits a consequential accumulation of the second messenger cyclic adenosine monophosphate (cAMP), which activates the cAMP-dependent protein kinase A (PKA)-dependent signaling cascade resulting in phosphorylation of targets, such as phospholamban, ryanodine receptor 2, troponin I, and MYPBC, key regulators of cardiac function. Whereas stimulation of either β_1 AR or β_2 AR leads to a rise in cAMP accumulation, the two receptor subtypes exert different effects, probably due to differential cAMP subcellular compartmentation.[131-133] In fact, while β_2 AR activation endows with more protective signaling by acting against myocardial apoptosis,[129, 134, 135] the β_1 AR subtype has been shown to be responsible for several harmful processes occurring during the progression to heart failure. Constitutive activation of β_1 AR *in vivo* causes pathological cardiac hypertrophy, associated with significant fibrosis and accelerated progression towards heart failure.[136, 137] On the other hand, transgenic mice with a modest overexpression of β_2 ARs showed enhanced cardiac contractility without any deleterious effects.[138] Due to their fundamental role in regulating cardiac function, β ARs are critical therapeutic targets and β_1 AR blockers have been clinically proven to be

beneficial for the treatment of patients with hypertension, ischemia, post-inflammatory cardiomyopathy, and heart failure.[123]

MicroRNAs (miRs) are small non-coding RNAs that negatively interfere with mRNA stability and translation by binding to the 3' untranslated region (UTR) of their target mRNAs.[139] The role of miRs under cardiac physiological and pathological conditions is well documented and accumulating evidence corroborates their potential as novel therapeutic targets.[140] One of the most abundant miRs in the heart is miR-133, which has been extensively studied by us and others.[141-144] In particular, its expression was found to be inversely related to cardiac hypertrophy and in human heart disease.[141]

Here we reveal miR-133 as a novel molecular player involved in the regulation of the β -adrenergic system in the heart. In particular, we demonstrate that miR-133 directly targets β_1 AR (*adbr1*) as well as several other components of the β_1 AR signaling cascade, including adenylate cyclase VI (AC_{VI} , *adcy6*), the catalytic subunit beta of cAMP-dependent protein kinase A (PKA C-Beta, *prkacb*), and the exchange protein activated by cAMP (EPAC, *epac*). Thus, miR-133 regulates the β_1 AR pathway at multiple levels, thereby modulating cardiac function.

Methods

A detailed description of methods is provided in the Online Data Supplement.

Results

MiR-133 modulates components of the β_1 AR signaling cascade

In a bioinformatic search for potential targets of miR-133, the β_1 adrenergic receptor (β_1 AR, *adbr1*) was among the predicted target (Online Table I). To determine whether miR-133 can directly target β_1 AR mRNA, its 3'UTR was cloned into the psiCHECK2 luciferase reporter vector and cotransfected with

a miR-133 expressing plasmid into 293 cells. A 60% reduction in luciferase activity was found in the presence of miR-133, whereas mutation of the miR-133 target site completely abolished the repression (Figure 1A). Similar results were obtained using synthetic miR-133 mimics (data not shown). Further confirmation was obtained by immunoprecipitation with biotinylated miR-133 oligo on adult mouse heart homogenate following by PCR analysis for *adrb1* mRNA on extracted total RNA (Figure 1D). Furthermore, in a loss-of-function experiment in nCMs, repression of miR-133 by Ad-Decoy133[141] resulted in a ~60% upregulation of β_1 AR protein (Online Figure I). Taken together these results demonstrate that β_1 AR is a direct target of miR-133.

Stimulation of β_1 AR with catecholamines regulates a wide range of biological processes through the activation of intermediate signaling components, such as the second messenger cAMP and subsequently protein kinase A (PKA). Thus, to determine whether additional regulators of the β_1 AR transduction cascade are potentially targeted by miR-133, we performed bioinformatics analysis, luciferase assays, target pull-down, and miR-133 loss-of-function experiments in nCMs. Our results revealed that both adenylate cyclase VI (AC_{VI} , *adcy6*), one of the main AC isoforms expressed in CMs,[145] and the catalytic subunit beta of cAMP-dependent protein kinase A (PKA C-Beta, *prkacb*) are targeted by miR-133 (Online Table I, Figure 1B-D, and Online Figure I, IIA). In addition, the Exchange protein activated by cAMP (Epac), an additional component of the β_1 AR signaling cascade, was also shown to be a predicted target of miR-133 (Online Table I) and validated by luciferase and immunoprecipitation assays (Online Figure IIB,C).

Thus, miR-133 can directly target multiple signal transduction molecules of the β_1 AR/cAMP/PKA pathway, consistent with recent evidence that a single miR can target several components of the same pathway.[146, 147]

MiR-133 modulates activation of b₁AR signaling in cardiomyocytes

Based on the results described above, we sought to determine the effect of miR-133 on the activation of b₁AR-dependent signaling using cAMP imaging in living cultured CMs. To this aim, control and Ad-miR133-infected CMs were transiently transfected with the fluorescent cAMP sensor EPAC1-cAMPs and challenged by b₁AR-selective stimulation through administration of norepinephrine (NE) (10 nmol/L) in the presence of the b₂AR selective antagonist ICI-118,551 (ICI) (100 nmol/L). As expected, this resulted in a rapid increase in cAMP levels in control (Ctl) cells, while the response was significantly reduced in miR-133 overexpressing CMs (peak $\Delta R/R_0$ (%): Ad-miR133 = 12.96 ± 0.05 ; Ctl = 34.12 ± 0.04 , $p < 0.01$) (Figure 2A, B). In support of the specificity of miR-133 in targeting b₁AR-dependent signaling, stimulation of CMs with the b₂AR selective agonist clenbuterol (CLB) (10 μ mol/L) caused a comparable increase in cAMP in miR-133 overexpressing and control CMs (Figure 2C). In addition, no effects of miR-133 on mRNA levels of b₂AR were found (Online Figure IIIB).

Since we found AC_{V1} to be negatively regulated by miR-133 (Figure 1B,D and Online Figure I, IIA), we next sought to determine whether miR-133 overexpression may have an effect on the ability of CMs to synthesize cAMP in response to direct activation of ACs. We thus performed an *in cell* AC activity assay by measuring the synthesis rate and maximal [cAMP] elicited by a submaximal concentration of the direct AC activator forskolin (FRSK) (5 μ mol/L). Notably, miR-133 overexpression reduced both the maximal amount and the rate of cAMP accumulation (steady state cAMP (DR/R₀ (%): Ad-miR133 = 22.0 ± 2.9 ; Ctl = 35.0 ± 6.8 , $p < 0.01$; accumulation rate (dR/min): Ad-miR133 = 0.56 ± 0.01 ; control = 0.1 ± 0.02 , $p < 0.01$; Figure 3A,B).

Based on our identification of PKA C-Beta as a target of miR-133 (Figure 1C,D and Online Figure I) as well as the reduced cAMP response (Figure 2A,B) and PKA-dependent phosphorylation of phospholamban

(PLN) in miR-133-overexpressing compared to control nCMs (Online Figure IIIA), we next hypothesized that PKA activity is reduced in miR-133-overexpressing nCMs. To test this, we transfected nCMs with the fluorescent PKA activity reporter AKAR3 that allows for correlation of dynamic changes in FRET with the kinetics of PKA phosphorylation. For this purpose, we treated AKAR3-expressing nCMs with a cell-permeable cAMP analog (10 $\mu\text{mol/L}$) to directly activate PKA. As expected, the rate of PKA phosphorylation of AKAR3 was significantly lower in miR-133-overexpressing nCMs compared to Ctl cells following treatment with the cAMP analog (phosphorylation rate (dR/min) Ad-miR133 = 1.7 ± 0.4 ; control = 3.6 ± 0.4 ; $p < 0.01$; Figure 3C).

Altogether, these results demonstrate that miR-133 is directly involved in the modulation of the $\beta_1\text{AR}$ signaling pathway by acting at multiple levels downstream of $\beta_1\text{AR}$ ($\beta_1\text{AR}$ - AC_{V1} - PKA).

MiR-133 modulates activation of $\beta_1\text{AR}$ signaling *in vivo*

To determine whether miR-133-dependent modulation of the $\beta_1\text{AR}$ signaling pathway is taking place also *in vivo*, we generated an inducible cardiac-specific transgenic mouse model (Tg133) in which the pri-miR-133a-2 sequence (chromosome 2) was inserted downstream of a TET-ON activation system.[148] When fed with dox-supplemented diet, Tg133 mice showed a 3.15 and 1.65 fold overexpression of pri-miR-133a-2 and mature miR-133, respectively, while no effect was observed on the expression of endogenous pri-miR-133a-1 (chromosome 18) (Figure 4A). Consistent with the overexpression of miR-133, WHSC2, a previously validated target of miR-133,[141] was downregulated in Tg133 *vs.* Ctl mice (Online Figure IVB). Furthermore, an inverse relationship between miR-133 and $\beta_1\text{AR}$ expression was confirmed in a receptor-density assay (Figure 4B). In agreement with results from a previous study,[143] induced Tg133 mice did not show any major phenotypic abnormalities compared to Ctl mice as evaluated by

echocardiographic analysis (Data not shown). However, in agreement with our *in vitro* data on neonatal cells (see above), freshly isolated adult CMs from Tg133 hearts showed blunted cAMP accumulation following treatment with 100 nmol/L of the β_1 AR selective agonist xamoterol (81.9 ± 2 pmol/mg ([cAMP]/protein) vs. 52.7 ± 6 pmol/mg in Ctl and Tg133 CMs, respectively; Figure 4C). Consistently, acute induction of miR-133 in Tg133 mice resulted in reduced left ventricular hemodynamic performance in response to dobutamine stimulation (Figure 4D). We next asked whether in a condition of chronic activation of β_1 AR signaling detrimental to cardiac performance,[149, 150] i.e. during left ventricular pressure overload induced by transverse aortic constriction (TAC), induction of miR-133 expression would be sufficient to prevent alterations in cardiac function. In support of this hypothesis, Tg133 mice subjected to TAC showed preserved cardiac performance and attenuated cardiac remodeling as demonstrated by echocardiography and histological analyses (Figure 5A, 6C, and Online Table III, Online Figure IVC). In agreement with our *in vitro* data, a reduction in mRNA and protein levels as well as density of β_1 AR was observed in Tg133 compared to Ctl mice 1 week after TAC (Figure 5B and Online Figure VIB), which was accompanied by decreased cAMP/PKA-dependent phosphorylation of PLN (Online Figure IVB and VIB). At the immunohistochemical level, no difference at basal level was found (data not shown), while a strong reduction in apoptosis and fibrosis was observed in Tg133 mice 3 and 12 weeks after TAC (Figure 6C and Online Figure VB).

To evaluate how the observed cardioprotection in Tg133 mice relates to that mediated by pharmacological blockade of β_1 signaling, C57J/B6 mice were subjected to TAC, whereafter half received treatment with a clinically relevant dose of metoprolol (350 mg/kg/day). Echocardiographic analysis revealed a reduction in the TAC-induced decrease in fractional shortening in metoprolol-treated mice (Online Figure VA) to an extent that is comparable to or lower that observed in Tg133 mice.

Furthermore, metoprolol administration prevented the expected downregulation of miR-133 1 week post TAC and maintained miR-133 at levels comparable to those of the sham group (Figure 5C). On the other hand, no significant differences in miR-133 levels between metoprolol-treated and untreated mice were found 3 weeks after TAC.

Altogether, these data show that miR-133 modulates the β_1 AR transduction axis both *in vitro* and *in vivo* and suggest that the partial protective effect of b-blockers might be due to the preservation of miR-133 expression levels during the first phase of pressure overload, which is the time frame when miR-133 expression is decreased.

MiR-133 protects cardiomyocytes from β_1 AR-induced apoptosis *in vitro* and *in vivo*

Since prolonged stimulation of CMs with β_1 AR has previously been shown to be associated with activation of apoptotic cell death,[151-154] we hypothesized that miR-133 overexpression affects nCM susceptibility to apoptosis in response to chronic β AR activation. To determine this, we stimulated Ad-miR133-infected and Ctl nCMs with different doses of NE in the presence of the β_2 AR antagonist ICI. Immunostaining for the apoptotic marker caspase-3 after 72 hours of treatment revealed a significant reduction in the fraction of caspase-3 positive nCMs in NE-treated miR-133 overexpressing nCMs compared to Ctl cells (Figure 6A and also Online Figure VIIA), indicating that miR-133 overexpression protects nCMs from β_1 AR-induced apoptosis. Conversely, miR133 downregulation, as obtained by infection with Ad-Decoy133, resulted in a significant increase in nCM apoptosis (Figure 6B), accompanied by a considerable decrease in cell density in response to prolonged β_1 AR activation (Online Figure VIIB). In agreement with our *in vitro* data, the fraction of apoptotic myocardial cells was significantly lower in Tg133 mice compared to Ctl mice both 1 and 3 weeks after TAC (Figure 6C and Online Figure VB). This was accompanied

by reduced fibrosis and resulted in cardioprotection in Tg133 mice (Figure 6C). In line with this, Tg133 mice at 1 week after TAC showed reduced levels of the β_1 but not β_2 -adrenergic receptor kinase (G protein-coupled receptor kinases (GRK) 2 and 3, respectively) (Figure 6D and also Online Figure IVD), which has previously been shown to exert a pro-death function.[155] Likewise, also the mRNA levels of identified miR-133 targets were downregulated in Tg133 mice after TAC (Figure 5B and Online Figure VIA).

Taken together, these data demonstrate that by targeting multiple components of the β_1 AR-signaling cascade, miR-133 protects CMs from β_1 AR-induced apoptosis.

Discussion

In this study we provide the first evidence that miR-133 controls the β_1 AR system at multiple levels along its signaling axis in CMs. In particular, we show that miR-133, by targeting the β_1 -receptor itself and its downstream effectors AC_{VI} and PKA C-Beta, is a key modulator of the β_1 AR-mediated accumulation of the second messenger cAMP (Figure 7). This result is in line with a growing body of evidence demonstrating that miRs play a role in modulating specific receptor pathways in CMs.[146, 147] For example miR-1, which together with miR-133 is one of the most highly expressed miRs in the heart and is transcribed from the same bicistronic unit as miR-133, was found by us and others to regulate the insulin-like growth factor 1 (IGF-1)/IGF1R signal transduction pathway,[147, 156] a key regulator of cardiac muscle trophism and function.

Recent studies have demonstrated a role of β AR signaling in controlling miR expression. For instance, a group of 18 miRs was reported to be differentially expressed in the heart in response to β AR agonist or antagonist treatment.[157] Similarly, Kim *et al.* recently showed altered expression levels of a number of miRs in response to treatment with the β -

arrestin 1-biased β AR agonist carvedilol.[158] In another study, β -blockers were found to induce Serum Responsive Factor (SRF)-mediated inhibition of miR-1 expression, which appeared to be correlated with PKA-dependent phosphorylation of SRF in response to β AR activation.[159] These data correlate with a study on patients with chronic heart failure, where altered miR expression was found to be associated with reduced catecholamine sensitivity.[160] Finally, the miR let-7f was found to directly target β_2 AR and to be negatively regulated by β_2 -agonist stimulation.[161] On the other hand, a direct link between miRs and the β_1 AR cascade has not previously been demonstrated.

Our data show that miR-133 specifically interferes with the β_1 AR signaling pathway and exclude any potential effect of the miR on β_2 AR signaling. In fact, no effect on the cAMP accumulation rate was observed in miR-133-overexpressing CMs treated with β_2 AR selective agonist. The miR-133 targeting of AC_{VI} , which has been found to be selectively coupled to β_1 AR, further supports its pathway-specificity for the β_1 axis. On the other hand, AC_V , which is not a miR-133 predicted target, is predominantly associated with activation of β_2 AR signaling.[162] Thus, miR-133 overexpression in CMs should change the balance between β_1 - and β_2 -dependent effects towards the β_2 AR dependent signaling pathway, resulting in cardioprotection and counteraction of deleterious effects due to activation of the β_1 AR. Apoptosis is among the detrimental processes that are triggered by β_1 AR activation, consistent with the reported anti-apoptotic role of miR-133.[143] In agreement with this, both our *in vitro* and *in vivo* data (Figure 6) show that miR-133 protects CMs against β_1 AR-induced apoptosis. Furthermore, mRNA levels of *grk2*, which is upregulated in heart failure exerting a pro-death function,[155] were downregulated in Tg133 mice 1 week after TAC (Figure 6D). On the other hand, no differences were found in mRNA levels of *grk3*, which is mainly associated with endothelin receptors.[163]

In the present study, we also demonstrated that miR-133 targets Epac (Online Figure IIB,C), which is involved in the modulation of cAMP levels through a negative feedback loop between the cAMP-specific phosphodiesterase (PDE4D3) and PKA.[164] Thus, the decreased cAMP levels in response to miR-133 overexpression may not only be due to downregulation of the miR-133 targets β_1 AR, AC_{VI}, and PKA C-Beta, but also to enhanced PDE4D3 activity consequent to Epac downregulation. Furthermore, Epac has been shown to associate with Ca²⁺/calmodulin kinase II (CaMKII) and β -arrestin at the β_1 AR,[165-167] suggesting that by targeting Epac, miR-133 affects the CaMKII-dependent signaling in the failing heart. Future studies are needed to shed more light on this matter.

Previous studies on transgenic mice constitutively overexpressing miR-133 have shown major discrepancies, most likely due to the different approaches used. In fact, whereas miR-133 overexpression driven by an early embryonic promoter (β -myosin heavy chain, β -MHC) caused a lethal phenotype with detrimental cardiac defects in survivors to adulthood,[142] a normal basal cardiac phenotype was obtained when transgenic miR-133 was stably overexpressed at a later post-developmental phase under the control of the α -MHC promoter.[143] In agreement with the latter study, our echocardiographic analysis on induced adult Tg133 mice showed no abnormalities under basal resting conditions compared to Ctl mice, though a reduction in fractional shortening was observed with extended time of miR induction (Online Figure IVC). On the other hand, whereas the α MHC-transgenic mouse model showed impaired cardiac performance in response to ventricular pressure overload, our inducible miR-133 transgenic mice exhibited preserved fractional shortening and attenuated cardiac remodeling (Figure 5, 6). These apparently contrasting results might be due to the different modalities of miR-133 expression and possibly to compensatory mechanisms that might be activated when miR-133 is constitutively overexpressed.

Conclusion

In this study we demonstrate with several complementary approaches that miR-133 targets distinct components of the β_1 AR pathway and provide evidence suggesting that restoration of miR-133 levels in patients might be used as a potential novel therapeutic strategy for the treatment of cardiovascular diseases. This is in line with our observation that downregulation of miR-133 levels in condition of pressure-overload can be counteracted by administration of a clinically relevant b-blocker. Current therapeutic strategies are mainly designed to achieve inhibition of endogenous levels of specific miRs *in vivo* through the use of miR-antisense oligos.[140] For example, downregulation of various miRs have been shown to have beneficial effect on cardiac fibrosis and remodeling,[168-170] regeneration,[171] and neoangiogenesis.[172] As of yet, overexpression of miRs *in vivo* has only been achieved through the use of viral vectors,[173] which as opposed to antisense technology, do not allow for transient miR modulation. Thus, the development of improved strategies for efficient and specific expression of miRs in the heart is needed before miR replacement can be envisioned as a therapeutic strategy.

Acknowledgments

The authors thank Alessandra Rodanò for her expertise and technical assistance.

Source of Funding

This work was supported in part by grants from: the Italian Ministry of University and Research FIRB-Futuro in Ricerca (RBF1213KA), the PNR-CNR Aging Program 2012-2014 to DC; an “Advanced” grant (CardioEpigen; 294609) from the European Research Council and a Transatlantic Network of Excellence on Foundation LeDucq to GC; the European Community Seventh Framework Program FP7/2007-2013 under

Grant Agreement HEALTH-F2-2009-241526, EUTrigTreat and Telethon-Italy (GGP11224) to MM; University of Padova (Progetto Giovani Studiosi 2010, contract: GRIC101133) to TZ.

Disclosure

None.

References

1. Bristow MR. Beta-adrenergic receptor blockade in chronic heart failure. *Circulation*. 2000;101:558-569
2. Vatner SF, Vatner DE, Homcy CJ. Beta-adrenergic receptor signaling: An acute compensatory adjustment-inappropriate for the chronic stress of heart failure? Insights from gsalpha overexpression and other genetically engineered animal models. *Circulation research*. 2000;86:502-506
3. Lohse MJ, Engelhardt S, Eschenhagen T. What is the role of beta-adrenergic signaling in heart failure? *Circulation research*. 2003;93:896-906
4. Koch WJ, Lefkowitz RJ, Rockman HA. Functional consequences of altering myocardial adrenergic receptor signaling. *Annual review of physiology*. 2000;62:237-260
5. Brodde OE, Michel MC. Adrenergic and muscarinic receptors in the human heart. *Pharmacological reviews*. 1999;51:651-690
6. Lefkowitz RJ. Seven transmembrane receptors: Something old, something new. *Acta Physiol (Oxf)*. 2007;190:9-19
7. Rockman HA, Koch WJ, Lefkowitz RJ. Seven-transmembrane-spanning receptors and heart function. *Nature*. 2002;415:206-212

8. Ishikawa Y, Homey CJ. The adenylyl cyclases as integrators of transmembrane signal transduction. *Circulation research*. 1997;80:297-304
9. Lohse MJ, Engelhardt S. Protein kinase a transgenes: The many faces of camp. *Circulation research*. 2001;89:938-940
10. Mongillo M, McSorley T, Evellin S, Sood A, Lissandron V, Terrin A, Huston E, Hannawacker A, Lohse MJ, Pozzan T, Houslay MD, Zaccolo M. Fluorescence resonance energy transfer-based analysis of camp dynamics in live neonatal rat cardiac myocytes reveals distinct functions of compartmentalized phosphodiesterases. *Circulation research*. 2004;95:67-75
11. Nikolaev VO, Moshkov A, Lyon AR, Miragoli M, Novak P, Paur H, Lohse MJ, Korchev YE, Harding SE, Gorelik J. Beta2-adrenergic receptor redistribution in heart failure changes camp compartmentation. *Science*. 2010;327:1653-1657
12. Hall RA. Beta-adrenergic receptors and their interacting proteins. *Seminars in cell & developmental biology*. 2004;15:281-288
13. Tevaearai HT, Eckhart AD, Walton GB, Keys JR, Wilson K, Koch WJ. Myocardial gene transfer and overexpression of beta2-adrenergic receptors potentiates the functional recovery of unloaded failing hearts. *Circulation*. 2002;106:124-129
14. Engelhardt S, Hein L, Wiesmann F, Lohse MJ. Progressive hypertrophy and heart failure in beta1-adrenergic receptor transgenic mice. *Proceedings of the National Academy of Sciences of the United States of America*. 1999;96:7059-7064
15. Bisognano JD, Weinberger HD, Bohlmeyer TJ, Pende A, Reynolds MV, Sastravaha A, Roden R, Asano K, Blaxall BC, Wu SC, Communal C, Singh K, Colucci W, Bristow MR, Port DJ. Myocardial-directed overexpression of the human beta(1)-adrenergic

- receptor in transgenic mice. *Journal of molecular and cellular cardiology*. 2000;32:817-830
16. Milano CA, Allen LF, Rockman HA, Dolber PC, McMinn TR, Chien KR, Johnson TD, Bond RA, Lefkowitz RJ. Enhanced myocardial function in transgenic mice overexpressing the beta 2-adrenergic receptor. *Science*. 1994;264:582-586
 17. Dorn GW, 2nd. Micrnas in cardiac disease. *Translational research : the journal of laboratory and clinical medicine*. 2011;157:226-235
 18. van Rooij E, Purcell AL, Levin AA. Developing microrna therapeutics. *Circulation research*. 2012;110:496-507
 19. Care A, Catalucci D, Felicetti F, Bonci D, Addario A, Gallo P, Bang ML, Segnalini P, Gu Y, Dalton ND, Elia L, Latronico MV, Hoydal M, Autore C, Russo MA, Dorn GW, 2nd, Ellingsen O, Ruiz-Lozano P, Peterson KL, Croce CM, Peschle C, Condorelli G. Microrna-133 controls cardiac hypertrophy. *Nature medicine*. 2007
 20. Liu N, Bezprozvannaya S, Williams AH, Qi X, Richardson JA, Bassel-Duby R, Olson EN. Microrna-133a regulates cardiomyocyte proliferation and suppresses smooth muscle gene expression in the heart. *Genes & development*. 2008;22:3242-3254
 21. Matkovich SJ, Wang W, Tu Y, Eschenbacher WH, Dorn LE, Condorelli G, Diwan A, Nerbonne JM, Dorn GW, 2nd. Microrna-133a protects against myocardial fibrosis and modulates electrical repolarization without affecting hypertrophy in pressure-overloaded adult hearts. *Circulation research*. 2010;106:166-175
 22. Trajkovski M, Ahmed K, Esau CC, Stoffel M. Myomir-133 regulates brown fat differentiation through prdm16. *Nature cell biology*. 2012;14:1330-1335
 23. Sunahara RK, Dessauer CW, Gilman AG. Complexity and diversity of mammalian adenylyl cyclases. *Annual review of pharmacology and toxicology*. 1996;36:461-480

24. Ganesan J, Ramanujam D, Sassi Y, Ahles A, Jentzsch C, Werfel S, Leierseder S, Loyer X, Giacca M, Zentilin L, Thum T, Laggerbauer B, Engelhardt S. Mir-378 controls cardiac hypertrophy by combined repression of mitogen-activated protein kinase pathway factors. *Circulation*. 2013;127:2097-2106
25. Elia L, Contu R, Quintavalle M, Varrone F, Chimenti C, Russo MA, Cimino V, De Marinis L, Frustaci A, Catalucci D, Condorelli G. Reciprocal regulation of microrna-1 and insulin-like growth factor-1 signal transduction cascade in cardiac and skeletal muscle in physiological and pathological conditions. *Circulation*. 2009;120:2377-2385
26. Suarez J, Gloss B, Belke DD, Hu Y, Scott B, Dieterle T, Kim YK, Valencik ML, McDonald JA, Dillmann WH. Doxycycline inducible expression of serca2a improves calcium handling and reverts cardiac dysfunction in pressure overload-induced cardiac hypertrophy. *American journal of physiology. Heart and circulatory physiology*. 2004;287:H2164-2172
27. Adameova A, Abdellatif Y, Dhalla NS. Role of the excessive amounts of circulating catecholamines and glucocorticoids in stress-induced heart disease. *Canadian journal of physiology and pharmacology*. 2009;87:493-514
28. Ganguly PK, Lee SL, Beamish RE, Dhalla NS. Altered sympathetic system and adrenoceptors during the development of cardiac hypertrophy. *American heart journal*. 1989;118:520-525
29. Singh K, Xiao L, Remondino A, Sawyer DB, Colucci WS. Adrenergic regulation of cardiac myocyte apoptosis. *Journal of cellular physiology*. 2001;189:257-265
30. Fujita T, Ishikawa Y. Apoptosis in heart failure. -the role of the beta-adrenergic receptor-mediated signaling pathway and p53-mediated signaling pathway in the apoptosis of cardiomyocytes. *Circulation*

- journal : official journal of the Japanese Circulation Society.*
2011;75:1811-1818
31. Zaugg M, Xu W, Lucchinetti E, Shafiq SA, Jamali NZ, Siddiqui MA. Beta-adrenergic receptor subtypes differentially affect apoptosis in adult rat ventricular myocytes. *Circulation.* 2000;102:344-350
 32. Zhu WZ, Wang SQ, Chakir K, Yang D, Zhang T, Brown JH, Devic E, Kobilka BK, Cheng H, Xiao RP. Linkage of beta1-adrenergic stimulation to apoptotic heart cell death through protein kinase a-independent activation of ca²⁺/calmodulin kinase ii. *The Journal of clinical investigation.* 2003;111:617-625
 33. Brinks H, Boucher M, Gao E, Chuprun JK, Pesant S, Raake PW, Huang ZM, Wang X, Qiu G, Gumpert A, Harris DM, Eckhart AD, Most P, Koch WJ. Level of g protein-coupled receptor kinase-2 determines myocardial ischemia/reperfusion injury via pro- and anti-apoptotic mechanisms. *Circulation research.* 2010;107:1140-1149
 34. Kumarswamy R, Lyon AR, Volkmann I, Mills AM, Bretthauer J, Pahuja A, Geers-Knorr C, Kraft T, Hajjar RJ, Macleod KT, Harding SE, Thum T. Serca2a gene therapy restores microrna-1 expression in heart failure via an akt/foxo3a-dependent pathway. *European heart journal.* 2012;33:1067-1075
 35. Hou Y, Sun Y, Shan H, Li X, Zhang M, Zhou X, Xing S, Sun H, Chu W, Qiao G, Lu Y. Beta-adrenoceptor regulates mirna expression in rat heart. *Medical science monitor : international medical journal of experimental and clinical research.* 2012;18:BR309-314
 36. Kim IM, Wang Y, Park KM, Tang Y, Teoh JP, Vinson J, Traynham CJ, Pironti G, Mao L, Su H, Johnson JA, Koch WJ, Rockman HA. Beta-arrestin1-biased beta1-adrenergic receptor signaling regulates microrna processing. *Circulation research.* 2014;114:833-844

37. Lu Y, Zhang Y, Shan H, Pan Z, Li X, Li B, Xu C, Zhang B, Zhang F, Dong D, Song W, Qiao G, Yang B. MicroRNA-1 downregulation by propranolol in a rat model of myocardial infarction: A new mechanism for ischaemic cardioprotection. *Cardiovascular research*. 2009;84:434-441
38. Funahashi H, Izawa H, Hirashiki A, Cheng XW, Inden Y, Nomura M, Murohara T. Altered microRNA expression associated with reduced catecholamine sensitivity in patients with chronic heart failure. *Journal of cardiology*. 2011;57:338-344
39. Wang WC, Juan AH, Panebra A, Liggett SB. MicroRNA let-7 establishes expression of beta2-adrenergic receptors and dynamically down-regulates agonist-promoted down-regulation. *Proceedings of the National Academy of Sciences of the United States of America*. 2011;108:6246-6251
40. Timofeyev V, Myers RE, Kim HJ, Woltz RL, Sirish P, Heiserman JP, Li N, Singapuri A, Tang T, Yarov-Yarovoy V, Yamoah EN, Hammond HK, Chiamvimonvat N. Adenylyl cyclase subtype-specific compartmentalization: Differential regulation of l-type Ca^{2+} current in ventricular myocytes. *Circulation research*. 2013;112:1567-1576
41. von Lueder TG, Gravning J, How OJ, Vinge LE, Ahmed MS, Krobert KA, Levy FO, Larsen TS, Smiseth OA, Aasum E, Attramadal H. Cardiomyocyte-restricted inhibition of G protein-coupled receptor kinase-3 attenuates cardiac dysfunction after chronic pressure overload. *American journal of physiology. Heart and circulatory physiology*. 2012;303:H66-74
42. McConnachie G, Langeberg LK, Scott JD. Akap signaling complexes: Getting to the heart of the matter. *Trends in molecular medicine*. 2006;12:317-323

43. Yoo B, Lemaire A, Mangmool S, Wolf MJ, Curcio A, Mao L, Rockman HA. Beta1-adrenergic receptors stimulate cardiac contractility and camkii activation in vivo and enhance cardiac dysfunction following myocardial infarction. *American journal of physiology. Heart and circulatory physiology*. 2009;297:H1377-1386
44. Anderson ME. Camkii and a failing strategy for growth in heart. *The Journal of clinical investigation*. 2009;119:1082-1085
45. Anderson ME, Brown JH, Bers DM. Camkii in myocardial hypertrophy and heart failure. *Journal of molecular and cellular cardiology*. 2011;51:468-473
46. Montgomery RL, Hullinger TG, Semus HM, Dickinson BA, Seto AG, Lynch JM, Stack C, Latimer PA, Olson EN, van Rooij E. Therapeutic inhibition of mir-208a improves cardiac function and survival during heart failure. *Circulation*. 2011;124:1537-1547
47. da Costa Martins PA, Salic K, Gladka MM, Armand AS, Leptidis S, el Azzouzi H, Hansen A, Coenen-de Roo CJ, Bierhuizen MF, van der Nagel R, van Kuik J, de Weger R, de Bruin A, Condorelli G, Arbones ML, Eschenhagen T, De Windt LJ. MicroRNA-199b targets the nuclear kinase dyrk1a in an auto-amplification loop promoting calcineurin/nfat signalling. *Nature cell biology*. 2010;12:1220-1227
48. Thum T, Gross C, Fiedler J, Fischer T, Kissler S, Bussen M, Galuppo P, Just S, Rottbauer W, Frantz S, Castoldi M, Soutschek J, Koteliansky V, Rosenwald A, Basson MA, Licht JD, Pena JT, Rouhanifard SH, Muckenthaler MU, Tuschl T, Martin GR, Bauersachs J, Engelhardt S. MicroRNA-21 contributes to myocardial disease by stimulating map kinase signalling in fibroblasts. *Nature*. 2008;456:980-984
49. Porrello ER, Johnson BA, Aurora AB, Simpson E, Nam YJ, Matkovich SJ, Dorn GW, 2nd, van Rooij E, Olson EN. Mir-15

- family regulates postnatal mitotic arrest of cardiomyocytes. *Circulation research*. 2011;109:670-679
50. Bonauer A, Carmona G, Iwasaki M, Mione M, Koyanagi M, Fischer A, Burchfield J, Fox H, Doebele C, Ohtani K, Chavakis E, Potente M, Tjwa M, Urbich C, Zeiher AM, Dimmeler S. MicroRNA-92a controls angiogenesis and functional recovery of ischemic tissues in mice. *Science*. 2009;324:1710-1713
51. Eulalio A, Mano M, Dal Ferro M, Zentilin L, Sinagra G, Zacchigna S, Giacca M. Functional screening identifies mirnas inducing cardiac regeneration. *Nature*. 2012;492:376-381

Supplemental Material

MiR-133 modulates the β_1 Adrenergic Receptor transduction cascade

Castaldi, MiR-133 targets β_1 AR pathway

Alessandra Castaldi, PhD; Tania Zaglia, PhD; Vittoria Di Mauro, MSc; Pierluigi Carullo, BSc; Giacomo Viggiani, MSc; Giulia Borile, MSc; Barbara Di Stefano, PhD; Gabriele Giacomo Schiattarella, MD; Maria Giovanna Gualazzi, PhD; Leonardo Elia, PhD; Giuliano Giuseppe Stirparo, MSc; Maria Luisa Colorito, PhD; Gianluigi Pironti, PhD; Paolo Kunderfranco, PhD; Giovanni Esposito, MD, PhD; Marie-Louise Bang, PhD; Marco Mongillo, MD, PhD; Gianluigi Condorelli, MD, PhD; Daniele Catalucci, PhD

Target prediction

Prediction of miR-133 targets was performed using publicly available algorithms: TargetScan (<http://www.targetscan.org/>), miRanda (<http://www.microna.org/>), PicTar (<http://pictar.bio.nyu.edu/>), PITA (http://genie.weizmann.ac.il/pubs/mir07/mir07_prediction.html), and miRDIP (<http://ophid.utoronto.ca/mirDIP/>). 3'UTRs of predicted targets were uploaded on the PITA database (http://genie.weizmann.ac.il/pubs/mir07/mir07_prediction.html) and scanned for miR-133 binding sites (Online Table I).

Luciferase assay

A 3' UTR segment of the *adrb1*, *adcy6*, *prkacb*, and *epac* mRNAs were subcloned by standard procedures into the psiCHECK-TM2 vector (Promega) immediately downstream of the stop codon of the Renilla luciferase gene. The miR-133 mature sequence was cloned into the pcDNA6.2-GW/EmGFP-miR vector according to the manufacturer's protocol (Invitrogen). 2.5×10^5 293 cells were transfected with psiCHECK-3'UTR and pcDNA6.2-GW/EmGFP-miR-133 plasmids. 48 h post transfection, cells were lysed and luciferase activity was measured as described by the manufacturer (Promega). To confirm specific targeting of the 3'UTR of target genes by miR-133, site-specific mutagenesis at the predicted sites for each target was performed using the QuikChange Site-Directed Mutagenesis Kit as described by the manufacturer (Stratagene). Mutated constructs were then tested in luciferase assays and rescue of chemiluminescent signal in the presence of miR-133 identified real targeting sites.

RNA immunoprecipitation

A synthetic biotinylated miR-133 oligo (IBA BioTAGnology) was used to immunoprecipitate the miR:RNA-target binding complexes from heart

homogenate as previously described.[174] mRNA targets were then amplified by PCR (primers are listed in Online Table II).

RNA isolation and quantification

Total RNA was extracted using TRIzol Reagent (Life Technologies). Reverse transcription of RNA for miR-133, U6, and Rnu5g expression analysis was performed using the miRCURY LNA™ Universal RT microRNA PCR Polyadenylation and cDNA synthesis kit (Exiqon). Quantitative polymerase chain reaction (qPCR) was performed with microRNA LNA™ PCR primers (Exiqon) using the Fast SYBR Green Master Mix (Life Technologies). Reverse transcription of RNA for pri-mir-133a-1, pri-mir-133a-2, as well as *adrb1*, *adrb2*, *adcy6*, *prkacb*, *grk2*, and *grk3* expression analyses was performed using the High Capacity cDNA Reverse Transcription Kit (Life Technologies), following by qPCR with custom designed oligos (shown in Online Table II) using the Fast SYBR Green Master Mix (Life Technologies). Relative expression analyses were performed using the $\Delta\Delta C(t)$ method.

Neonatal cardiomyocyte isolation and culture

Hearts from 1-2 days old Sprague Dawley rats were minced in ADS (5 mM glucose, 106 mM NaCl, 5.3 mM KCl, 20 mM Hepes, 0.8 mM Na₂HPO₄, and 0.4 mM MgSO₄, pH7.4) and enzymatically dissociated with collagenase A (0.4 mg/ml) (Roche) and pancreatine (1.2 mg/ml) (Sigma). Cells were cultured for 24 hours in medium containing 67% DMEM, 17.5% M199, 10% HS, 5% NCS, L-glutamine, and antibiotics (all from Invitrogen), plated on laminin-coated dishes (10 $\mu\text{g}/\text{cm}^2$) (BD) at a density of 6×10^4 cells/cm², and maintained in a humidified atmosphere (5% CO₂) at 37°C. At the second day, cardiomyocytes (CMs) were cultured in a medium with low serum concentration.[141]

FRET imaging of cultured cardiomyocytes

24 hours after seeding, neonatal CMs (nCMs) were transfected with the appropriate FRET-based sensor, GcAMPs (for cAMP accumulation measurements, courtesy of Dr. Martin Lohse) or the fluorescent PKA activity reporter AKAR3 (for PKA activity, kind gift of Dr. Jin Zhang) using transfectin (Bio-Rad) as recommended by the manufacturer. After five hours, the medium was changed and approximately 5×10^5 nCMs were infected with either Ad-Empty or Ad-miR133 at different multiplicity of infection (MOI) as stated in the Results section and maintained in complete culture medium until the start of the imaging experiments. Cells were transferred to Hepes-buffered Ringer-modified saline (in mmol/L, 125 NaCl, 5 KCl, 1 Na_3PO_4 , 1 MgSO_4 , 5.5 glucose, 1.8 CaCl_2 , 20 Hepes, pH 7.4) kept at room temperature, and imaged on an inverted Olympus IX50 microscope coupled to a CCD camera (Sensicam QE, PCO) and a custom built beam-splitter optical device (F. Mammano, Venetian Institute of Molecular Medicine). Images were acquired using custom developed software and processed using ImageJ (National Institutes of Health). FRET changes were determined by measuring the background-subtracted 480 nm/535 nm fluorescence emission upon excitation at 430 nm. FRET values were expressed as $\Delta R/R_0$, where R_0 is the ratio at $t = 0$ s and $\Delta R = R - R_0$. Norepinephrine (NE), forskolin (FRSK), clenbuterol (CLB), ICI-118,551 (ICI), and Isobutylmethylxantine (IBMX) (all from Sigma) were delivered to the cells using separate perfusion lanes. For the AC activity assay, the rate of cAMP increase was estimated by calculating the slope of CFP/YFP emission ratio change (dR/dt) in GcAMP transfected cells between 100 and 150 sec after FRSK addition. For the PKA activity assay, AKAR transfected cells were incubated with 10 mmol/L of the cell permeable cAMP analogue 8-(4-Chlorophenylthio)-N⁶-phenyladenosine-3',5'-cyclic monophosphate (8-CPT-6-Phe-cAMP, Biolog, DE), and the 535 nm/480 nm emission ratio was

compared in Ad-miR133 *vs.* control cells. No differences were observed in Ad-Empty infected cells compared to control (Ctl) cells (data not shown).

cAMP assay in freshly isolated adult cardiomyocytes

CMs were isolated from 2-month-old wild-type and Tg133 male mice using standard enzymatic techniques, whereafter calcium was gradually reintroduced.[141] cAMP accumulation in response to selective β_1 AR stimulation was evaluated in freshly isolated cell through incubation with increasing concentrations (0.1, 1, and 10 μ mol/L) of xamoterol (Tocris) for 15 minutes at 37°C, after which cAMP levels were measured using the Cyclic AMP EIA Kit (Cayman) following the manufacturer's instructions.

Western blot analysis

Cells or tissues were lysed in RIPA buffer containing (in mmol/L) 10 Tris HCl pH7.2, 150 NaCl, 5 EDTA, 1% Triton-X, 0.1% SDS, complete protease inhibitor cocktail (Roche), 100 μ mol/L Sodium Orthovanadate, and 10 mmol/L P-nitrophenylphosphate. 30 mg of extracted proteins were loaded on 4-12% acrylamide gels and Western blot analysis was performed using the following antibodies: β_1 AR (SantaCruz, sc-568), WHSC2 (Abcam, Ad1481), PLN (Novus Biological, NEB300-582), PLN P-16 (Abcam, Ab15000), AC ν I (Sigma SAB2100054), PRKACB (Sigma SAB1302543), α -tubulin (Abcam 18251), and GAPDH (Cell Signaling, 2128); HRP-secondary antibodies were from Cell Signaling. ECL (Thermo Fisher Scientific) was used for protein detection using a Chemidoc MP Imaging System (Bio-Rad) and densitometry analysis was performed using Image Lab software 5.0 (Bio-Rad).

Immunofluorescence analysis

Cultured CMs were fixed with 4% paraformaldehyde (PFA) for 30 min at 4°C, permeabilized with 1X PBS supplemented with 1% BSA and 0.1%

Triton X-100 (all from Sigma) and stained with antibodies against cleaved caspase-3 antibody (Cell Signaling Technology, 9662) or cardiac troponin I[175] diluted in 1X PBS supplemented with 1% BSA for 2 hours at 37°C. Cy3-conjugated secondary antibodies from the Jackson ImmunoResearch Laboratories were used and nuclei were counterstained with DAPI (Sigma). Cells were analyzed using a Leica TCS SP5 confocal microscope.

b₁AR Receptor Density

Myocardial sarcolemmal membranes were prepared by homogenizing whole hearts in ice-cold buffer containing 50 mM HEPES (pH 7.3), 150 mM KCl, and 5 mM EDTA. Total βAR density was determined by incubating 25 μg of the above homogenate with a saturating concentration of ¹²⁵I-cyanopindolol (125I-CYP) (Perkin Elmer) in 500 μl of binding buffer.[176] Nonspecific binding was determined in the presence of 20 mmol/L alprenolol (Perkin Elmer). Binding assays were conducted at 37°C for 60 min and terminated by rapid vacuum filtration over glass fiber filters, which were subsequently washed and counted in a gamma counter. Specific binding was reported as fmol of receptor per mg of membrane protein.

Apoptosis assay

Non-infected, Ad-Empty-, and Ad-miR133 infected nCMs were subjected to chronic treatment (72 hours) with 0.1, 1, and 10 (μmol/L) NE either in the absence or in presence of 0.1, 1, and 10 (μmol/L) of the b₂AR antagonist ICI, and compared to non-treated cells. The same experimental protocol was followed in CMs infected with Ad-Decoy[141] and relative non-infected and Ad-Empty infected controls. At the end of the pharmacological treatment, nCMs were fixed and co-stained with antibodies against cleaved caspase-3 and cardiac troponin I as described above. Neonatal CMs were analyzed using a confocal microscope and cell density as well as the number of caspase-3 positive CMs/total nCMs were estimated. Three coverslips for

each experimental group were analyzed and a total of three different cell cultures were tested.

Histochemical analysis

Histochemical analyses were performed on 5 mm thick paraffin sections of heart specimens. H&E- and Azan Mallory-stainings were performed as previously described.[177] For immunofluorescence staining, slides were heated in 10 mM sodium citrate (pH 6.0) for antigen retrieval. After rinsing in dH₂O, sections were incubated with antibodies against smooth muscle actin (Sigma, A2547) and desmin (Abcam, AB8592), and subsequently Cy2 and Cy3-conjugated secondary antibodies (The Jackson ImmunoResearch Laboratories) before counterstaining with Toto-3 (Life Technologies). Apoptosis was determined using the *In Situ* Cell Death Detection AP Kit (Boehringer Mannheim). Specimens pretreated with DNase I served as positive control. Fluorescence acquisition was performed using a Leica TCS SP5 confocal microscope.

Animals

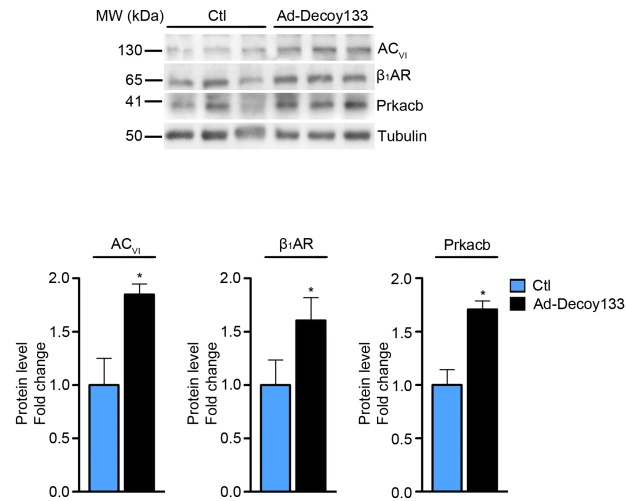
All mouse procedures on mice were performed according to institutional guidelines in compliance with national (4D.L. N.116, G.U., suppl. 40, 18-2-1992) and international law and policies (EEC Council-Directive 86/609, OJ L 358,1,12-12-1987; NIH Guide for the Care and Use of Laboratory Animals, US National Research Council-1996 and new directive 2010/63/EU). The protocol was approved by the Italian Ministry of Health. Special attention was paid to animal welfare and to minimize the number of animals used and their suffering. A targeting construct for inducible miR-133 expression was generated by cloning a DNA fragment containing the Tet operon, the minimal CMV promoter, the miR-133a-2 sequence, and a polyA termination sequence. Positive founder mice (F0) were crossed with mice expressing the reverse tetracycline-responsive transcriptional activator

rtTA under the control of the cardiac-specific α -Myosin Heavy Chain (α -MHC),[148] kindly provided by Dr. Wolfgang Dillmann (University of California San Diego, CA). Double transgenic mice (Tg) were backcrossed for six generations into the C57Bl/6J strain background. All experiments were performed on 12-week-old male mice with at least 8 animals per group. Induction of cardiac-specific expression of miR-133 in Tg mice was obtained by administration of doxycycline (Dox, 500 mg/Kg) to their food pellet as described in the text. Ctl receive the same Dox treatment as Tg133. For hemodynamic studies, cardiac catheterization was performed using a 1.4 French (0.46 mm) conductance catheter (Millar Instruments Inc.) inserted retrograde through the right carotid artery into the left ventricle, where pressure was recorded. A polyethylene-50 catheter was placed into the right external jugular vein for dobutamine infusion. True zero was obtained in saline at the end of each experiment and any offset was corrected. After bilateral vagotomy, basal pressures were again measured, and β -adrenergic responsiveness was assessed with graded doses of dobutamine, as described.[178] In β -blocker experiments, 2-month-old C57Bl/6J male mice were subjected to transverse aortic constriction (TAC), and metoprolol (350mg/kg/day, Sigma) was given in the drinking water as previously reported.[179] For each group, sham operated animals were used as controls. B-mode echocardiography and TAC were performed using standard techniques.[174]

Statistical analysis

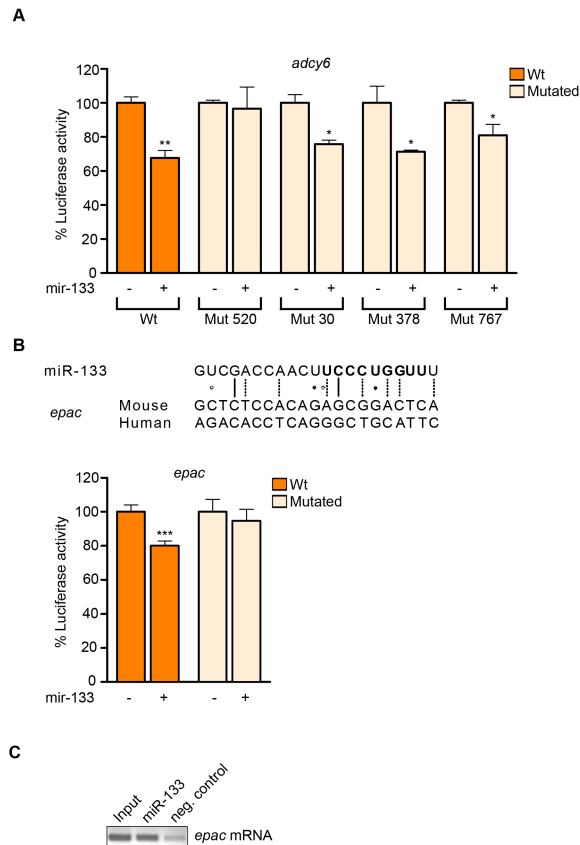
All data are expressed as mean \pm s.e.m. Comparison between experimental groups was performed using the unpaired Student's t-test or ANOVA tests using Prism 6.0 software (GraphPad Software, Inc.). A value of at least $P < 0.05$ was considered statistically significant.

Online Figures



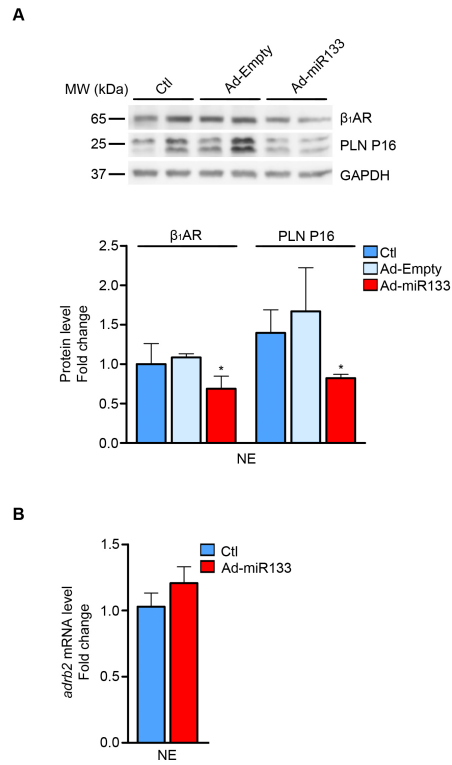
Online Figure I

Online Figure I. MiR-133 loss-of-function upregulates protein levels of β₁AR, Adcy6, and Prkacb. Western Blot and densitometric analysis for β₁AR, AC_{v1}, and Prkacb on total protein lysates from nCMs infected or not with Ad-Decoy133 (MOI = 50; n = 3). Tubulin was used as loading control. *, P < 0.05.



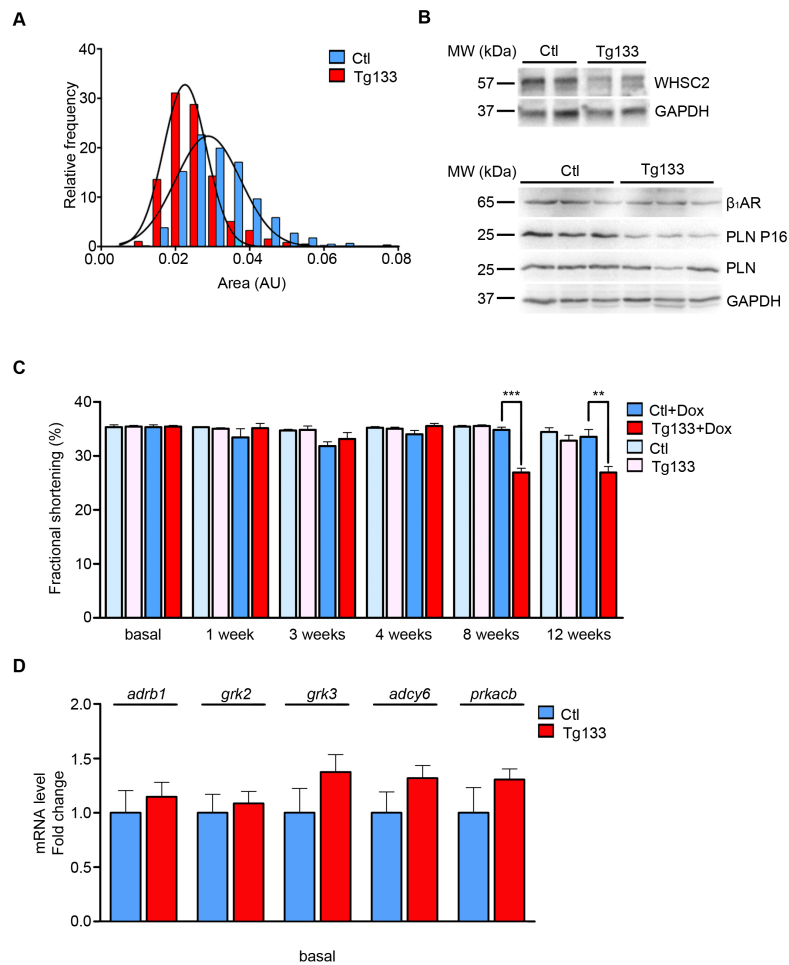
Online Figure II

Online Figure II. MiR-133 targets Adcy6 and Epac **A**, Luciferase reporter activity for all Adcy6 predicted sites (n=3). **B**, Conserved binding site for miR-133 in the 3'UTR of *epac* (**up**) and corresponding luciferase reporter activity (**bottom**) (n=3). For sequence alignments, filled and empty dots (□) represent conserved and non-conserved wobble pairs, respectively; continuous and dashed lines represent conserved or non-conserved residues, respectively. **C**, Representative PCR analysis of *epac* mRNA co-immunoprecipitated with biotinylated miR-133 oligo. Input = pre-immunoprecipitated RNA (positive control); miR-133 = biotinylated miR-133; neg; Control = no oligo (n= 3). *, P<0.05**, P < 0.01; ***, P < 0.001.



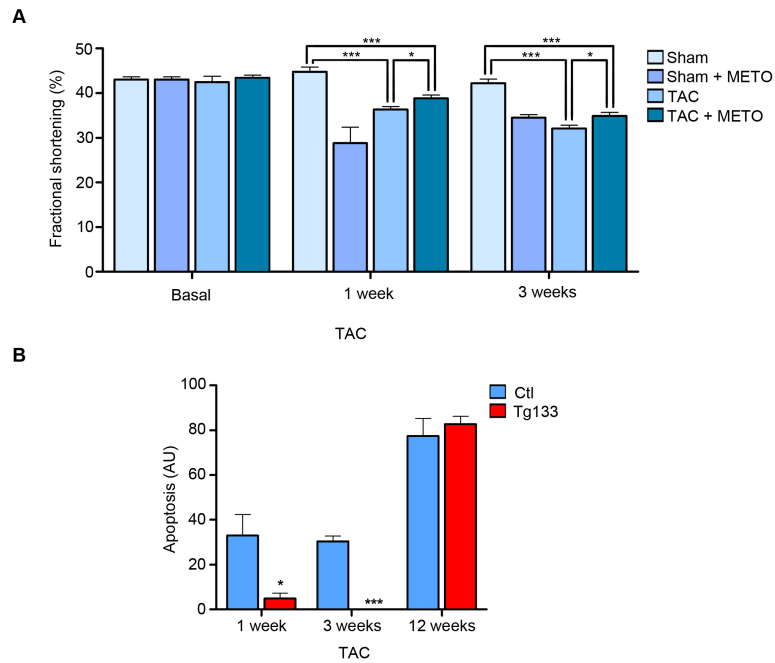
Online Figure III

Online Figure III. β_1 ARs, but not β_2 ARs are targeted by miR-133. A, Western blot and densitometric analyses for β_1 AR and PLN (total and phosphorylated form at the PKA consensus site, Ser16) on cell lysate from NE-treated miR-133 and control (non-infected and AdEmpty infected) nCMs (n = 3). GAPDH was used as loading control. **B,** *Adrb2* mRNA levels in NE-treated nCMs infected with Ad-miR133 compared to Ctl (n = 3). *, P<0.05.



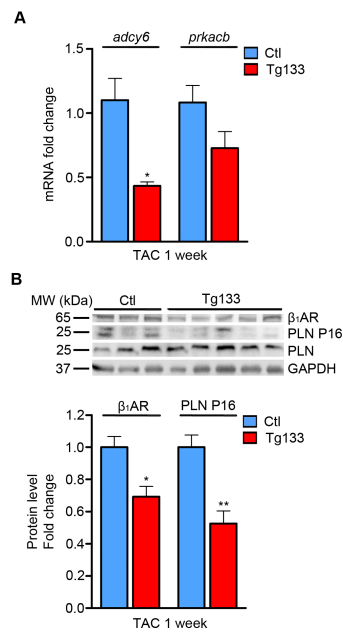
Online Figure IV

Online Figure IV. Tg133 mice **A**, Cell size measurements of single adult CMs isolated from Tg133 and Ctl mice 1 week after Dox administration (n = 600, 3 animals per group). **B**, Western blot analysis for expression of WHSC2 (**top**), β_1 AR, and PLN (total and phosphorylated form at the PKA consensus site, Ser16) (**bottom**) on left ventricular extracts from Tg133 and Ctl mice after 2 days of Dox administration (n = 3). GAPDH was used as loading control. **C**, Fractional shortening (%) in Tg133 and Ctl sham mice fed with normal or Dox-supplemented diet (n = 6). *, $P < 0.05$; **, $P < 0.01$; ***, $P < 0.001$. **D**, qRT-PCR on left ventricular extracts from Tg133 and Ctl mice after 2 days of Dox administration (n = 5).



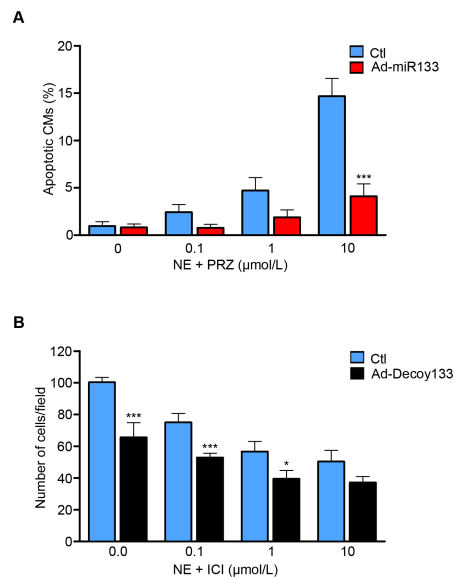
Online Figure V

Online Figure V. Metoprolol administration to TAC mice. **A**, Fractional shortening (%) in C57J/B6 mice administered or not with metoprolol at baseline as well as 1 and 3 weeks after TAC (n = 10). **B**, Quantification of apoptotic cells in heart sections from Tg133 and Ctl mice 1, 3, and 12 weeks after TAC. *, P<0.05; ***, P<0.005.



Online Figure VI

Online Figure VI. Tg133 mice subjected to TAC. A, qRT-PCR analysis for miR-133 target mRNAs in Tg133 compared to Ctl mice 1 week after TAC (n = 3). **B,** Western blot and densitometric analysis for β_1 AR and PLN (phosphorylated/total) on left ventricular lysates from Tg133 and Ctl mice 1 week after TAC. *, P<0.05; **, P<0.001.



Online Figure VII

Online Figure VII. MiR-133 determines the apoptotic response following β AR-chronic stimulation. **A**, Percentage of caspase-3 positive nCMs following NE-stimulation in the presence of the α -blocker prazosin (1 mmol/L). **B**, Cell density evaluated in cultures of Ctl and Ad-Decoy133 infected nCMs both at baseline and following 72 hours of treatment with NE in the presence of ICI (n=150 cells per group). *P < 0.05; *** P < 0.005.

Online Table I. Bioinformatic target prediction for miR-133. Validated targets are highlighted. dGduplex considers the binding free energy of the miRNA-target duplex, where the miRNA and the target pair according to the pairing forces imposed by the seed; dGopen describes the free energy lost by unpairing the target-site nucleotides; ddG represents the total miR-target interaction score that equals the difference between dGduplex and dGopen.

Target gene	Position	Seed	dGduplex	dGopen	ddG
<i>adrb1</i>	816	8:1:1	-19,05	-6,35	-12,9
<i>adrb1</i>	209	8:1:1	-11,85	-9,29	-2,55
<i>prkacb</i>	693	8:1:1	-15,06	-11,88	-3,17
<i>prkacb</i>	640	8:1:1	-8,95	-11,06	2,11
<i>epac</i>	60	7:1:1	-11,6	-11,19	-0,4
<i>epac</i>	180	7:1:1	-13,54	-12,26	-1,27
<i>epac</i>	103	7:1:1	-20,21	-13,23	-6,97
<i>gnai1</i>	648	8:1:1	-15,6	-12,77	-2,82
<i>gnai2</i>	334	8:0:1	-20,8	-16,25	-4,54
<i>gnai2</i>	65	8:1:1	-14,8	-14,8	0,42
<i>gnai3</i>	551	8:1:1	18,4	-9,31	-9,08
<i>gnai3</i>	40	8:1:1	-14,8	-6,96	-7,83
<i>gnai3</i>	87	8:0:1	-16,3	-12,36	-3,93
<i>gnai3</i>	511	8:1:1	-12,9	-11,26	-1,63
<i>gnai3</i>	1000	8:1:1	-9,1	-11,17	2,07
<i>gnas</i>	909	8:1:1	-18,46	-10,22	-8,23
<i>gnas</i>	481	8:1:1	-9,33	-9,71	0,38
<i>gnas</i>	453	8:1:1	-10,08	-12,22	1,42
<i>gnas</i>	528	8:0:1	-11,73	-13,25	1,52
<i>grk2</i>	447	8:1:1	-14,6	-16,96	2,36

<i>grk2</i>	1247	8:1:1	-21.3	-14.33	-6.96
<i>grk2</i>	254	8:1:0	-16.4	-13.28	-3.11
<i>grk2</i>	337	8:1:1	-18.2	-15.91	-2.28
<i>grk2</i>	2722	8:1:1	-14.8	-17.87	3.07
<i>adcy6</i>	378	8:1:1	-18.41	-7.52	-10.88
<i>adcy6</i>	30	8:0:0	-21.8	-14.66	-7.13
<i>adcy6</i>	767	8:1:1	-13.27	-13.55	0.28
<i>adcy6</i>	520	8:1:0	-16.9	-21.16	4.26

Online Table II. PCR and qPCR primers.

PCR

<i>Fw adrb1</i>	ctcatcgtggtgggtaacgtg
<i>Rev adrb1</i>	acacacagcacatctaccgaa
<i>Fw prkacb</i>	ttgccacaactgactggattgc
<i>Rev prkacb</i>	agtgtgagctccaggctatctt
<i>Fw adcy6</i>	agcacgttgccatggagatgaa
<i>Rev adcy6</i>	agcttgtaaaccgggcaaaga
<i>Fw epac</i>	tatctgcctagccctgcatctt
<i>Rev epac</i>	gccagctgaccttcattgttct

qPCR

<i>Fw pri-mir133a-1</i>	gggaacctetaatacctgtcatgc
<i>Rev pri-mir133a-1</i>	ggctgtccatgtgtaataatcaatgc
<i>Fw pri-mir133a-2</i>	gacagaacctatcttcttctggag
<i>Rev pri-mir133a-2</i>	agccttgaagagtccttgctg
<i>Fw adrb1</i>	ctcatcgtggggtaacgtg
<i>Rev adrb1</i>	acacacagcacatctaccgaa
<i>Fw adrb2</i>	gggaacgacagcgacttctt
<i>Rev adrb2</i>	gccaggacgataaccgacat
<i>Fw adcy6</i>	atctactgcttggcgtccat
<i>Rev adcy6</i>	agtccagcccatcaaaggt
<i>Fw prkacb</i>	aagcctagccaaagttgctg
<i>Rev prkacb</i>	gcagtgttcccatgacc
<i>Fw grk2</i>	gaaagcagacacaggcaaga
<i>Rev grk2</i>	acgagggaaagcatgatcc
<i>Fw grk3</i>	ctgttccccaacagactgg
<i>Rev grk3</i>	ggtcagtagactttgccgaga

Online table III. Echocardiographic parameters of Tg133 and Ctl mice at different time points post TAC.

	1 wk post TAC		3 wks post TAC		4 wks post		8 wks post		12 wks post	
	Tg133 (n=8)	Ctl (n=8)								
	±28.76 ±	±27.04 ±	±28.20 ±	±30.42 ±	±30.08 ±	±31.37 ±	±31.69 ±			
	0.53	0.90	0.63	0.45	1.25	1.22	1.16	1.15	1.27	
	±1.008 ±	±1.035 ±	±1.044 ±	±1.008 ±	±1.045 ±	±1.069 ±	±1.045 ±	±1.056 ±	±1.037 ±	
	0.008	0.002	0.009*	0.015	0.004	0.011	0.004	0.015	0.002	
	±3.115 ±	±3.533 ±	±3.646 ±	±4.089 ±	±3.646 ±	±4.197 ±	±3.886 ±	±4.329 ±	±3.963 ±	
	0.012	0.020	0.019*	0.063	0.049*	0.123	0.022	0.120	0.007*	
	±1.013 ±	±1.051 ±	±1.060 ±	±1.038 ±	±1.060 ±	±1.067 ±	±1.042 ±	±1.060 ±	±1.038 ±	
	0.007	0.005	0.003*	0.009	0.015	0.013	0.004	0.014	0.004	
	±1.310 ±	±1.343 ±	±1.345 ±	±1.294 ±	±1.345 ±	±1.388 ±	±1.355 ±	±1.366 ±	±1.357 ±	
	0.006	0.005	0.012	0.016	0.005*	0.013	0.006	0.011	0.006	
	±1.987 ±	±2.301 ±	±2.373 ±	±3.017 ±	±2.373 ±	±3.178 ±	±2.586 ±	±3.307 ±	±2.635 ±	
	0.026	0.033	0.020*	0.075	0.069*	0.155	0.027*	0.153	0.007*	
	±1.321 ±	±1.365 ±	±1.360 ±	±1.341 ±	±1.350 ±	±1.374 ±	±1.360 ±	±1.357 ±	±1.350 ±	
	0.007	0.003	0.004	0.006	0.006	0.023	0.005	0.006	0.004	
	±36.20 ±	±34.87 ±	±35.00 ±	±26.23 ±	±35.00 ±	±24.47 ±	±33.46 ±	±23.77 ±	±33.50 ±	
	0.60	0.57	0.39*	1.32	1.07*	1.43	0.53*	1.42	0.24*	
	±513 ±	±496 ±	±483 ±	±492 ±	±483 ±	±518 ±	±525 ±	±505 ±	±521 ±	
	8	10	7	13	6	9	5	11	9	

posterior wall thickness in diastole; IVSs, systolic intraventricular septal wall thickness; LVIDs, left ventricular end-systolic inner diameter; LVPWs, left ventricular posterior wall thickness in systole; FS, left ventricular fractional

Basal	
Ctl	Tg133
(n=8)	(n=8)
Weight	27.9927.76 ±
(g)	± 0.66 0.59
IVSd	0.951 ±0.974 ±
(mm)	0.013 0.008
LVIDd	3.094 ±3.125 ±
(mm)	0.048 0.008
LVPWd	0.978 ±0.955 ±
(mm)	0.010 0.041
IVSs	1.265 ±1.270 ±
(mm)	0.009 0.007
LVIDs	1.982 ±2.017 ±
(mm)	0.040 0.031
LVPWs	1.265 ±1.271 ±
(mm)	0.010 0.005
FS	35.97 ±35.48 ±
(%)	0.37 0.31
HR	504 ± 496 ±
(bpm)	9 7

References

1. Varrone F, Gargano B, Carullo P, Di Silvestre D, De Palma A, Grasso L, Di Somma C, Mauri P, Benazzi L, Franzone A, Jotti GS, Bang ML, Esposito G, Colao A, Condorelli G, Catalucci D. The circulating level of fabp3 is an indirect biomarker of microrna-1. *Journal of the American College of Cardiology*. 2013;61:88-95
2. Care A, Catalucci D, Felicetti F, Bonci D, Addario A, Gallo P, Bang ML, Segnalini P, Gu Y, Dalton ND, Elia L, Latronico MV, Hoydal M, Autore C, Russo MA, Dorn GW, 2nd, Ellingsen O, Ruiz-Lozano P, Peterson KL, Croce CM, Peschle C, Condorelli G. Microrna-133 controls cardiac hypertrophy. *Nature medicine*. 2007
3. Saggin L, Gorza L, Ausoni S, Schiaffino S. Troponin i switching in the developing heart. *The Journal of biological chemistry*. 1989;264:16299-16302
4. Koch WJ, Rockman HA, Samama P, Hamilton RA, Bond RA, Milano CA, Lefkowitz RJ. Cardiac function in mice overexpressing the beta-adrenergic receptor kinase or a beta ark inhibitor. *Science*. 1995;268:1350-1353
5. Catalucci D, Zhang DH, DeSantiago J, Aimond F, Barbara G, Chemin J, Bonci D, Picht E, Rusconi F, Dalton ND, Peterson KL, Richard S, Bers DM, Brown JH, Condorelli G. Akt regulates l-type ca²⁺ channel activity by modulating cavalpha1 protein stability. *The Journal of cell biology*. 2009;184:923-933

6. Suarez J, Gloss B, Belke DD, Hu Y, Scott B, Dieterle T, Kim YK, Valencik ML, McDonald JA, Dillmann WH. Doxycycline inducible expression of serca2a improves calcium handling and reverts cardiac dysfunction in pressure overload-induced cardiac hypertrophy. *American journal of physiology. Heart and circulatory physiology*. 2004;287:H2164-2172
7. Condorelli G, Drusco A, Stassi G, Roncarati R, Iaccarino G, Russo MA, Gu Y, Chung C, Latronico M, Napoli C, Sadoshima J, Croce CM, Ross J, jr. Akt induces enhanced myocardial contractility and cell size in vivo in transgenic mice. *Proc. Natl. Acad. Sci. USA*. 2002
8. Harding VB, Jones LR, Lefkowitz RJ, Koch WJ, Rockman HA. Cardiac beta ark1 inhibition prolongs survival and augments beta blocker therapy in a mouse model of severe heart failure. *Proceedings of the National Academy of Sciences of the United States of America*. 2001;98:5809-5814

Figure legends

Figure 1. MiR-133 targets key components of the β_1 AR transduction cascade. A-C, Conserved binding site for miR-133 in 3'UTRs of (**up**) and luciferase reporter activity (**bottom**) for *adbr1* (A), *adcy6* (B), and *prkacb* (C), respectively. For sequence alignments, filled and empty dots (\square) represent conserved and non-conserved wobble pairs, respectively; continuous and dashed lines represent conserved and non-conserved residues, respectively. For luciferase assays, 293 cells were co-transfected with 3' UTRs cloned into the psiCHECK-TM2 luciferase vector and miR-133 cloned into the pcDNATM6.2-GW/ EmGFP-miR vector. **, P < 0.01; ***, P < 0.001; n = 3. **D**, Representative PCR analyses of target mRNAs co-immunoprecipitated with biotinylated miR-133 oligo. Input = pre-immunoprecipitation RNA (positive control); miR-133 = biotinylated miR-133; neg; Control = no oligo. (n = 3).

Figure 2. MiR-133 modulates β_1 AR signaling *in vitro*. **A**, Effect of norepinephrine (NE, 10 nmol/L) on cAMP levels upon β_2 AR blockage with ICI (100 nmol/L) in control (blue) and Ad-miR133 (red) neonatal CMs transfected with the cAMP sensor Epac1-cAMPs (representative traces). Maximal cAMP accumulation was elicited with FRSK (25 mmol/L) and IBMX (100 mmol/L) **B**, Quantification of the average cAMP change measured in single cells upon β_1 AR stimulation with NE (10 nmol/L) and β_2 AR blockage with ICI (100 nmol/L). Values are expressed as % change in the 480 nm/545 nm emission ratio of Epac1-cAMP following NE stimulation and normalized to the

maximal response obtained with FRSK plus IBMX. cAMP accumulation was highly (about 60%) reduced in miR-133 overexpressing CMs (Ad-miR133, n = 9; controls, n = 10). **C**, Quantification of the average cAMP change measured in single cells upon selective β_2 AR stimulation with CLB (10 mmol/L), showing no significant changes in β_2 AR response (Ad-miR133, n = 8; Ctl, n = 10). ***, P < 0.001. No significant differences were observed in Ad-Empty infected cells compared to Ctl cells. MOI = 25.

Figure 3. MiR-133 modulates cAMP signaling *in vitro*. **A**, Effect of miR-133 on AC activity, as assayed in single cells expressing Epac1-cAMP and stimulated with the direct AC activator FRSK (5 mmol/L). The trace represents the average of 18 Ctl and 7 miR-133 overexpressing CMs. Bars indicate s.e.m. **B**, cAMP synthesis rate as estimated by measuring the % increase in the rate of 480 nm/545 nm Epac1-cAMP emission per minute upon stimulation with FRSK (5 mmol/L) (Ad-miR133, n = 7; Ctl, n = 18). MiR-133 overexpression causes a significant decrease in cAMP accumulation rate. **C**, Effect of miR-133 on PKA activity as assayed in single cells expressing AKAR3 and treated with the cell-permeable cAMP analogue 8-CPT-6-Phe-cAMP (10 mmol/L). A significant decrease in PKA phosphorylation rate of AKAR3 was found in miR-133 overexpressing CMs compared to control cells (Ad-miR133, n = 10; Ctl, n = 12). Bars indicate s.e.m. **P < 0.01. No differences were observed in Ad-Empty infected cells, compared to Ctl cells. MOI = 25.

Figure 4. MiR-133 affects β -adrenergic stimulation *in vivo*. **A**, mRNA expression levels of mature and precursor miR-133 in Tg133 mice compared to Ctl mice 2 days after Dox administration (n = 11). **B**, Cardiac β_1 AR density, as evaluated in a radioligand binding assay, was significantly reduced in Tg133 mice compared to Ctl mice after Dox administration (n = 11). **C**, Effect of selective β_1 AR stimulation with xamoterol on cAMP accumulation in adult CMs isolated from Tg133 and Ctl mice. No cAMP increase was observed in Tg133 CMs (n = 4). **D**, Evaluation of max dP/dt during dobutamine stress test in Tg133 mice and Ctl mice after Dox administration (Ctl, n = 8; Tg133, n = 9). Bars indicate s.e.m. *P < 0.05; **P < 0.01, ***P < 0.005; ****P < 0.001.

Figure 5. MiR-133 modulates cardiac dysfunction *in vivo*. **A**, Fractional shortening (%) in Tg133 and Ctl mice at baseline and after Dox administration at different time points (from 1 to 12 weeks) after TAC as determined by echocardiography (Ctl, n = 8; Tg133, n = 8). The graph shows significant cardioprotection in Tg133 mice. **B**, mRNA (**left panel**, qRT-PCR) and protein (**middle panel**, densitometric analysis of Western blot in Suppl. Figure 6B) levels as well as membrane receptor density (**right panel**, radioligand binding assay) of β_1 AR in Tg133 and Ctl mice 1 week after TAC. **C**, qRT-PCR for miR-133 on left ventricular extracts from TAC and sham operated mice both in the presence and absence of metoprolol (n = 10 mice per group). Metoprolol treatment prevented miR-133 downregulation 1 week after TAC. Bars indicate s.e.m. *P < 0.05; ***P < 0.005.

Figure 6. MiR-133 reduces cardiomyocyte apoptosis induced by chronic activation of β_1 AR signaling both *in vitro* and *in vivo*. **A**, Percentage of caspase-3 positive CMs evaluated in Ctl and Ad-miR133 nCMs treated or not with different doses of NE and ICI for 72 hours (n = 150 cells per group). MiR-133 overexpression reduces NE-induced apoptosis. MOI = 50. **B**, Percentage of caspase-3 positive cells evaluated in Ctl and Ad-Decoy133-infected nCMs treated or not with different doses of NE and ICI for 72 hours. Ad-Decoy-induced downregulation of miR-133 increases the percentage of apoptotic CMs compared to Ctl cells. No differences were observed in Ad-Empty infected cells, compared to Ctl cells (n = 150 CMs per group). MOI = 25. **C**, Tunel staining (green signal) of heart sections from Tg133 and Ctl mice 1, 3, and 12 weeks after TAC. Tissues were costained with desmin antibody (red signal) and nuclei were counterstained with Toto-3 (blue signal). Scale bar: 5 mm. **D**, qRT-PCR on left ventricular extracts from Tg133 and Ctl mice 1 week after TAC. The mRNA level of the pro-death *grk2* gene was reduced by ~20% in Tg133 compared to Ctl mice, while the *grk3* mRNA level was unchanged. Bars indicate s.e.m. *P < 0.05; **P < 0.01, ***P < 0.005.

Figure 7. Working model. Schematic representation of miR-133 targeting key components of the β_1 AR transduction cascade.

Novelty and Significance

What is known?

- MiR-133 expression is inversely related to cardiac hypertrophy and human cardiac disease;
- β -blockers are used for the treatment of cardiovascular diseases;
- β_1 -adrenergic receptor (β_1 AR) signaling exerts pro-apoptotic effects whereas miR-133 plays an anti-apoptotic role.

What New Information Does This Article Contribute?

- MiR-133 directly targets the β_1 AR transduction cascade at the level of β_1 AR, adenylyl cyclase VI (Adcy_{VI}), and PKA C-Beta (Prkacb);
- MiR-133 overexpression protects cardiomyocytes (CMs) against β_1 AR-dependent apoptosis;
- β -blockers prevent miR-133 downregulation in response to mechanical pressure overload by transverse aortic constriction (TAC), and transgenic mice with inducible and cardiac specific miR-133 show cardioprotection during TAC.

In conditions of pathological stress, activation of the β_1 AR signaling is a causative factor in the chain of events leading to the decline in cardiac function. In line with this, therapeutic use of β -blockers has been shown to ameliorate heart function. Based on a combination of *in vitro* and *in vivo* approaches, we here demonstrate that the β_1 AR

transduction cascade is directly regulated by miR-133, which is downregulated in response of ventricular pressure overload. In particular, we found that *i)* miR-133 overexpression reduces cAMP accumulation in β_1 AR-agonist-treated neonatal and adult CMs, and *ii)* mice with inducible and cardiac-specific overexpression of miR-133 show cardioprotection during TAC by preventing, at least in part, the activation of pathological effects (*e.g.* apoptosis) due on β_1 AR activation. Thus, we demonstrate for the first time a direct correlation between β_1 -adrenergic signaling and miR-133 and provide proof of concept that restoration of miR-133 levels in conditions of heart failure (HF) might be used as a potential novel therapeutic strategy for the treatment of HF patients.

Chapter 5

Bio-Inspired Negatively-Charged Calcium Phosphate Nanocarriers for Cardiac Delivery of MicroRNAs

Di Mauro V, Iafisco M, Salvarani N, Vacchiano M, Carullo P,
Ramírez-Rodríguez GB, Patrício T, Tampieri A, Miragoli M,
Catalucci D.

Published on Nanomedicine (Lond). 2016 Apr;11(8):891-906. doi:
10.2217/nmm.16.26. Epub 2016 Mar 16.

ABSTRACT

Aim: To develop biocompatible and bioresorbable negatively-charged calcium phosphate nanoparticles (CaP-NPs) as an innovative therapeutic system for the delivery of bioactive molecules to the heart.

Materials & methods: CaP-NPs were synthesized via a straightforward one-pot biomineralization-inspired protocol employing citrate as a stabilizing agent and regulator of crystal growth. CaP-NPs were administered to cardiac cells *in vitro* and effects of treatments were assessed. CaP-NPs were administered *in vivo* and delivery of microRNAs was evaluated. **Results:** CaP-NPs efficiently internalized into cardiomyocytes without promoting toxicity or interfering with any functional properties. CaP-NPs successfully encapsulated synthetic microRNAs, which were efficiently delivered into cardiac cells *in vitro* and *in vivo*. **Conclusions:** CaP-NPs are a safe and efficient drug-delivery system for potential therapeutic treatments of polarized cells such as cardiomyocytes.

Keywords: Calcium Phosphate Nanoparticles, microRNA, cardiomyocytes, nanomedicine, drug delivery systems

Cardiovascular disease (CVD) is a worldwide growing problem that afflicts close to 1% of the population and causes 17.3 million annual premature deaths (http://www.who.int/cardiovascular_diseases/en/). Causes include ischemic, toxic, genetic, post-inflammatory, and structural defects, overall resulting in a mortality of ~50% within 5 years from diagnosis [180]. Clinical management of CVDs has improved during the last decades, but despite significant

advancements, these pathologies still lead to a poor quality of life and reduced longevity. Moreover, the prognosis has been described as more malignant than cancer. Altogether, this entails the critical need to further understand the mechanisms underlying CVDs, to identify innovative therapeutic compounds, as well as to develop more efficient and safe drug-delivery systems. MicroRNAs (miRNAs; miRs) are small regulatory RNA molecules shown to be disease-specific biomarkers and key regulators of cardiac dysfunction [181, 182]. In line with this, significant effort has been put into developing new therapeutic tools designated to correct levels of miRNAs found to be dysregulated in CVDs [183]. Modified antisense oligonucleotides such as 2-O-methyl-modified ones, antagomirs, and locked nucleic acids have been largely applied for therapeutic knockdown of miRNA levels both in *in vitro* and *in vivo* models of CVDs [181]. On the other hand, approaches aimed at increasing the *in vivo* levels of miRNAs are still not optimal and require drastic improvements and new solutions. In fact, current miRNA mimics in terms of *in vivo* delivery, stabilization, efficacy of over-expression, and cell targeting, have resulted so far to be inadequate, with use of miRNA-expressing adeno-associated viruses (AAV) as the only alternative strategy [173, 184]. However, the long-term miRNA expression associated with AAV technology drastically limits any therapeutic approach that requires short-term and/or interval drug administration.

Nanoparticle (NP) delivery platforms hold great promise to overcome such limitations, providing an alternative strategy for more efficient, controlled, and safe drug-delivery approaches. In fact, NPs potentially bind and deliver a large plethora of agents such as

conventional drugs and more recently, nucleotides [185-187]. Additionally, NPs can offer a substantial protection of the payload against immediate diffusion from or degradation in the bloodstream and at the injury site, thus enabling controlled drug release and sustained therapeutic stimulus [187]. However, while largely investigated in the cancer field, the development and use of efficient NPs for the treatment of CVDs is still in its infancy. In fact, to the best of our knowledge, only liposomes, NPs based on synthetic polymers or silica, and micelles have been investigated so far for the delivery of various therapeutic molecules to myocardial cells [188-192]. However, in many cases, their use is drastically limited due to the lack of biocompatibility, reduced or very slow biodegradability [193], uncontrolled drug release in the bloodstream, poor encapsulation efficacy, and poor stability during storage [194]. Additionally, optimization of the synthesis of cardiac-compatible NPs requires improved colloidal stability, and specific size, shape, and surface charge [195]. In line with this, we recently demonstrated that polystyrene latex NPs are less toxic for cardiac cells when generated with a negative surface charge, which is compatible with the intrinsic charge of well-polarized excitable cells (*i.e.* cardiomyocytes) and facilitates the formation of life-compatible nanopores and cellular internalization of NPs [196]. However, the slow dissolution and cell accumulation of polystyrene latex restricts the use of these NPs for therapeutic approaches. In summary, there is still a strong need for the identification of new formulations based on biocompatible and biodegradable negatively-charged NPs to overcome the limitations of NPs currently used for CVD treatment.

The aim of the present study was the generation of innovative and effective negatively-charged calcium phosphate nanoparticles (CaP-NPs) for the delivery of novel therapeutic drugs (*i.e.* miRNAs) into cardiac tissue. To this end, a simple and straightforward one-pot mineralization synthesis protocol using citrate as stabilizing agent has been adopted. The biocompatibility and the mechanism of internalization of CaP-NPs in cardiac cells were obtained and the proof-of-concept for the ability of CaP-NPs to deliver miRNAs *in vivo* into cardiac tissue was provided.

Material & Methods

Synthesis of calcium phosphate nanoparticles

Functional CaP-NPs were generated according to a quick and simple protocol. Briefly, two aqueous solutions of (a) CaCl₂ (10-50 mM) + Na₃Cit (40-200 mM) and (b) Na₂HPO₄ (12-60 mM) were mixed (1:1 v/v, 5 mL total) and the pH was adjusted to 8.5, adding NaOH aqueous solution. The mixed solution was kept in a water bath at 37 °C for different times ranging from 5 to 60 min. When drug conjugation was performed, aqueous solution of synthetic unmodified and unprotected miRNA duplexes (1-10 µg/ml, IBA, Germany) was added to the above mixed solution. To remove unreacted reagents, the CaP-NP suspension was washed three times by centrifugation or dialyzed for 6 hours across a cellulose dialysis membrane with a cut-off of 3500 Da and immersed in 400 mL Milli-Q water. The suspension was recovered and stored in a fridge at 4 °C. The amount of CaP was evaluated by freeze-drying the sample suspensions and

weighting the inorganic residual. The final concentration of aqueous CaP suspension ranged from 60 to 300 $\mu\text{g/ml}$ as a function of reagent concentration.

Characterization of CaP-NPs and CaP-NP-miRs

Size distribution and surface charge of CaP-NPs were evaluated by dynamic light scattering (DLS) and ζ -potential, respectively. CaP-NP suspensions were characterized without any dilution by DLS using a Zetasizer Nano Series (Malvern, UK) by backscatter detection ($\lambda=630$ nm, $\theta=173^\circ$). Particle size (reported as Z-average of hydrodynamic diameter) was calculated as the average of three measurements of 10 runs for 10 seconds at 37 °C. ζ -potential measurements through electrophoretic mobility were carried out with a Zetasizer Nano analyzer (Malvern, UK) using disposable folded capillary cells (DTS1061; Malvern, UK) at 25 °C, suspending CaP-NPs in 10 mM HEPES buffer at pH 7.4. Three separate measurements (100 runs each) were collected in each case. Colloidal stability, size, and photon counts were recorded continuously for 300 min. Infrared spectra of freeze-dried samples were collected using a Nicolect 380 spectrometer (Thermo Fisher Scientific, USA) with a resolution of 2 cm^{-1} . 1 mg of sample was mixed with 150 mg of anhydrous potassium bromide (KBr). The mixture was pressed at 10 T pressure into a 7 mm diameter disc. A pure KBr disk was used as blank. Transmission electron microscopy (TEM) images and energy dispersive X-Ray (EDS) spectrum were collected using a FEI Tecnai F20 ST microscope operating at 200 kV. An aliquot of 20 μL of CaP-NP suspension was placed on carbon/formvar coated-copper grid for 5

min. The grid was then washed with ultrapure water and dried by manual blotting.

Cell line and primary cell culture

HL-1 cells were grown in Claycomb medium (Sigma-Aldrich) supplemented with 10% FBS (Sigma-Aldrich), 1% penicillin-streptomycin (Pen-Strep 10000 U/ml, Lonza), 1% ultraglutamine 1 (200 mM, Lonza), and 1 mM norepinephrine (Sigma-Aldrich) in gelatin/fibronectin pre-coated T75 flasks. After reaching full confluence, cells were split 1:3 according to Dr. Claycomb's instructions [197]. Adult cardiomyocytes were isolated as previously described [177, 198].

Viability, cytotoxicity and caspase 3-7 assays

Trypan blue assay. HL-1 cells were seeded at 10×10^4 cells/well in pre-coated 24-well plates (1 h, 37 °C). All experiments were performed in triplicate. The day after seeding, HL-1 cells were washed with PBS 1X and treated with different doses of CaP-NPs, ranging from 500 µg/ml to 3.9 µg/ml. After 24 h, HL-1 cells were collected with trypsin-EDTA, re-suspended in Claycomb complete medium, and counted in a Trypan blue solution (Sigma-Aldrich). The percentage of dead cells over total number of cells was calculated.

Viability, cytotoxicity, and caspase 3-7 assays. HL-1 cells or freshly isolated adult cardiomyocytes were seeded at 1×10^4 cells/well density in pre-coated 96-well plates (1 h, 37 °C), and different doses of CaP-NPs were administered as specified in the text. All experiments were performed in triplicate. Viability, cytotoxicity, and caspase-3/7

activities were measured using the ApoTox-Glo triplex Assay (Promega™), according to the manufacturer's instructions. Fluorescence and bioluminescence reactions were measured using a Synergy™ H4 Hybrid Multi-Mode Microplate Reader (BioTek).

Inhibition of endocytosis

Clatrin inhibitor (PitStop2, abcam) and dynamin inhibitor (MiTMAB, abcam) were used at 1 μ M. After 30 min incubation at 37 °C, cells were treated with CaP-NPs for 24 h and processed as described in the text.

RNA isolation and quantification

Total RNA was extracted using PureZol Reagent (Biorad). Reverse transcription of RNA for miR-133, cel-miR-39, and U6 was performed using the miRCURY LNA™ Universal RT microRNA PCR Polyadenylation and cDNA synthesis kit (Exiqon). Quantitative polymerase chain reaction (qPCR) was performed with microRNA LNA™ PCR primers (Exiqon) using the GoTaq® qPCR Master Mix (Promega). Relative expression was calculated using the $\Delta\Delta$ (Ct) method.

Luciferase assay

The miR-133 luciferase sensor [198] was transfected into HEK-293 cells using Lipofectamine 2000 (Invitrogen), following the manufacturer's protocol. After 5 h, cell medium was changed and miRNA-loaded CaP-NPs added to the medium. 6 h post-treatment,

cells were lysed and luciferase activity was measured as described by the manufacturer (Promega).

Confocal microscopy

HL-1 cells were seeded at 5.0×10^4 cells/well on VWR Micro cover slips coated with gelatin/fibronectin in complete Claycomb medium, and then incubated overnight at 37 °C, 5% CO₂. The following day, HL-1 cells were treated with CaP-NP-FITC. 24h post treatment, cultured cells were fixed using 4 % paraformaldehyde at room temperature, followed by treatment in PBS containing 0.2 % Triton X-100 (PBST) for 5 min. After three washes with PBS, nuclei were counterstained with DAPI (4',6-Diamidino-2-Phenylindole, Dihydrochloride, Life Technology) for 5 min at room temperature. Fluorescent images were taken with a laser scanning confocal microscope (Olympus, FV1000/SIMS)

[177].

Patch-Clamp recordings

Electrophysiological parameters of HL-1 cells and primary ventricular cardiomyocytes freshly isolated from adult mouse were measured using standard whole-cell voltage clamp and patch-clamp techniques. Experiments were conducted at room temperature. Patch pipette filling solution contained (in mmol/L): K-aspartate 120, NaCl 10, MgATP 3, CaCl₂ 1, EGTA 10, and Hepes 5 (pH 7.2) with a free cytosolic Ca²⁺ concentration of 10⁻⁸ M. Analog signals were amplified, digitized (2.8 kHz), and filtered (1 kHz) with an MultiClamp 700B patch clamp amplifier integrated with an Axon's

Digidata 1440A AD/DA interface, and stored on a computer for off-line analysis using Clampfit v.10.3. Experimental protocols were controlled using Clampex software (version 10.3 of pClamp, Axon Instruments). Pipette resistances ranged from 2 to 3 MOhm and pipette potentials were zeroed before cell contact. Liquid junction potential corrections calculated by the pClamp software were performed off-line after experiments. Preparations were superfused with Hank's balanced salt solution (pH 7.40, buffered with 10 mmol/L HEPES) at 2-3 ml/min at RT. Seal resistances were 2-10 GOhm. Rupturing the cell membrane in the patch resulted in access resistances of 2-10 MOhm. Clampex patch clamp amplifier allowed series resistances (70% to 90%) and whole cell capacitances electronic compensation. Action potentials (APs), resting membrane potential (RMP), input resistance (R_{in}), membrane capacitance (C_m) as well as sodium (I_{Na}), calcium ($I_{Ca,L}$) and net membrane currents (NMCs) were measured in both single HL-1 and adult ventricular cardiomyocytes in current and voltage clamp mode. RMP was measured in current clamp modality, applying 10 sec long current stimuli with the current value set to zero ($pA=0$). C_m was measured utilizing a sinusoidal voltage stimulus and processing the resulting sinusoidal current using a phase-sensitive detector or "lock-in amplifier" implemented either in Clampex hardware or software. R_{in} was calculated from voltage changes in response to 5 pA hyperpolarizing current steps from holding potentials. APs from which parameters as AP threshold (APTh), amplitude (APA), duration (APD₉₀) and maximal upstroke velocity (dV/dt_{max}) were measured, were elicited with depolarizing current steps of 10 pA (3 ms) until threshold-APs were obtained.

Threshold-Aps were after repeated 10 times at a rate of 1Hz and the 10th AP used for measurements.

To study the effect of nanoparticles (NPs) on I_{Na} , $I_{Ca,L}$ and NMCs of HL-1 cells and adult ventricular cardiomyocytes, standard step protocols and downward directed ramp were applied. In downward directed ramp protocols, the membrane was clamped from 50 to -110 mV over 5000 ms (32 mV s^{-1} in order to inactivate voltage gated ion channels) from a holding potential of -80 mV for two times at a rate of 0.1 Hz and $I_{Ca,L}$ was blocked by addition of 0.2 mM nifedipine. To obtain sodium current I-V relationships, 100 ms long voltage steps were applied, ranging from -90 to 65 mV from a holding potential of -80 mV at a rate of 0.33 Hz. Calcium I-V relations were obtained by measuring activated currents at different test potentials (300 ms, from -30 to 75 mV at a rate of 0.25Hz) from a holding potential of -40 mV. Steady state activation curves were derived from each I/V relation and were described by fitting experimental points with the Boltzmann equation. To take into account the variations in cell size, current amplitude were normalized to C_m through all measurements. In sodium current experiments, the patch pipette filling solution, and the Hank's balanced salt solution were properly modified in order to bypass technical issues related to the capacity of the patch clamp amplifier to track the fast sodium change in current and series resistance. Patch clamp current and voltage traces were acquired at least at 5kHz, depending on the protocol applied.

Cardiomyocyte contractility and Ca²⁺ transient recordings

Adult cardiomyocytes and HL-1 cells were loaded with 1 μ M Fura-2 acetoxymethyl (ThermoFischer Scientific), field stimulated at 1.0 Hz and recorded using an IonOptix System (Milton, MA, USA), as previously described [177].

Statistics

Values are given as mean \pm SD. Data were compared using the 2-tailed Student *t* test or Two-Way ANOVA and Bonferroni Test. Differences between data sets were considered significant at $p < 0.05$. All data were analyzed using Prism 6.0 software (GraphPad Software, Inc.).

Mice

All procedures on mice were performed according to institutional guidelines in compliance with national (D.L. N.26, 04/03/2014) and international law and policies (new directive 2010/63/EU). The protocol was approved by the Italian Ministry of Health. Special attention was paid to animal welfare and to minimize the number of animals used and their suffering. All experiments were performed on 10-week-old C57B6J male mice. Solutions were administered by retro-orbital administration as described elsewhere [199].

Results & Discussion

Synthesis and characterization of CaP-NPs

Living organisms adopt complex biomineralization processes to produce nanostructured materials endowed with high biocompatibility and stability [200]. These nano-materials, when synthetically prepared

with chemical-physical features very close to the biogenic ones, can therefore be ideal systems for biomedical applications, particularly as nano-carriers for drug delivery [201, 202]. Synthetic biomimetic CaP-NPs, which resemble the main inorganic component of bones, teeth, and also some pathological calcification, show high biocompatibility and pH-sensitive stability that facilitates the complete release of payload upon dissolution in biological acidic environments such as endosomes and lysosomes [203-205]. The complete dissolution of CaP in its ionic constituents (Ca^{2+} and PO_4^{3-}) prevents undesirable NP accumulation in cells and tissues, a drawback often encountered with other inorganic and metallic NPs [206]. Based on this evidence, we generated CaP-NPs using a one-pot synthesis method, in which the biocompatible organic molecule citrate plays a relevant role in the mechanism of CaP crystallization. The benefit of citrate-based synthesis concerns the stabilization of CaP-NPs at the early stage of crystallization, which is due to the binding of citrate ions to the CaP surface. In fact, whereas a broad distribution in particle size is obtained when calcium and phosphate are mixed in solution in the absence of crystal-growth inhibitor, the adjustment of the citrate amount in solution allowed us to control morphology, crystallinity, and size of CaP-NPs [207]. Notably, a similar effect might occur *in vivo* in bones where citrate interacting at the surface of biogenic apatite nanocrystals (citrate accounts for about 5.5 wt% of the total organic component of bone tissue nanocrystals) can limit their further growth and renders the mineral surface more hydrophobic to interact with collagen [207, 208].

Dynamic Light Scattering (DLS) was used to monitor the effect of citrate on size and colloidal stability of CaP-NPs. Mean particle size (reported as Z-average) as well as count rate of the reaction medium were continuously recorded for 60 min. As shown in **figure 1a**, incremental doses of sodium citrate (Na_3Cit) significantly limited the growth of CaP-NPs, as evidenced by the slow increase in the mean particle size as a function of the crystallization time. Moreover, higher Na_3Cit concentrations also improved the colloidal stability of NPs as shown **figure 1b** where the count rate of CaP-NPs prepared in the presence of 40 and 80 mM of Na_3Cit remained nearly constant for 60 min compared to conditions at 0 and 20 mM Na_3Cit . These results confirmed that no sedimentation occurred. Therefore, an initial Na_3Cit concentration of 80 mM was selected for the further studies since it gave the best results in terms of size and colloidal stability of CaP-NPs.

The next step was to determine the most suitable time for crystallization through the evaluation of the chemical structure, size, and surface charge of CaP-NPs. At determined crystallization times ranging from 5 to 30 min, CaP-NPs were washed three times by centrifugation, freeze-dried and then analyzed by Fourier Transform Infrared spectroscopy (FT-IR) and DLS. **Figure 1c** displays the FT-IR spectra of CaP-NPs crystallized at different times showing the typical bands of CaP compound [(*i.e.* PO_4^{3-} vibration bands at 560–603 (ν_4), 962 (ν_1), and 1000–1104 cm^{-1} (ν_3) [209]]. Moreover, since the synthesis was not carried out under inert gas, FT-IR spectra exhibited bands at 870 (ν_2) and 1420 cm^{-1} (ν_3) assignable to CO_3^{2-} vibrations, which are characteristic for non-apatitic carbonates and B-type

carbonate substitution (CO_3 substitution for PO_4^{3-}), respectively [209]. The band at *ca.* 1600 cm^{-1} , assignable to citrate (ν_{asOCO}) [209], was also clearly visible in all samples. In addition, the narrowing of the bands at $560\text{-}603\text{ cm}^{-1}$ revealed that amorphous CaP turned into a more crystalline state, following a time-dependent process. The amorphous to crystalline transformation was quantitatively evaluated by means of the splitting factor (**Table 1**), a well-reported index for the evaluation of crystallinity degree of CaP-based materials [210]. Additionally, while an increase in CaP-NP size was observed as a function of crystallization time, no significant variation was found for ζ -potential and polydispersity index (PDI), which remained stable under all conditions (**Table 1**). In particular, ζ -potential values were negative, indicating that citrate covered the surface of NPs, thus providing a negative surface charge.

To remove any unreacted ions after 5 min of crystallization, which gave the most promising results in terms of size of CaP-NPs for the further application as drug delivery system, we applied a dialysis step that, in contrast to other purification procedures, such as centrifugation and freeze-drying or even purification by desalting columns, prevents some irreversible agglomeration of adjacent particles. Thus, the removal of unreacted ions was assessed by measuring the conductivity of the dialysis medium (outside the membrane) as a function of time, which showed a plateau after 6 hours of treatment (**Supplementary Figure 1a**). This conductivity plateau indicated that the equilibrium of ionic exchange from the reaction medium to the dialysis medium was reached and a large majority of the unreacted ions were removed. Z-average, PDI, and ζ -

potential of CaP-NPs after 6 hours of dialysis were 129 ± 2 nm, 0.18 ± 0.10 , and -31.5 ± 1.5 mV, respectively. These results indicated that dialysis, in contrast to the washing step via centrifugation (data not shown), drastically decreased the mean size of CaP-NPs as well as narrowed size distribution (low PDI) while preserving a constant negative ζ -potential, which is a fundamental prerequisite for the use of nano-carriers in excitable cardiac cells [196]. In addition, the stability of CaP-NPs after washing by dialysis was evaluated by DLS measurements for 300 min (**Supplementary Figure 1b**). A constant particle size as well as mean count rate demonstrated that neither aggregation nor sedimentation occurred.

Finally, morphological analysis by Transmission Electron Microscopy (TEM) revealed CaP-NPs as round shape particles of about 20–50 nm in diameter (**Figure 1d**). The smaller size determined by TEM in comparison to that quantified by DLS is consistent with the ability to analyze the dried solid material diameter via the TEM technique in contrast to DLS, which gives the hydrodynamic size distribution in suspension of solid particle, organic layers, and surrounding liquid. Moreover, selected area electron diffraction (SAED) pattern (**Figure 1d**, inset) confirmed their amorphous nature (*i.e.* presence of diffuse rings rather than spots) while energy dispersive X-ray (EDX) analysis (**Supplementary Figure 1c**) corroborated their chemical composition (*i.e.* presence of Ca and P together with C, O, and Cu from the copper grid coated with carbon/formvar support film).

CaP-NP biocompatibility and cellular internalization

Our next objective was to test the biocompatibility of optimized CaP-NPs by subjecting HL-1 cardiac cells to incremental doses of CaP-NPs (0 to 500 $\mu\text{g}/\text{ml}$). As demonstrated by Trypan blue exclusion assay (**Figure 2a**), HL-1 cells largely tolerated an acute administration of CaP-NPs, showing an increase in mortality rate only at higher doses (>125 mg/ml) and 24 h post administration. This finding was further supported by a viability, cytotoxicity and caspase 3-7 assay, which showed a significant increased levels of apoptotic activity only with chronic administration of higher concentrations (≥ 250 mg/ml) of CaP-NPs (**Figure 2b and Supplementary Figure 2**). We tested biocompatibility also on adult cardiomyocytes subjected to the same dose/responses for CaP-NPs and no differences were observed (**Supplementary Figure 3**). Based on these results, a concentration of 20 mg/ml was chosen for the subsequent studies.

Cellular internalization was evaluated by exposing HL-1 cells to CaP-NPs conjugated to the fluorescein isothiocyanate (FITC). Confocal microscopy revealed distinct vesicular compartmentation, confirming the internalization of CaP-NP-FITC (**Figure 2c**). To determine whether the internalization was due to active mechanisms of endocytosis, specific inhibitors of clathrin and dynamin, which are involved in the initial processes of endocytosis and invagination from the plasma membrane, were used. Following pre-treatment with these inhibitors, HL-1 cells were exposed to increasing concentrations of CaP-NPs, and a Trypan blue exclusion assay was performed as described above. In accordance with our previous studies of negative-charged nanoparticles [211], inhibition of dynamin- and clathrin-

mediated endocytosis significantly reduced cellular toxicity at all doses of CaP-NPs, suggesting that internalization occurs via conventional clathrin- and dynamin-mediated endocytosis (**Figure 2a**). Altogether, the above findings demonstrate that CaP-NPs efficiently internalize into the cytoplasmic intracellular space of cardiac cells without inducing toxicity or apoptosis.

Effects of CaP-NPs on cardiomyocyte function

One of the main concerns in using calcium-based NPs is their potential interference with functional properties of excitable and contractile cells, such as cardiomyocytes. Thus, to evaluate any potential effect that CaP-NPs might have on cellular physiological properties and functions, a complete electrophysiological evaluation was performed on HL-1 cells as well as primary ventricular cardiomyocytes freshly isolated from adult mouse. To this end, HL-1 and adult cardiomyocytes were exposed to 20 $\mu\text{g/ml}$ of CaP-NPs for 24 hours (chronic stimulation) or 5 hours (acute stimulation), respectively. As shown in **Supplementary Figure 4**, results from voltage clamp experiments showed no effect of CaP-NPs on any of the typical characteristics of cell excitability, including membrane potential (V_m), membrane capacitance (C_m), membrane resistance (R_m), threshold of the action potential (AP), AP amplitude (APA), maximum speed of ascent of the AP (dV/dt_{max}), and AP duration (APD). Similarly, analyses of the main ionic currents underlying the typical cardiac cell AP (sodium, calcium and potassium currents measured by appropriate steps and ramp protocols) showed no significant differences between controls and treated cells under both

chronic (**Figure 3**) and acute conditions (**Figure 4**). Ramps protocols shown in figure 3a and 4a,b were used to measure net membrane currents which represent the activation of at least three time independent or slowly activating K^+ currents (I_{K1} , I_{Kr} and I_{Ks}). [212].

Finally, we evaluated adult cardiomyocyte contractility and intracellular calcium transients, a process associated with the excitation-contraction coupling of cardiac cells [213]. As shown in **Supplementary Table 1**, no significant alterations were found between treated and untreated conditions, further supporting the evidence that administration of CaP-NPs does not alter cellular functional properties of cardiac cells. Similarly, no significant alterations in intracellular calcium transients were found in HL-1 treated cells (**Supplementary Table 2**).

Taken together, these findings indicate good biocompatibility of CaP-NPs for cardiac cells, suggesting their potential use as drug nanocarriers for CVDs.

CaP-NPs encapsulate and deliver miRNAs into cardiac cells

We next asked whether CaP-NPs can efficiently bind synthetic compounds (*e.g.* miRNAs) and thus potentially be used as effective nanocarriers for intracellular drug delivery. For this purpose, different amounts of synthetic unmodified and unprotected miRNA duplexes (ranging from 1 to 10 $\mu\text{g mL}^{-1}$) were added to the reaction medium during the one-pot CaP-NP synthesis protocol described above. DLS analysis revealed that the size of CaP-NP-miRNAs (CaP-NP-miRs) increased as a function of miRNA amount, while PDI values and surface charge remained close to those of miRNA-free CaP-NPs

(**Table 2**). The increase in size could be associated with an effective interaction of miRNAs with CaP-NPs, while unaltered surface charge and PDI indicated that also in this case citrate homogeneously covered the NP surface. A scheme of a possible formation mechanism of CaP-NP-miRs is shown in **Figure 5a**. TEM analysis of CaP-NP-miRs (**Figure 5b**) revealed round shape NPs of approximately 20-30 nm in diameter similar to miRNA-free CaP-NPs. In addition, the presence of diffuse rings in the SAED pattern of CaP-NP-miRs (**Figure 5b** inset) validated their amorphous nature, suggesting that the presence of miRNA under these experimental conditions did not induce or accelerate the crystallization mechanism of CaP-NPs.

To evaluate the efficiency of miRNA delivery, we exposed HL-1 cells to CaP-NP-miRs (carrying either the muscle-enriched miR-133 or the not-mammalian *C. elegans* cel-miR-39-3p) and measured intracellular levels of miRNAs at different time points post-treatment. For these experiments CaP-NP-miRs were prepared using the maximum initial concentration of miRNA. As shown in **Figure 6a,b**, qRT-PCR analyses of total RNA revealed an effective time-dependent increase in the levels of intracellular delivered miRNA, confirming the effective encapsulation of both miRNAs into CaP-NPs as well as their cellular uptake. A similar result of CaP-NP-mediated uptake of miRNA was confirmed in adult cardiomyocytes (**Supplementary Figure 5**). Additionally, a cell-based luciferase assay confirmed that the administered CaP-NP-miR-133 efficiently repressed a miR-133-specific target [198] (**Figure 6c**).

Altogether, our findings provide evidence that functionalized CaP-NPs possess an intrinsic ability to carry functional miRNAs into cardiac cells.

Uptake of CaP-NP-miRs *in vivo*

As a final step, we evaluated as a proof-of-concept the *in vivo* efficiency of CaP-NPs as drug delivery system. In particular, CaP-NP-miRs (complexed with the exogenous cel-miR-39-3p) were administered to 10-week-old mice by retro-orbital injection (once a day for three consecutive days), whereafter qRT-PCR analyses were performed on total RNA isolated from various tissues. As shown in **Figure 7**, a significant accumulation of cel-miR-39-3p was found in the left ventricle as well as liver, spleen, and kidney, whereas no signals were detected in brain, likely due to the high filtering efficiency of the hematic-encephalic barrier. These results demonstrate the capacity of our formulation for intracellular drug delivery *in vivo*.

Discussion

In this report, a novel and safe drug-delivery system based on bio-inspired negatively-charged CaP-NPs was generated. To the best of our knowledge this represents the first cross-domain study that, ranging from functional chemistry to molecular and cellular cardiac physiology, provides important advances in the field of cardiovascular nanomedicine.

When selecting suitable nano-carriers for drug delivery, several concerns hindering the potential clinical translation of NPs (*i.e.* the

biodegradability of the materials, the toxicity of degradation by-products, the toxic structural features of NPs, and protection of the payload) need to be taken into account [214]. CaP, a synthetic carrier resembling biogenic compounds, has ideal properties of biocompatibility, bioresorbability, and biodegradability because of its structural and chemical similarity with the mineral component of bones and teeth [215]. Furthermore, CaP-based carriers provide the further improvement of non-immunogenicity and minimal or absent toxicity [203, 204].

An additional advantage of CaP-NPs is related to the fact that at acidic pH, as found in endosomes and lysosomes after cellular intake, these nano-carriers rapidly dissolve into their ionic constituents facilitating the release of their cargo into the cytoplasm without any residual accumulation in cells and tissues, a critical drawback often encountered with other inorganic and metallic NPs [216].

The concept of preparing CaP-NPs for the encapsulation of RNA or DNA molecules, as opposed to surface decoration or adsorption where the therapeutic agent is not protected from the biological environment, is not new *per se* [217]. This strategy requires the presence of a capping agent to prevent the formation of large polydisperse and polymorphous micro-sized particles [218], and a variety of capping agents mainly based on synthetic polymers such as polyethylene glycol (PEG) [219], poly(methacrylic acid) (PMAA) [220], or polyethylenimine (PEI) [221] have been already used to stabilize CaP particles for gene delivery. However, synthetic polymers such as PEI, are cytotoxic and not suitable for the *in vivo* delivery of nucleic acids [222, 223]. Therefore the identification of alternative and more “bio-

friendly” stabilizing agents is an effective need. In this study, we have modified the conventional synthesis of CaP-NPs by including Na₃Cit in the synthesis process providing: *i*) improvement in the control of CaP growth tailoring the final dimensions, *ii*) enhancement of colloidal stability, and *iii*) negative surface charge. In addition, and in contrast to previous synthetic polymers, we employed citrate, which is a fully biocompatible organic molecule present in several biological environments such as the bone apatite surface [224]. Finally, by applying a final step of dialysis, we drastically reduced the mean size of CaP-NPs and increased their stability. In the last years, other authors employed citrate as stabilizing agent to prepare effective CaP-NPs as non-viral vectors for the delivery of nucleic acids [225-227]. However, here, differently from the previous works, miRNA was included during the synthesis of CaP-NP assisted by citrate, with the aim to encapsulate the active agent into the NPs as opposed to surface decoration for the reasons described above.

We recently introduced the concept that excitable cells are prone to (electro)toxicity. In fact, by measuring passive and active electrophysiologic properties of cardiomyocytes subjected to charged synthetic NPs, we found that polarized cells have a selective compatibility for negatively charged NPs [211, 228]. In agreement with these results, the negatively charged CaP-NPs generated in this study did not affect any of the functional parameters we measured in cardiac cells. In particular, we did not observe any changes in passive membrane properties, known to be a signature of arrhythmogenesis [228]. The relevance of these results points to a promising employment of CaP-NPs for cardiac related applications *in vivo*.

The functionalization of CaP-NPs with a negatively-charged surface is beneficial also for crossing the lipid bilayer of the cell membrane. Our results showed that internalization of CaP-NPs occurs via clathrin-mediated active endocytosis, which is in line with our previous study [211]. However, in a recent study it was also shown that CaP internalization in HeLa and COS7 cells follows the caveolae-mediated path [229]. While this process is indeed effective in those cells [229], the caveolae-mediated internalization is most likely not occurring in excitable cells such as cardiomyocytes and HL-1 where on the other hand caveolae and lipid-rafts constitute well-organized microdomains deputed for the thorough regulation of cardiac ion channel function [230]. This is in line with our data showing that administration of CaP-NPs to cardiac cells does not induce any alteration in cell membrane capacitance (**Supplementary Figure 4c**), an index of absence of pinocytosis or caveosome endocytosis of lipid rafts [231].

Nowadays, a great effort is made toward the identification of nano-formulations capable of specific delivery of small therapeutic agents (*i.e.* nucleic acids or peptides) to tissues and cells [232]. To meet this demand, we have used an innovative approach for the generation of CaP-NPs, which can easily and cost-effectively bind miRNAs, small nucleic acids with enormous therapeutic potentials. In particular, we showed that CaP-NP-miRs are *i)* efficient for *in vitro* and *in vivo* miRNA-delivery, and *ii)* able to target polarized tissues, such as the heart, although further improvements are still required to overcome limitations associated with cell-type specific targeting. In addition, the approach of encapsulating miRNAs into CaP-NPs bypasses potential

problems occurring with the majority of current miRNA delivery systems. In fact, in contrast to surface decoration or adsorption approaches, this approach increases the stability and functionality of miRNAs.

Conclusions

In summary, our study provides the proof-of-concept for an innovative, safe, and efficient CaP drug-delivery system in which the homogeneity of the nano-complex can be controlled by adding citrate during the crystallization process. The resulting CaP-NPs were biocompatible with the viability and electrophysiology of a cardiac cell line and primary cardiomyocytes. In addition, CaP-NPs were demonstrated to carry and efficiently release miRNAs both *in vitro* and *in vivo*. All together, we envisage that the current study will open up new avenues for the potential application of CaP-NPs in the context of cardiac nanomedicine.

Future Perspective

In this study we developed bioinspired and negatively surface charged nanoparticles, which are able to encapsulate and carry miRNAs into cardiac cells both *in vitro* and *in vivo*. In the emerging field of nanomedicine, controlling the negative charge of the nanocarriers in terms of negative surface potential can be beneficial in facilitating the targeting of hyperpolarized and excitable organs. Further prospective studies, together with a long-term *in vivo* toxicity evaluation and comparison with other delivery systems, will provide evidence-based data to support the use of this nano-approach for the treatment of cardiovascular diseases. Additionally, key investigations in support of

effective human translatability and personalized medicine applications would require experimentations in cultured induced pluripotent stem cells derived cardiomyocytes from cardiac pathologies. This will contribute with better understanding of doses, toxicity and the beneficial miRNA effect together with the possibility to carry other drugs, peptides or siRNAs to the diseased heart. Altogether, this will open up the potential use of bioinspired and surface charged nanoparticles for future therapeutic approaches.

Figure Legends

Figure 1. Chemical-physical and morphological characterization of CaP-NPs. (a) Mean particle size (Z-Average) and (b) count rate (Counts) as a function of time, analyzed by DLS during CaP-NPs crystallization in the absence (0 mM) and presence of Na₃Cit at different concentrations. (c) FT-IR spectra of CaP-NPs prepared in the presence of Na₃Cit (80 mM) at different crystallization times (*i.e.* 5, 10, 20, and 60 min). (d) TEM image of CaP-NPs. inset: corresponding SAED pattern.

Figure 2. Biocompatibility of HL-1 cardiac cells to CaP-NPs. (a) Cell toxicity as measured by Trypan blue exclusion assay in HL-1 cells treated as indicated. (b) Apoptosis detection via activated caspase 3 and 7 assay in HL-1 cells treated with increasing concentration of CaP-NPs. (c) Cellular internalization of FITC-conjugated CaP-NPs (green); Nucleus (Blue). §§§ p <0.001 compared to conditions of no CaP-NP treatment (NT) using Two-way Anova followed by Dunnet's multiple comparison test. * p <0.05; **p

<0.005; *** $p < 0.001$ calculated for each CaP-NP dose using Two-way Anova followed by a Bonferroni's test.

Figure 3. Voltage-current relationship (I-V curve) in HL-1 cells exposed to CaP-NPs. (a) Top row. Net membrane current I-V curves for control (left, black) and exposed (right, grey) HL-1 cells. Bottom row. Superimposition of the two curves (left) and net membrane current difference curve (right). (b) Sodium current traces for both conditions. Bottom. I-V curve for sodium currents and voltage-dependency of sodium channel activation (g/g_{max} , right) for control (black) and exposed (grey) HL-1 cells.

Figure 4. Sodium and calcium currents in adult ventricular myocytes exposed to CaP-NPs. (a) Net membrane current I-V curves for control (black) and exposed (grey) adult ventricular myocytes. (b) Superimposition of the two curves (left) and net membrane current difference curve (right). (c and d) Top row. Representative sodium current traces (c) and calcium current traces (d) acquired at both conditions. Bottom row. I-V curves for sodium (c) and calcium (d) currents and the related voltage-dependencies of the activation.

Figure 5. CaP-NP-miR assembly (a) Schematic illustration of the formation mechanism of CaP-NP-miRs; (b) TEM images of CaP-NP-miRs; inset: corresponding SAED pattern.

Figure 6. *In vitro* CaP-NP delivery into a cardiac cell line. (a-b) qRT-PCR on HL-1 cells treated for 6 and 12h with CaP-NP-miRs

loaded with miR-133a (up) and cel-miR-39-3p (down). (c) Luciferase reporter activity measured on HEK-293 cells transfected with a luciferase sensor and treated for 6 h with CaP-NP-miR carrying miR-133.

Figure 7. *In vivo* administration of CaP-NP-miRs. qRT-PCR performed on total RNA from various organs following three days of retro-orbital injection of CaP-NP-miRs carrying cel-miR-39-3p.

Executive summary

Objective

- To develop biocompatible and bioresorbable negatively-charged calcium-phosphate nanoparticles (CaP-NPs) as an innovative therapeutic system for the delivery of bioactive molecules to the heart.

Experimental setup

- CaP-NPs were synthesized via a straightforward one-pot biomineralization-inspired protocol employing citrate as a stabilizing agent and regulator of crystal growth.
- CaP-NPs were administered to cardiac cells *in vitro* and the effects of treatments were assessed.
- CaP-NPs were delivered *in vivo*.

Results

- CaP-NPs efficiently internalized into cardiomyocytes.
- CaP-NPs do not promote cell toxicity nor interfere with any functional properties of cardiomyocytes.
without promoting toxicity or interfering with any functional properties.
- CaP-NPs successfully encapsulated synthetic microRNAs, which were efficiently delivered into cardiac tissue *in vitro* and *in vivo*.

Conclusion

- CaP-NPs are a safe and efficient drug-delivery system for potential therapeutic treatments of polarized cells such as cardiomyocytes.

Supporting Information

Supporting Information is available Online.

ACKNOWLEDGMENTS

This work was supported by the Flagship project Nanomax – miRnano National Research Council grant to DC, MM, MI, and a Young investigator grant from the Italian Ministry of Health (GR-2009-1530528) to MM. HL-1 cells used in this study were kindly provided by Dr. W. Claycomb.

References

1. Mosterd A, Hoes AW. Clinical epidemiology of heart failure. *Heart* 93(9), 1137-1146 (2007).
2. Olson EN. MicroRNAs as therapeutic targets and biomarkers of cardiovascular disease. *Science translational medicine* 6(239), 239ps233 (2014).
3. Romaine SP, Tomaszewski M, Condorelli G, Samani NJ. MicroRNAs in cardiovascular disease: an introduction for clinicians. *Heart* 101(12), 921-928 (2015).
4. Poller W, Hajjar R, Schultheiss HP, Fechner H. Cardiac-targeted delivery of regulatory RNA molecules and genes for the treatment of heart failure. *Cardiovasc Res* 86(3), 353-364 (2010).
5. Eulalio A, Mano M, Dal Ferro M *et al.* Functional screening identifies miRNAs inducing cardiac regeneration. *Nature* 492(7429), 376-381 (2012).

6. Quattrocelli M, Crippa S, Montecchiani C *et al.* Long-term miR-669a therapy alleviates chronic dilated cardiomyopathy in dystrophic mice. *Journal of the American Heart Association* 2(4), e000284 (2013).
7. Fitzgerald KT, Holladay CA, Mccarthy C, Power KA, Pandit A, Gallagher WM. Standardization of models and methods used to assess nanoparticles in cardiovascular applications. *Small* 7(6), 705-717 (2011).
8. Matoba T, Egashira K. Nanoparticle-mediated drug delivery system for cardiovascular disease. *International heart journal* 55(4), 281-286 (2014).
9. Suarez S, Almutairi A, Christman KL. Micro- and Nanoparticles for Treating Cardiovascular Disease. *Biomaterials science* 3(4), 564-580 (2015).
10. Chang MY, Yang YJ, Chang CH *et al.* Functionalized nanoparticles provide early cardioprotection after acute myocardial infarction. *Journal of controlled release : official journal of the Controlled Release Society* 170(2), 287-294 (2013).
11. Gray WD, Che P, Brown M, Ning X, Murthy N, Davis ME. N-acetylglucosamine conjugated to nanoparticles enhances myocyte uptake and improves delivery of a small molecule p38 inhibitor for post-infarct healing. *Journal of cardiovascular translational research* 4(5), 631-643 (2011).
12. Verma DD, Hartner WC, Levchenko TS, Bernstein EA, Torchilin VP. ATP-loaded liposomes effectively protect the

- myocardium in rabbits with an acute experimental myocardial infarction. *Pharm Res* 22(12), 2115-2120 (2005).
13. Canyon SJ, Dobson GP. Protection against ventricular arrhythmias and cardiac death using adenosine and lidocaine during regional ischemia in the in vivo rat. *Am J Physiol-Heart C* 287(3), H1286-H1295 (2004).
 14. Liu M, Li M, Wang G *et al.* Heart-targeted nanoscale drug delivery systems. *Journal of biomedical nanotechnology* 10(9), 2038-2062 (2014).
 15. Thakor AS, Gambhir SS. Nanooncology: the future of cancer diagnosis and therapy. *CA: a cancer journal for clinicians* 63(6), 395-418 (2013).
 16. Eloy JO, Claro De Souza M, Petrilli R, Barcellos JP, Lee RJ, Marchetti JM. Liposomes as carriers of hydrophilic small molecule drugs: strategies to enhance encapsulation and delivery. *Colloids and surfaces. B, Biointerfaces* 123 345-363 (2014).
 17. Kobayashi K, Wei JJ, Iida R, Ijiro K, Niikura K. Surface engineering of nanoparticles for therapeutic applications. *Polym J* 46(8), 460-468 (2014).
 18. Miragoli M, Novak P, Ruenraroengsak P *et al.* Functional interaction between charged nanoparticles and cardiac tissue: a new paradigm for cardiac arrhythmia? *Nanomedicine* 8(5), 725-737 (2013).
 19. Claycomb WC, Lanson NA, Jr., Stallworth BS *et al.* HL-1 cells: a cardiac muscle cell line that contracts and retains phenotypic characteristics of the adult cardiomyocyte.

- Proceedings of the National Academy of Sciences of the United States of America* 95(6), 2979-2984 (1998).
20. Catalucci D, Zhang DH, Desantiago J *et al.* Akt regulates L-type Ca²⁺ channel activity by modulating Cavalpha1 protein stability. *The Journal of cell biology* 184(6), 923-933 (2009).
 21. Castaldi A, Zaglia T, Di Mauro V *et al.* MicroRNA-133 modulates the beta1-adrenergic receptor transduction cascade. *Circulation research* 115(2), 273-283 (2014).
 22. Bang C, Batkai S, Dangwal S *et al.* Cardiac fibroblast-derived microRNA passenger strand-enriched exosomes mediate cardiomyocyte hypertrophy. *The Journal of clinical investigation* 124(5), 2136-2146 (2014).
 23. Beniash E. Biomaterials--hierarchical nanocomposites: the example of bone. *Wiley interdisciplinary reviews. Nanomedicine and nanobiotechnology* 3(1), 47-69 (2011).
 24. Morgan TT, Muddana HS, Altinoglu EI *et al.* Encapsulation of organic molecules in calcium phosphate nanocomposite particles for intracellular imaging and drug delivery. *Nano Lett* 8(12), 4108-4115 (2008).
 25. Iafisco M, Palazzo B, Martra G *et al.* Nanocrystalline carbonate-apatites: role of Ca/P ratio on the uptake and release of anticancer platinum bisphosphonates. *Nanoscale* 4(1), 206-217 (2012).
 26. Iafisco M, Delgado-Lopez JM, Varoni EM *et al.* Cell surface receptor targeted biomimetic apatite nanocrystals for cancer therapy. *Small* 9(22), 3834-3844 (2013).

27. Rodriguez-Ruiz I, Delgado-Lopez JM, Duran-Olivencia MA *et al.* pH-responsive delivery of doxorubicin from citrate-apatite nanocrystals with tailored carbonate content. *Langmuir* 29(26), 8213-8221 (2013).
28. Li D, He J, Huang X *et al.* Intracellular pH-responsive mesoporous hydroxyapatite nanoparticles for targeted release of anticancer drug. *RSC Advances* 5(39), 30920-30928 (2015).
29. Lacerda L, Bianco A, Prato M, Kostarelos K. Carbon nanotubes as nanomedicines: from toxicology to pharmacology. *Adv Drug Deliv Rev* 58(14), 1460-1470 (2006).
30. Delgado-López JM, Frison R, Cervellino A, Gómez-Morales J, Guagliardi A, Masciocchi N. Crystal Size, Morphology, and Growth Mechanism in Bio-Inspired Apatite Nanocrystals. *Advanced Functional Materials* 24(8), 1090-1099 (2014).
31. Davies E, Muller KH, Wong WC *et al.* Citrate bridges between mineral platelets in bone. *Proceedings of the National Academy of Sciences of the United States of America* 111(14), E1354-1363 (2014).
32. Delgado-Lopez JM, Iafisco M, Rodriguez I, Tampieri A, Prat M, Gomez-Morales J. Crystallization of bioinspired citrate-functionalized nanoapatite with tailored carbonate content. *Acta Biomater* 8(9), 3491-3499 (2012).
33. Termine JD, Posner AS. Infra-red determination of the percentage of crystallinity in apatitic calcium phosphates. *Nature* 211(5046), 268-270 (1966).

34. Novak P, Shevchuk A, Ruenraroengsak P *et al.* Imaging single nanoparticle interactions with human lung cells using fast ion conductance microscopy. *Nano Lett* 14(3), 1202-1207 (2014).
35. Spindler AJ, Noble SJ, Noble D. Comparison of step and ramp voltage clamp on background currents in guinea-pig ventricular cells. *Experimental physiology* 84(5), 865-879 (1999).
36. Bers DM. Cardiac excitation-contraction coupling. *Nature* 415(6868), 198-205 (2002).
37. Doane TL, Burda C. The unique role of nanoparticles in nanomedicine: imaging, drug delivery and therapy. *Chem Soc Rev* 41(7), 2885-2911 (2012).
38. Roveri N, Palazzo B, Iafisco M. The role of biomimetism in developing nanostructured inorganic matrices for drug delivery. *Expert opinion on drug delivery* 5(8), 861-877 (2008).
39. Singh N, Jenkins GJ, Asadi R, Doak SH. Potential toxicity of superparamagnetic iron oxide nanoparticles (SPION). *Nano reviews* 1 (2010).
40. Jung H, Kim SA, Yang YG, Yoo H, Lim SJ, Mok H. Long chain microRNA conjugates in calcium phosphate nanoparticles for efficient formulation and delivery. *Archives of pharmaceutical research* 38(5), 705-715 (2015).
41. Xie Y, Chen Y, Sun M, Ping Q. A mini review of biodegradable calcium phosphate nanoparticles for gene delivery. *Current pharmaceutical biotechnology* 14(10), 918-925 (2013).

42. Kakizawa Y, Kataoka K. Block Copolymer Self-Assembly into Monodisperse Nanoparticles with Hybrid Core of Antisense DNA and Calcium Phosphate. *Langmuir* 18(12), 4539-4543 (2002).
43. Kakizawa Y, Furukawa S, Ishii A, Kataoka K. Organic-inorganic hybrid-nanocarrier of siRNA constructing through the self-assembly of calcium phosphate and PEG-based block anionomer. *Journal of controlled release : official journal of the Controlled Release Society* 111(3), 368-370 (2006).
44. Devarasu T, Saad R, Ouali A *et al.* Potent calcium phosphate nanoparticle surface coating for in vitro and in vivo siRNA delivery: a step toward multifunctional nanovectors. *Journal of Materials Chemistry B* 1(36), 4692-4700 (2013).
45. Vilar G, Tulla-Puche J, Albericio F. Polymers and drug delivery systems. *Current drug delivery* 9(4), 367-394 (2012).
46. Moghimi SM, Symonds P, Murray JC, Hunter AC, Debska G, Szewczyk A. A two-stage poly(ethylenimine)-mediated cytotoxicity: implications for gene transfer/therapy. *Molecular therapy : the journal of the American Society of Gene Therapy* 11(6), 990-995 (2005).
47. Hu YY, Rawal A, Schmidt-Rohr K. Strongly bound citrate stabilizes the apatite nanocrystals in bone. *Proceedings of the National Academy of Sciences of the United States of America* 107(52), 22425-22429 (2010).
48. Banik M, Basu T. Calcium phosphate nanoparticles: a study of their synthesis, characterization and mode of interaction with

- salmon testis DNA. *Dalton transactions* 43(8), 3244-3259 (2014).
49. Li J, Chen YC, Tseng YC, Mozumdar S, Huang L. Biodegradable calcium phosphate nanoparticle with lipid coating for systemic siRNA delivery. *Journal of controlled release : official journal of the Controlled Release Society* 142(3), 416-421 (2010).
 50. Banik M, Mukherjee R, Patra M *et al.* Spectrofluorimetric study on in vitro interaction between calcium phosphate nanoparticle and salmon testis DNA. *J Nanopart Res* 16(1), 1-11 (2013).
 51. Savi M, Rossi S, Bocchi L *et al.* Titanium dioxide nanoparticles promote arrhythmias via a direct interaction with rat cardiac tissue. *Particle and fibre toxicology* 11 63 (2014).
 52. Olton DY, Close JM, Sfeir CS, Kumta PN. Intracellular trafficking pathways involved in the gene transfer of nanostructured calcium phosphate-DNA particles. *Biomaterials* 32(30), 7662-7670 (2011).
 53. Maguy A, Hebert TE, Nattel S. Involvement of lipid rafts and caveolae in cardiac ion channel function. *Cardiovasc Res* 69(4), 798-807 (2006).
 54. Nichols B. Caveosomes and endocytosis of lipid rafts. *Journal of cell science* 116(Pt 23), 4707-4714 (2003).
 55. Dizaj SM, Jafari S, Khosroushahi AY. A sight on the current nanoparticle-based gene delivery vectors. *Nanoscale research letters* 9(1), 252 (2014).

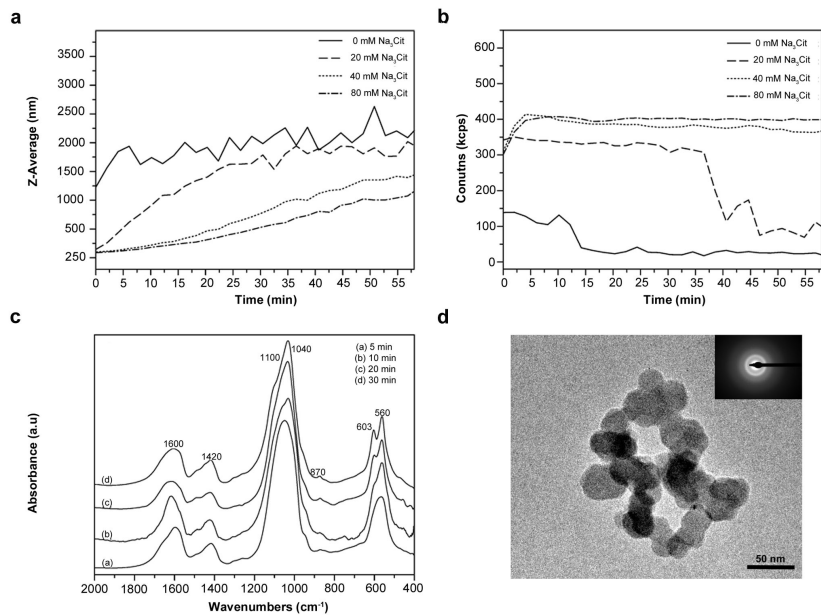


Figure 1

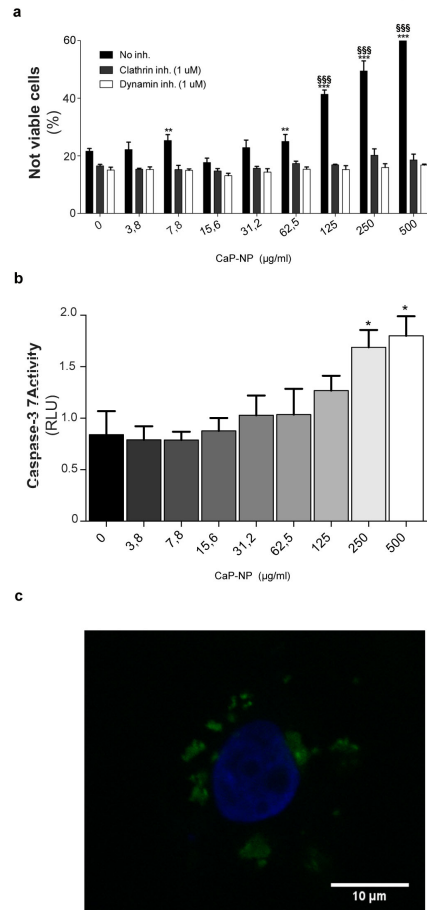


Figure 2

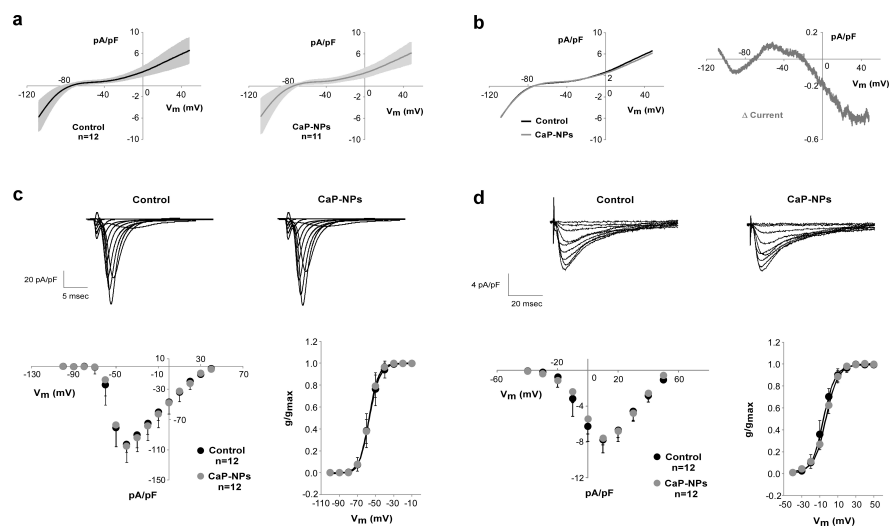


Figure 3

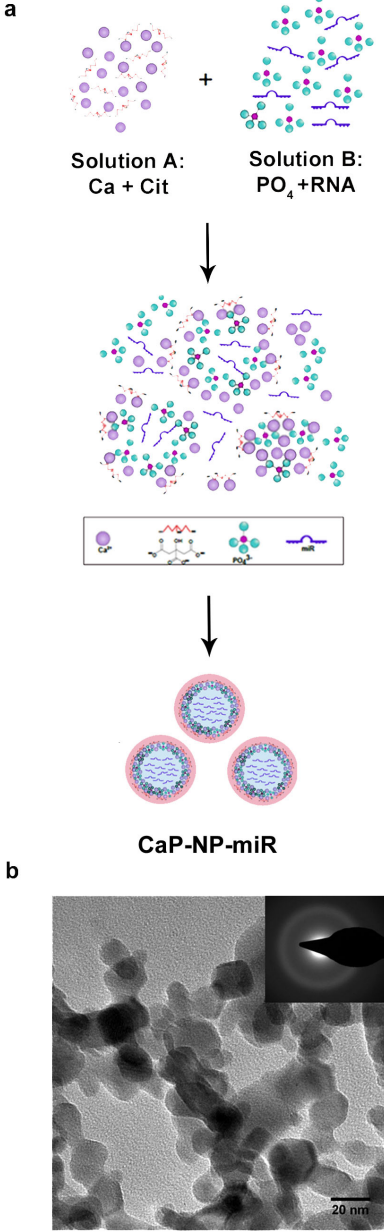


Figure 5

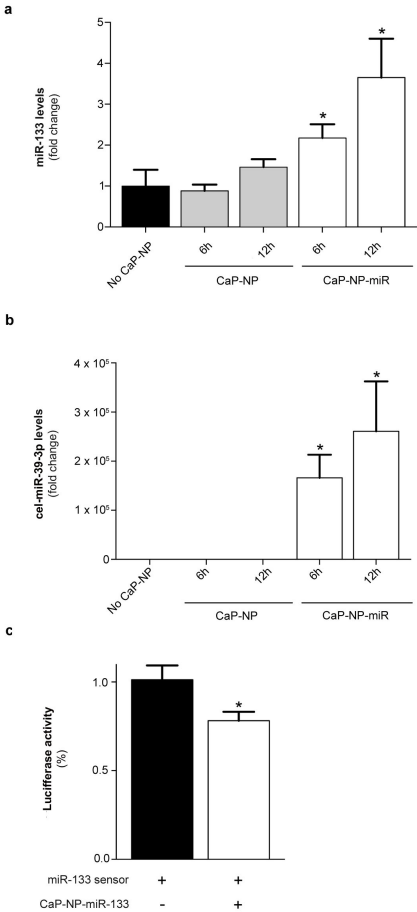


Figure 6

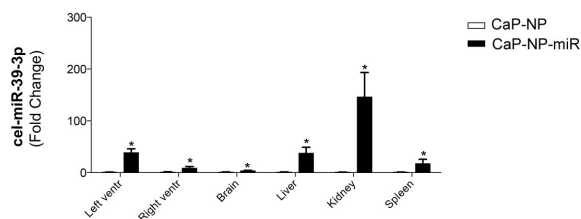


Figure 7

Crystallization time (min)	Splitting factor (SF) ^a	Z-average (nm)	PDI	ζ-potential (mV)
5	No calculable	1175 ±	0.55 ±	-26.9 ±
		110	0.03	0.6
10	1.76	1656 ±	0.52 ±	-25.9 ±
		408	0.03	0.9
20	2.16	2405 ±	0.38 ±	-26.1 ±
		402	0.02	0.7
60	2.25	3376 ±	0.44 ±	-30.4 ±
		851	0.02	1.3

Table 1. Splitting factor (SF), Z-average, polydispersity index (PDI) and ζ-potential of freeze-dried CaP-NPs (synthesized in the presence of 40 mM of Na₃Cit) as a function of crystallization time. (a) Calculated from FT-IR spectra (SF: measure consists on sum of

the heights of the stretching of phosphates peaks at 603 and 560 cm^{-1} and divided by the height of the valley between them at $\approx 588 \text{ cm}^{-1}$; all heights were measured above a baseline drawn from approximately 780 to 495 cm^{-1}).

miRNA ($\mu\text{g mL}^{-1}$)	Z-average (nm)	PDI	ζ -potential (mV)
0	129 ± 2	0.18 ± 0.10	-31.5 ± 1.5
1	156 ± 6	0.23 ± 0.10	-29.6 ± 2.6
5	199 ± 11	0.20 ± 0.05	-36.6 ± 1.6
10	225 ± 6	0.17 ± 0.05	-32.1 ± 3.0

Table 2. Z-average, polydispersity index (PDI), ζ -potential of CaP-miRs miRNAs as a function of miRNA added during the synthesis.

Supplementary Information

Supplementary Figure 1. (a) Conductivity evolution of dialysis medium as a function of time; (b) Mean particle size (Z-Average) and count rate (Counts) as a function of time, of CaP-NPs after dialysis (analyzed by DLS in 10 mM HEPES buffer at pH 7.0 and 25°C); (c) Energy dispersive X-ray (EDX) analysis of the best-in-class CaP-NPs after the purification step.

Supplementary Figure 2. Viability, cytotoxicity and caspase 3-7 assay. (a, b) Dose-response graph plotting both vitality and cytotoxicity measured in HL-1 after 5 and 12h of exposition to increasing doses of CaP-NPs, respectively. (c, d) Apoptosis detection via activated caspase 3 and 7 assay in HL-1 cells after 5 and 12h of treatment with increasing concentration of CaP-NPs, respectively. No significant differences were observed. (n =3).

Supplementary Figure 3. Viability, cytotoxicity and caspase 3-7 assay. (a) Dose-response graph plotting both vitality and cytotoxicity of freshly isolated adult cardiomyocytes subjected for 5h to increasing doses of CaP-NPs. (b) Apoptosis detection via activated caspase 3 and 7 assay in freshly isolated adult cardiomyocytes after 5h of exposition to increasing concentration of CaP-NPs. No significant differences were observed. (n =3).

Supplementary Figure 4. Passive properties and action potential characteristics for cardiac cells exposed *in vitro* to CaP-NPs. (a) Box-plots of passive properties (resting membrane potential,

membrane capacitance and membrane resistance) for HL-1 cells unexposed (black) and exposed (grey) to 20 $\mu\text{g/ml}$ CaP-NPs. **(b)** Representative elicited threshold-action potentials in adult ventricular cardiomyocyte exposed to 20 $\mu\text{g/ml}$ CaP-NPs. **(c)** Adult ventricular cardiomyocytes passive properties and action potential characteristics. Top row: Same as a for HL-1 cells. Middle row. Action potential threshold (pico amperes, pA) and amplitude (millivolt, mV) measured in unexposed and exposed cells. Bottom row. Maximal upstroke velocity (dV/dt_{max} of the action potential overshoot, V/s) and action potential duration (millisecond, ms calculated at the 90% of repolarization) in both conditions.

Supplementary Figure 5. *In vitro* delivery of CaP-NP-miR into primary adult cardiomyocytes (cmc). qRT-PCR performed on freshly isolated cmc after 5h of treatment with CaP-NPs loaded with cel-miR-39-3p. *** $p < 0.001$. (n =3).

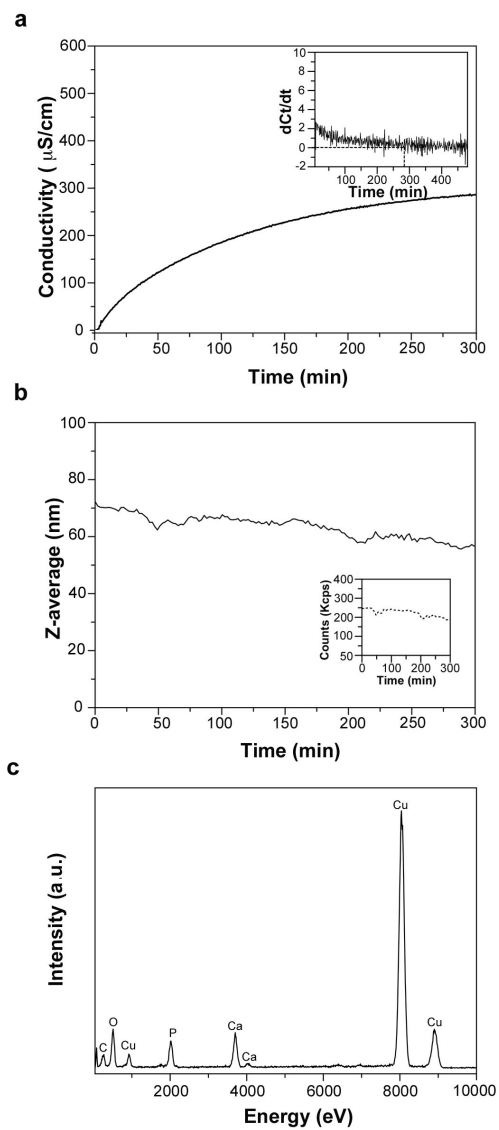


Figure S11

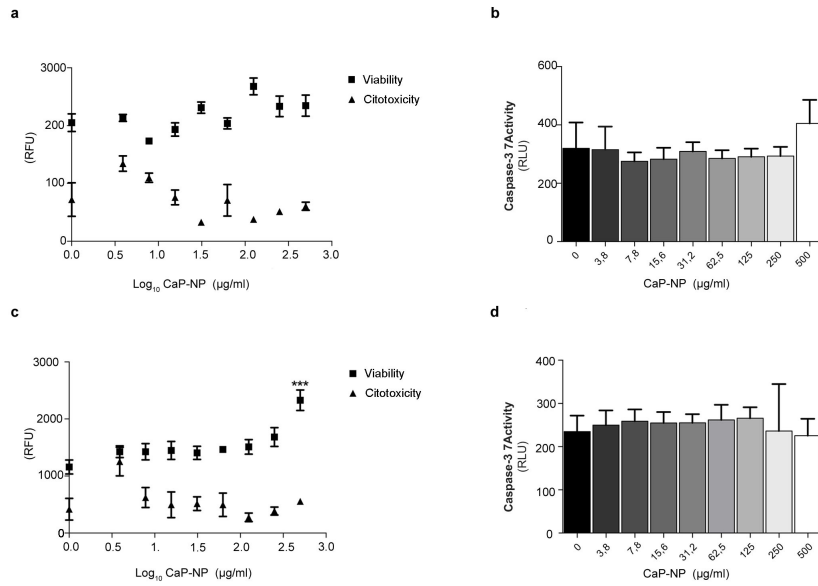


Figure S12

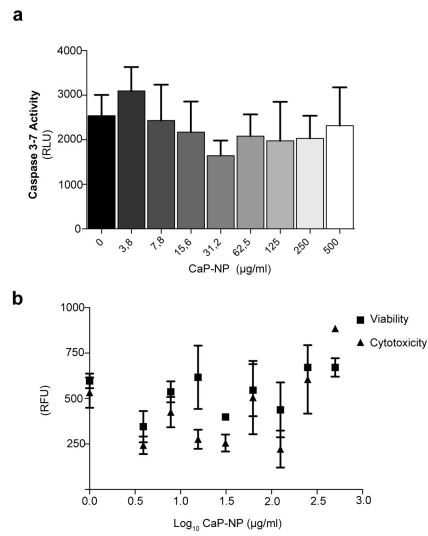
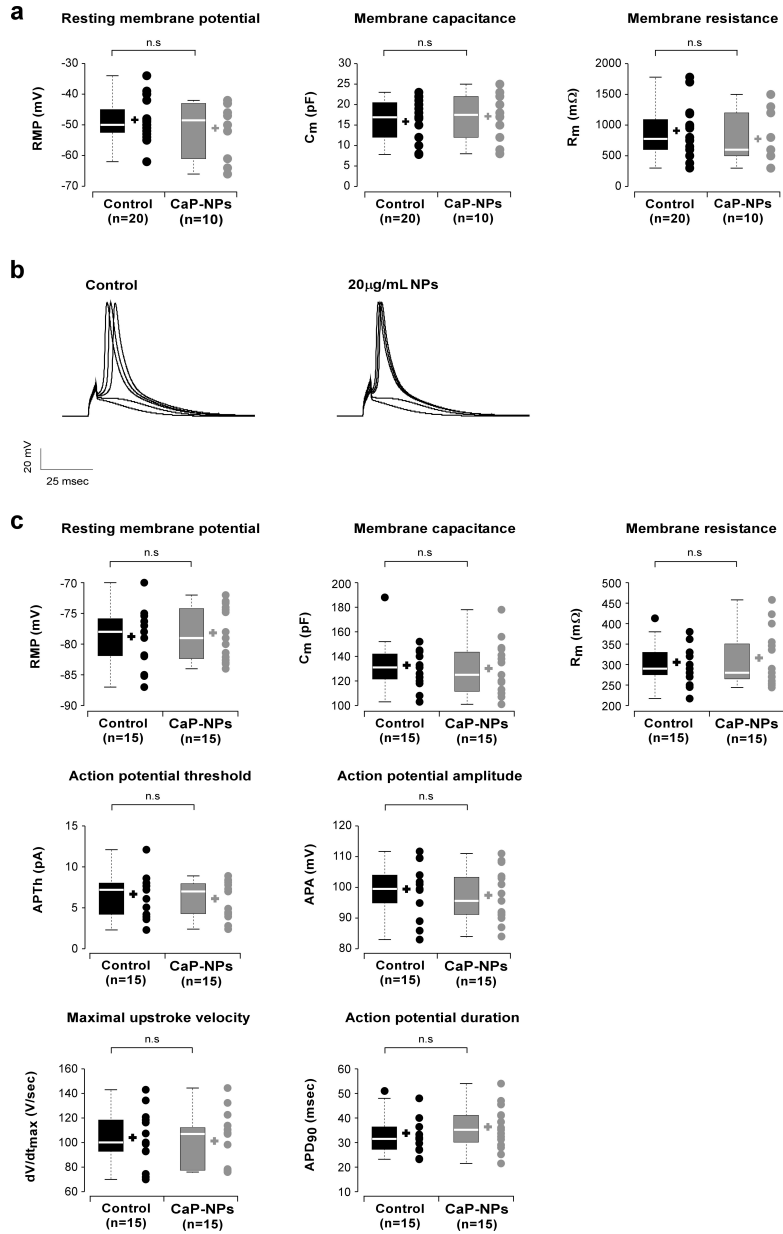


Figure S13



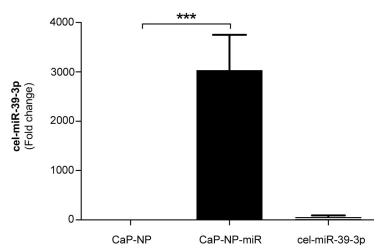


Figure S15

	CTL	CaP-NP
Ca²⁺ transient amplitude	11.35 ±	12.83 ±
(Δ360/380)	0.60	0.88
Resting Ca²⁺ (360/380)	0.943 ±	1.075 ±
	0.059	0.011
Time to peak 90% (msec)	0.084 ±	0.111 ±
	0.004	0.007*

Supplementary table 1. Ca²⁺ transient parameters in HL-1 cells treated or not with CaP-NPs. * = P<0.05. (n = 15).

	CTL	CaP-NP
Contractility		
Fractional shortening (% rest. cell. length)	6.128 ± 1.044	6.464 ± 1.097
Resting sarcomere length (µm)	1.761 ± 0.013	1.727 ± 0.005
Time to peak 90%(msec)	0.056 ± 0.02	0.048 ± 0.004
Ca ²⁺ transient		
Ca²⁺ transient amplitude (Δ360/380)	18.01 ± 2.32	15.89 ± 3.381
Resting Ca²⁺ (360/380)	1.110 ± 0.031	1.290 ± 0.017
Time to peak 90% (msec)	0.034 ± 0.004	0.043 ± 0.001

Supplementary table 2. Cell contractility and Ca²⁺ transient parameters in adult cardiomyocytes treated or not with CaP-NPs. (n = 17). No significant differences were observed

Chapter 6

MiR-153/Kv7.4: a novel molecular axis in the regulation of hypertension

Maffei A, Di Mauro V, Catalucci D, Lembo G.

Characterized by a steady increase in blood pressure values, hypertension is a complex, multifactorial disease resulting from a combination of environmental and genetic factors. Blood pressure is a function of peripheral resistance, which in turn depends on arterial diameter. Several molecular mechanisms have been described as regulators of arterial diameter both chronically, leading to vascular remodelling, and acutely, by contraction or relaxation of vascular smooth muscle in the vessel wall. Although decades of research proposed several advances in anti-hypertensive therapies, there are still patients with uncontrolled hypertension, thus pressing the search for novel mechanisms underlying hypertension and its related cardiovascular modifications.

MicroRNAs, small noncoding RNAs that target messenger RNAs at the post-transcriptional level, are involved in virtually all biological processes, including cellular proliferation, apoptosis, and differentiation¹. Deregulation of many individual microRNAs has been linked to the development and progression of cardiovascular diseases, thus highlighting the potential therapeutic importance of targeting microRNAs². The investigation of molecular mechanism regulated by microRNAs and the identification of novel microRNA targets in the pathogenesis of hypertension is a rapidly expanding area that can lead to the development of new treatment approaches for hypertension initiation¹.

Here, Carr et al. report that miR153 can alter arterial structure and function in hypertensive rats via translational inhibition of Kv7.4, a voltage-gated potassium channel present on vascular smooth muscle cells³.

Kv7.4 is an important regulator of arterial diameter acting by relaxing human⁴ and animal⁵ arteries. Voltage-gated potassium channels are able to repolarize smooth muscle cell membrane to the resting membrane potential, by allowing exit of potassium from the cell in response to membrane depolarization⁶. A decrease in Kv7.4 expression in animal models of hypertension, including the spontaneously hypertensive rat, had already been observed by the same Authors⁷, and linked to the decreased vasorelaxation typically observed in hypertension.

In the paper published on this issue of Cardiovascular Research, the Authors have extended their previous analysis on Kv7.4 decreased expression in hypertensive rats, showing that such decrease cannot be observed in cerebral arteries. This could be interesting in view of a possible future therapy interfering with these mechanisms. Actually, such a therapy would decrease blood pressure without affecting cerebral autoregulation, which is usually shifted towards higher blood pressure in hypertension⁸. This is not trivial, since the shift in autoregulation impairs the tolerance of the cerebral circulation to blood pressure reduction, so that a sudden decrease in blood pressure might induce a cerebral ischemia.

More important, the Authors focused on the mechanisms underlying the decrease in Kv7.4 expression, demonstrating a fundamental role for miR-153. Starting from a bioinformatics screening for potential putative microRNAs binding sites on Kv7.4 3'UTR, the authors selected miR-153, whose expression in SHR arteries was also inversely correlated to Kv7.4 protein. By luciferase reporter assay, the authors first assessed the directed binding of miR-153 on the 3' UTR

of kv7.4. Moreover, in order to elucidate the effective role of miR-153 in hypertension, the Authors transfected mesenteric arteries of wild type rats with a synthetic mimic of miR-153. After 24h of transfection the authors were able to observe significant morphological changes in the arteries, in terms of an increase in the media/lumen ratio, in average wall thickness and in the tunica media, which recapitulate an SHR-like phenotype.

It is unclear whether this effect was obtained through the regulation of Kv7.4 expression. Kv7 channels had already been involved in hypertrophic remodelling of pulmonary arteries in an animal model of pulmonary hypertension⁹. However, in this previous publication the vascular remodelling could simply be a side effect due to the restoration of normal pressure values by the intervention adopted, without involving Kv7 channels directly. Thus, whether Kv7.4 can be involved in vascular remodelling remains to be clarified, and would constitute an interesting direction for new research on this subject.

In conclusion, the work of Carr et al. provided for the first time a role for miR153 in contributing to chronic increased blood pressure in an animal model of hypertension, raising the possibility to design novel miR153-related therapies against vascular remodelling in hypertension. On the other hand, the Authors are also aware that microRNAs can potentially regulate a plethora of different target molecules. Thus, in order to improve the therapeutic efficacy and reduce side effects, further investigation of all the spectrum of miR-153 targets genes, as well as therapeutic strategy/delivery for the correction of miR-154 up-regulation, will be necessary.

References

1. Hartmann D, Thum T. MicroRNAs and vascular (dys)function. *Vascul Pharmacol.* 2011;55:92-105.
2. Jamaluddin MS, Weakley SM, Zhang L, Kougiyas P, Lin PH, Yao Q, and Chen C. MiRNAs: roles and clinical applications in vascular disease. *Expert Rev Mol Diagn.* 2011;11:79–89.
3. Carr G, Barrese V, Stott JB, Povstyan OV, Jepps TA, Zheng D, Jamshidi Y, Greenwood IA, Figueiredo HB. microRNA-153 targeting of KCNQ4 contributes to vascular dysfunction in hypertension. *Cardiovascular Research* 2016;
4. Ng FL, Davis AJ, Jepps TA, Harhun MI, Yeung SY, Wan A, Reddy M, Melville D, Nardi A, Khong TK, Greenwood IA. Expression and function of the K⁺ channel KCNQ genes in human arteries. *Br J Pharmacol.* 2011;162:42-53.
5. Jepps TA, Bentzen BH, Stott JB, Povstyan OV, Sivaloganathan K, Dalby-Brown W, Greenwood IA. Vasorelaxant effects of novel Kv 7.4 channel enhancers ML213 and NS15370. *Br J Pharmacol.* 2014;171:4413-24.
6. Ko EA, Park WS, Firth AL, Kim N, Yuan JX, Han J. Pathophysiology of voltage-gated K⁺ channels in vascular smooth muscle cells: modulation by protein kinases. *Prog Biophys Mol Biol.* 2010;103:95-101.
7. Jepps TA, Chadha PS, Davis AJ, Harhun MI, Cockerill GW, Olesen SP, Hansen RS, Greenwood IA. Downregulation of Kv7.4 channel activity in primary and secondary hypertension. *Circulation.* 2011;124:602-11.

8. Strandgaard S. Autoregulation of cerebral blood flow in hypertensive patients. The modifying influence of prolonged antihypertensive treatment on the tolerance to acute, drug-induced hypotension. *Circulation* 1976;53:720-7.
9. Morecroft I, Murray A, Nilsen M, Gurney AM, MacLean MR. Treatment with the Kv7 potassium channel activator flupirtine is beneficial in two independent mouse models of pulmonary hypertension. *Br J Pharmacol.* 2009;157:1241-9.

Chapter 7

The importance of being ncRNAs: from bit players as “junk DNA” to rising stars on the stage of the pharmaceutical industry

Vittoria Di Mauro^{1,2} and Daniele Catalucci¹

¹Humanitas Clinical and Research Center, Rozzano, Milan, Italy and National Research Council, Institute of Genetics and Biomedical Research, Milan Unit, Milan, Italy

²University of Milan Bicocca, Milan, Italy

Correspondence to: Daniele Catalucci and Vittoria Di Mauro.

¹Humanitas Clinical and Research Center, Rozzano, Milan, Italy and National Research Council, Institute of Genetics and Biomedical Research, Milan Unit, Milan, Italy

²University of Milan Bicocca, Milan, Italy

Email: daniele.catalucci@cnr.it; Vittoria.Di_Mauro@humanitasresearch.it

Key Words: ncRNAs, miRNAs, lncRNAs, cardiovascular diseases, therapeutic approaches

Running Title: ncRNAs for the translational medicine

Regulatory networks that orchestrate heart development and adaptation have always been under profound investigation, mainly because the heart is the first organ to form and function in order to sustain the entire life of the organism (1). Consequently, alterations in the molecular pathways controlling heart development as well as adaptation to physiological and environmental stress might result in cardiac pathological conditions, which represent the leading causes of death worldwide (2).

For many years it has been assumed that only functional proteins, encoded by genomic sequences containing open reading frames, were accountable in playing crucial roles in almost all biological processes, including cardiac physiology and pathologies (3). However, only 2% of the eukaryotic genome codes for proteins, which is why the formerly called “junk DNA” has become an expanding area of interest. Indeed, the latest advances in sequencing technologies and initiatives such as ENCODE (*Encyclopedia of DNA Elements*) have highlighted that the mammalian genome is actively transcribed into a myriad of non-coding transcripts, collectively defined as ncRNAs (4). In the context of the cardiovascular system, only recently it has become evident how these ncRNAs may play a crucial role in the gene regulatory networks that control physiological and pathological development (5).

Here, we discuss the review of Li *et al.* (6) which summarizes the role and function of miRNAs and lncRNAs in cardiac disease and how they interact with each other to finely regulate the molecular

events in ischemic heart diseases. We then underline recent advances involving the targeting of both miRNAs and lncRNAs and the consequent challenges for their exploitation in the pharmaceutical industry (7).

Based on size, ncRNAs can be classified into 2 categories: 1) small ncRNAs that comprise microRNAs (miRNAs), PIWI-interacting RNA (piRNAs) and endogenous short interfering RNAs (siRNAs); and 2) long noncoding RNAs (lncRNAs).

MicroRNAs (miRNAs) are 19-24 nucleotides long, and mainly function as negative regulators of gene expression, since they can influence the stability and the subsequent translation of nascent mRNA transcripts (8-10). Indeed, miRNAs inhibit mRNA translation and/or mRNA stability through base-pairing with the 3' untranslated regions within transcripts (11). Ultimately, several studies have also demonstrated the presence of mature miRNAs in the nuclear compartment, where they can act on the stability of nuclear transcripts, silence or activate transcription at specific gene promoters through epigenetic modifications and modulate co-transcriptional alternative splicing events (12).

Since the first discovery in *C. elegans* in 1993 (13), there was a remarkable gain in knowledge regarding regulation, expression and functionality of miRNAs in many human diseases, including cardiovascular pathologies (14). Van Rooij *et al* found that some miRNAs (miR-23a, miR-23b; miR-24, miR-195 and miR-214) were able to induce an hypertrophic response in cardiomyocytes (15). Successive studies revealed that other miRNAs can affect the development of hypertrophy. This is the case of miR-133, that was

demonstrated to be inversely related to cardiac hypertrophy (16). Carè *et al* showed for the first time, that *in vitro* overexpression of miR-133 blocks the up-regulation of different hallmarks of hypertrophy. On the contrary, even in absence of stress stimuli, the *in vivo* suppression of endogenous miR-133 with a decoy sequence was responsible of a massive cardiac hypertrophy response. Moreover, the cardio-protective effects of this miRNA was also demonstrated by Castaldi *et al*, who described that through its action on different effectors of the β_1 -Adrenergic cascade, miR-133 preserved cardiac performance and attenuated pathological remodeling in a mouse model of induced cardiac hypertrophy (17).

Alteration in miRNAs expression was also found to be associated in other models of cardiac diseases such as myocardial infarction (MI), a condition caused by coronary artery occlusion, that in turn results in death of cardiomyocytes and fibrosis. Among the dysregulated miRNAs, miR-21, which is preferentially expressed in cardiac-fibroblasts, was demonstrated to increase the development of fibrosis (18).

This rapidly expanding interest in miRNAs led to the development of increasingly sophisticated techniques of RNA sequencing, that in turn allowed the discovery of the second class of relevant ncRNAs: lncRNAs. lncRNAs are defined as RNA molecules of more than 200 nucleotides in length, lacking a significant open reading frame (ORF), and classified according to their genomic positioning as sense, antisense, intronic, divergent, or intergenic. Contrary to miRNAs, lncRNAs do not interact only with transcripts, but depending on their site/subcellular location, can exert several

different functions ^[4]. Some lncRNAs elicit their function in the cytosol mainly by regulating protein localization, mRNAs translation and stability (19). However, the majority of lncRNAs are located in the nucleus, where they control gene expression by interaction with transcription factors or histone-modifying enzymes. In the heart, one of the most well-studied lncRNAs is the myosin heavy chain-associated RNA transcript *Mhrt* (20). *Mhrt* was demonstrated to inhibit cardiac hypertrophy by antagonizing the function of Brg1, a chromatin-remodelling factor responsible for expression of many hypertrophic genes.

Despite a large number of studies have revealed that miRNAs and lncRNAs equally contribute in the onset of cardiac diseases, only recently it has been suggested that miRNAs and lncRNAs can react with each other, pointing out a novel level of complexity in the already well-orchestrated regulatory network of ncRNAs. As discussed by Li *et al* the interactions between miRNAs and lncRNAs can be mechanistically divided into: 1) lncRNAs acting as a sponge/decoy of miRNAs; 2) lncRNAs as precursor of miRNAs; 3) miRNA-triggering lncRNAs decay, and 4) competition for mRNA targets. Among these, the most characterized mechanism in the ischemic heart is the absorption of miRNAs by lncRNAs. Nonetheless, more detailed studies are required to further dissect the full mechanistic network of cross-talk between miRNAs and lncRNAs.

The strong association between aberrant expression of ncRNAs and pathological conditions has corroborated the concept that manipulation of miRNAs or lncRNAs could represent a new

frontier for innovative therapeutic strategies. Indeed, though most of the work in this field has been done in cancer therapy, the application of ncRNA-based therapeutic approaches for the treatment of cardiac diseases has been facing a rapid spreading towards pre-clinical and clinical phases (5). With respect to miRNA-based therapies, the knowledge of their mechanism of action and the frequent abnormal up-regulation in some pathologies has prompted the development of three main approaches: 1) expression vectors (miRNA sponges), 2) small-molecule inhibitors and 3) antisense oligonucleotides (ASOs) (21). The first technology was described by Ebert *et al* and it was conceived as reporter vector containing multiple miRNA-binding sites. When delivered into cells, the binding sites would serve as decoys for the targeted miRNA, thereby reversing the suppression of endogenous target genes (22). The second strategy is based on low molecular-weight compounds, which interfere with miRNA function, targeting different steps of miRNA pathways. These small molecules can interfere with the transcript of primary miRNAs or inhibit miRNA processing by interfering with Dicer activity or even with their loading into Argonaute 2 (AGO2) to form an active RNA-induced silencing complex (RISC). In this field a pioneering study was the work of Gumireddy *et al.* who demonstrated that azobenzene was able to directly inhibit the action of miR-21(23). The third technology was certainly the most studied and currently used. It is based on chemically modified miRNA-targeting antisense oligonucleotides (anti-miRs) designed to target specific miRNA and bind with high affinity. So far,

various chemical modifications (*i.e.* 2'-OME; cholesterol and Locked Nucleic Acid) are available in order to facilitate the cellular uptake and the specificity of these anti-miRs (16, 24-26).

In addition to the silencing of miRNAs, their up-regulation to physiological levels has become a goal for research institutes as well as for pharmaceutical industries. However, the approaches to optimize miRNA overexpressing tools have been rather inadequate so far (27). The synthetic RNA-duplexes known as “mimics” are largely used to emulate miRNA function. However, since they must function as a miRNA and become recognized by the RISC complex, the necessary chemical modifications have been so far limited (28). Thus, deeper studies in developing chemical stabilization and/or delivery modifications are required to increase the biological effects. This represents the current limiting step for this technology to become an acceptable avenue for future clinical studies.

In light of the chemical tools that have already been developed for miRNA manipulation, analogue approaches are now applied for new therapeutic strategies towards the use of lncRNA-based tools. However, despite lncRNA modulators (*i.e.* gapmers) has started to be used for different *in vitro* and *in vivo* studies, (29, 30) more efforts are still required for overcoming some obstacles for their exploitation in translational medicine. Additionally, the poor rate of lncRNA conservation between species makes the designed compounds difficult to be translated towards pre-clinical and clinical studies. Moreover, side-effects have to be carefully evaluated because of the more complicated mechanism of action

of lncRNAs (31). In addition, further limitations exist as a result of their targeting efficiency, which is related to the nuclear compartmentalization of the majority of lncRNAs.

Besides the chemistry used for down- or up-modulation of the altered ncRNAs, a further difficulty is the successful and safe delivery of the therapeutic compound to target tissues. To overcome this obstacle, a new frontier has been recently examined by the world of nanomaterials. In fact, nanostructured biomaterials with their physicochemical properties such as small and controllable size, biocompatibility and biodegradable chemical composition, high reactivity and functional structure, might successfully face the drug delivery limitations of traditional approaches (32). Additionally, the non-immunogenicity of some biomaterials and the incorporation of the therapeutic molecules loaded within nanocarriers facilitate the therapeutic preservation against potential immunogenicity reactions and enzymatic degradation, respectively (33). Furthermore, functionalization of nanocarriers with cell-specific targeting moieties (*i.e.* aptamers or peptides) might enable a more specific targeting thus avoiding side effects due to uncontrolled biodistributions of the drug in other organs.

In conclusion, the field of ncRNA therapeutics is still in its infancy and yet already there are promising data. However, before we might use these new therapeutic tools regularly, more detailed functional and structural investigations are necessary to better characterize the biology of ncRNAs and the proper approach for their modulation. It is reasonable to think that the more we learn

about the contribution of ncRNAs in diseases, the higher the chances for achieving a better diagnosis and prognosis will be. Thus, the scientific community and pharmaceutical companies must band together to pursue this goal in order to obtain more rigorous tools that will eventually be acceptable for clinical trials and subsequently be used as therapeutic tools for a wide range of diseases in the coming years.

Acknowledgments

We thank the Dr. Christina Pagiatakis for critical reading of the manuscript.

Foundings

This work was supported by grant from the Italian Ministry of University and Research FIRB (Fondo per gli Investimenti della Ricerca di Base)-Futuro in Ricerca (RBF12I3KA).

Provenance: This is a Guest Commentary commissioned by Section Editor Zhijun Han, MD (Department of Laboratory Medicine, Wuxi Second Hospital, Nanjing Medical University, Wuxi, Jiangsu, China).

Comment on:

J Cardiovasc Pharmacol Ther. 2016 Sep 15. pii: 1074248416667600. [Epub ahead of print]

The Role of MicroRNA and LncRNA-MicroRNA Interactions in Regulating Ischemic Heart Disease. **Findings**

This work was supported by grant from the Italian Ministry of University and Research FIRB (Fondo per gli Investimenti della Ricerca di Base)-Futuro in Ricerca (RBFR12I3KA).

References

1. Olson, E.N., *A decade of discoveries in cardiac biology*. Nature medicine, 2004. **10**(5): p. 467-474.
2. Schonrock, N., R.P. Harvey, and J.S. Mattick, *Long noncoding RNAs in cardiac development and pathophysiology*. Circulation research, 2012. **111**(10): p. 1349-1362.
3. Kataoka, M. and D.-Z. Wang, *Non-coding RNAs including miRNAs and lncRNAs in cardiovascular biology and disease*. Cells, 2014. **3**(3): p. 883-898.
4. Frank, S., et al., *A lncRNA Perspective into (Re) Building the Heart*. Frontiers in Cell and Developmental Biology, 2016. **4**.
5. Esteller, M., *Non-coding RNAs in human disease*. Nat Rev Genet, 2011. **12**(12): p. 861-74.
6. Li, N., et al., *The Role of MicroRNA and LncRNA-MicroRNA Interactions in Regulating Ischemic Heart Disease*. Journal of cardiovascular pharmacology and therapeutics, 2016.

7. Matsui, M. and D.R. Corey, *Non-coding RNAs as drug targets*. Nature Reviews Drug Discovery, 2016.
8. Grishok, A., et al., *Genes and mechanisms related to RNA interference regulate expression of the small temporal RNAs that control C. elegans developmental timing*. Cell, 2001. **106**(1): p. 23-34.
9. Hutvagner, G., et al., *A cellular function for the RNA-interference enzyme Dicer in the maturation of the let-7 small temporal RNA*. Science, 2001. **293**(5531): p. 834-838.
10. Van Rooij, E. and E.N. Olson, *microRNAs put their signatures on the heart*. Physiological genomics, 2007. **31**(3): p. 365-366.
11. Markham, D.W. and J.A. Hill, *MicroRNAs and heart failure diagnosis miR-acle or miR-age?* Circulation research, 2010. **106**(6): p. 1011-1013.
12. Roberts, T.C., *The microRNA biology of the mammalian nucleus*. Molecular Therapy-Nucleic Acids, 2014. **3**(8): p. e188.
13. Lee, R.C., R.L. Feinbaum, and V. Ambros, *The C. elegans heterochronic gene lin-4 encodes small RNAs with antisense complementarity to lin-14*. Cell, 1993. **75**(5): p. 843-854.
14. Kumarswamy, R. and T. Thum, *Non-coding RNAs in cardiac remodeling and heart failure*. Circulation research, 2013. **113**(6): p. 676-689.
15. van Rooij, E., et al., *A signature pattern of stress-responsive microRNAs that can evoke cardiac hypertrophy and heart*

- failure*. Proceedings of the National Academy of Sciences, 2006. **103**(48): p. 18255-18260.
16. Care, A., et al., *MicroRNA-133 controls cardiac hypertrophy*. Nature medicine, 2007. **13**(5): p. 613-618.
 17. Castaldi, A., et al., *MicroRNA-133 modulates the β -adrenergic receptor transduction cascade*. Circulation research, 2014. **115**(2): p. 273-283.
 18. Thum, T., et al., *MicroRNA-21 contributes to myocardial disease by stimulating MAP kinase signalling in fibroblasts*. Nature, 2008. **456**(7224): p. 980-984.
 19. Skroblin, P. and M. Mayr, *"Going long": long non-coding RNAs as biomarkers*. Circulation research, 2014. **115**(7): p. 607-609.
 20. Uchida, S. and S. Dimmeler, *Long noncoding RNAs in cardiovascular diseases*. Circulation research, 2015. **116**(4): p. 737-750.
 21. Li, Z. and T.M. Rana, *Therapeutic targeting of microRNAs: current status and future challenges*. Nature reviews Drug discovery, 2014. **13**(8): p. 622-638.
 22. Ebert, M.S., J.R. Neilson, and P.A. Sharp, *MicroRNA sponges: competitive inhibitors of small RNAs in mammalian cells*. Nature methods, 2007. **4**(9): p. 721-726.
 23. Gumireddy, K., et al., *Small-Molecule Inhibitors of MicroRNA miR-21 Function*. Angewandte Chemie International Edition, 2008. **47**(39): p. 7482-7484.
 24. Elmén, J., et al., *LNA-mediated microRNA silencing in non-human primates*. Nature, 2008. **452**(7189): p. 896-899.

25. Van Rooij, E., et al., *Dysregulation of microRNAs after myocardial infarction reveals a role of miR-29 in cardiac fibrosis*. Proceedings of the National Academy of Sciences, 2008. **105**(35): p. 13027-13032.
26. Bonauer, A., et al., *MicroRNA-92a controls angiogenesis and functional recovery of ischemic tissues in mice*. Science, 2009. **324**(5935): p. 1710-1713.
27. Thum, T., *MicroRNA therapeutics in cardiovascular medicine*. EMBO molecular medicine, 2012. **4**(1): p. 3-14.
28. van Rooij, E., A.L. Purcell, and A.A. Levin, *Developing microRNA therapeutics*. Circulation research, 2012. **110**(3): p. 496-507.
29. Viereck, J., et al., *Long noncoding RNA Chast promotes cardiac remodeling*. Science translational medicine, 2016. **8**(326): p. 326ra22-326ra22.
30. Wheeler, T.M., et al., *Targeting nuclear RNA for in vivo correction of myotonic dystrophy*. Nature, 2012. **488**(7409): p. 111-115.
31. Creemers, E.E. and E. van Rooij, *Function and Therapeutic Potential of Noncoding RNAs in Cardiac Fibrosis*. Circulation research, 2016. **118**(1): p. 108-118.
32. Singh, S., et al., *Nanoparticle based drug delivery system: advantages and applications*. Indian Journal of Science and Technology, 2011. **4**(3): p. 177-180.
33. Di Mauro, V., et al., *Bioinspired negatively charged calcium phosphate nanocarriers for cardiac delivery of MicroRNAs*. Nanomedicine, 2016. **11**(8): p. 891-906.

